

UNIVERSITY OF ZAGREB
FACULTY OF CHEMICAL ENGINEERING AND TECHNOLOGY

Bruno Zelić

**Study of the Process Development for *Escherichia coli* Based Pyruvate
Production**

DISSERTATION

Zagreb, July 2003.

Bibliographic facts:**UDK: 66:676.011:681.5.015:301.172=20(043)****Scientific area: technical sciences****Scientific field: chemical engineering****Institutions:** - Faculty of Chemical Engineering and Technology, University of Zagreb, Croatia

- Institute of Biotechnology 2, Research Center Jülich, Germany

Supervisor: Prof. Dr. Đurđa Vasić-Rački**Number of pages: 119****Number of figures: 72****Number of tables: 25****Number of supplements: 6****Number of literature cited: 127****Date of defense: July 11th 2003.****Members of the commission:**

1. Prof. Dr. Christian Wandrey, Institute of Biotechnology, Research Center Jülich, Germany
2. Prof. Dr. Đurđa Vasić-Rački, Faculty of Chemical Engineering and Technology, University of Zagreb, Croatia
3. Prof. Dr. Želimir Kurtanjek, Faculty of Food Technology and Biotechnology, University of Zagreb, Croatia

Dissertation is stored at:

1. Library of Faculty of Chemical Engineering and Technology, University of Zagreb, Marulićev trg 20
2. National and University Library Zagreb, Hrvatske bratske zajednice bb
3. Library of University of Rijeka, Dolac 1
4. Library of University of Split, Livanjska 5
5. Library of University of Osijek, Trg sv. Trojstva 3

This work was funded by the DBU (Deutsche Bundesstiftung Umwelt), grant number AZ 13040/05. The work was conducted at the facilities of the Institute of Biotechnology 2 of the Research Center Jülich, Germany.

I wish to express my appreciation to the following people for their help, support and guidance to make this piece of work a reality.

Prof. Dr. Đurda Vasić-Rački for the effective supervision of my career and this work, for the numerous helpful discussions and for friendly working atmosphere in last seven years.

Prof. Dr. Christain Wandrey for supervising this work and for giving me the opportunity to perform the research part of this thesis in his laboratories. This enabled me access to the diverse infrastructure and the fantastic working atmosphere I experienced at the Institute of Biotechnology 2 at the Research Center Jülich.

Dr. Ralf Takors for his extensive help during this work and for his thorough critics on this thesis.

Dr. Tanja Gerharz and Prof. Dr. Michael Bott for great cooperation on the "Pyruvate" project.

Ms. Marianne Hess for making my life and stay in Jülich as pleasant as possible.

B. Sc. Silvia Zaja for friendship and tremendous help during my stay in Jülich.

M. Sc. Freddy D. N. Tita-Nwa, B. Sc. Ana Vrsalović, B. Sc. Srđan Gostović, Ms. Heidi Haase-Reiff, B. Sc. Hans-Jürgen Brandt and M. Sc. Andreas Franz for their extensive work and help in the laboratories.

The people at the Institutes of Biotechnology 1 and 2, especially the people of the Fermentation Group that helped in many ways for the success of this work.

My parents Ana and Ante, my brother Ozren and my grandfather Đuro for love, care and support.

Last but not least my wife Aisa and my daughter Anais for love, support, understanding and always being there for me. I love you.

To Anais and Aisa.

Theme of the dissertation "Study of the process development for *Escherichia coli* based pyruvate production" was accepted on the meeting of the Faculty Council of the Faculty of Chemical Engineering and Technology, University of Zagreb (September 23. 2002.).

Sažetak

Sinteza velikog broja produkata kemijske, farmaceutske i prehrambene industrije sadrži reakcije dehidriranja. Za te reakcije uobičajena je primjena višestupnjevite kemije zaštitnih grupa, različitih organskih otapala i vrlo često teških metala kao katalizatora. K tome, visoke temperature pred- i nad-tlakovi neophodni za provedbu kemijskog dehidriranja čine ovakove sinteze skupim, kompleksnima i nepovoljnima za okoliš.

Zbog toga je u zadnjih dvadesetak godina razvijen veliki broj procesa koji za svoju provedbu koriste biokatalizatore. Primjenom biodehidriranja sintetski put je skraćen, procesi se provode u fiziološkim uvjetima, izbjegnuta je upotreba teških metala kao katalizatora, sporedni produkti su lako razgradljivi i neotrovni, što čini biotransformacije jednostavnijima za provedbu i ekološki prihvatljivima.

Industrijska upotreba biokatalizatora za provedbu reakcija dehidriranja vrlo je raširena, primjerice pri proizvodnji Vitamina C i anti-diabetika MiglitolTM. Moderne metode metaboličkog inženjerstva omogućuju provedbu velikog broja reakcija biodehidriranja korištenjem rekombinantnih produkcijskih mikroorganizama prilagođenih provedbi željenih reakcija, primjerice kroz ekspresiju gena bitnih za proizvodnju željenog produk(a)ta, "isključivanjem" neželjenih sporednih reakcija itd.

Pirogroždana kiselina se upotrebljava u farmaceutskoj (sinteza L-DOPA i L-efedrina), prehrambenoj (dodatak hrani) i agrokemijskoj industriji. U novije vrijeme pronađeno je da upotreba pirogroždane kiseline smanjuje broj slobodnih radikala i ima inhibicijski utjecaj na neke tumore. Tabletirana natrijeva sol pirogroždane kiseline jedan je od vodećih dijabetičkih proizvoda u svijetu u zadnjih pet godina.

Klasični kemijski način proizvodnje pirogroždane kiseline je piroliza vinske kiseline uz prisustvo KHSO_4 i teških metala kao katalizatora pri 200 ° C. Kako je u zadnjih dvadesetak godina porastao zahtjev za primjenu čistijih tehnologija u industrijskoj proizvodnji tako je razvijeno i više procesa dobivanja pirogroždane kiseline upotrebom biokatalizatora. Jedan od njih je i proces dobivanja pirogroždane kiseline iz glukoze upotrebom rekombinantne *Escherichia coli*.

U ovom radu je razvijen i optimiran novi proces dobivanja pirogroždane kiseline, upotrebom metodologije kemijskog inženjerstva, bilanciranja i modeliranja procesa, te identifikacije i optimiranja procesnih parametara u cilju postizanja maksimalnog iskorištenja pirogroždane kiseline na glukozi, maksimalnog prostornog vremenskog iskorištenja i konačne koncentracije pirogroždane kiseline.

Razvijena su četiri različita procesa proizvodnje pirogroždane kiseline: semi-kontinuirani, ponovljivi semi-kontinuirani proces, kontinuirani proces s povratnim tokom biomase i kontinuirani proces s potpuno integriranom separacijom pirogroždane kiseline (kao separacijski proces korištena je elektrodijaliza).

Razvijen je i model procesa biokonverzije glukoze u pirogroždanu kiselinu, procijenjeni parametri modela te ocjenjena valjanost istoga. Također je razvijen i model procesa elektrodijalize.

Ključne riječi: razvoj procesa, *Escherichia coli*, piruvat, model procesa, potpuno integrirana separacija produkta

Summary

The commercial demand for pyruvic acid has increased greatly in past decades owing to its various applications, e. g. as an effective starting material for the synthesis of many drugs, agrochemicals and nowadays in food industry as a fat burner. The main goal in this project was the development of a pyruvate production process from glucose with a high molar pyruvate/glucose yield (approaching 2 mol pyruvate/mol glucose) and space-time yield using a recombinant *Escherichia coli* YYC202 strain. This strain is completely blocked in its ability to convert pyruvate in acetyl-CoA or acetate, resulting in acetate-auxotrophy during growth in glucose minimal medium.

Due to the strain genotype, acetate availability was assumed to represent a key fermentation variable. Experimental studies identified a "simple" correlation between acetate consumption rate (*ACR*) and CO₂ production rate (*CTR*) with an optimum equal molar ratio. Therefore, *CTR* (calculated on-line by CO₂ and O₂ exhaust gas analysis) was used for on-line calculation and regulation of the acetate feed (acetate limiting, saturating and accumulating conditions could be established). Glucose closed-loop control was established and series of fed-batch processes were performed. At optimal process conditions final pyruvate titer higher than 700 mmol dm⁻³ (62 g dm⁻³), integral molar yields of 1.11 mol pyruvate/mol glucose and a space time yield (*STY*) of 42 g dm⁻³ d⁻¹ were achieved. Evidence was obtained that high extra-cellular pyruvate concentration inhibits the process.

To face this problem with process engineering means, repetitive fed-batch experiments with cell retention were performed. Molar yield pyruvate/glucose was improved up to 1.7 mol mol⁻¹. *STY* was increased more than 300 % and has reached 145 g dm⁻³ h⁻¹. Continuous process with cell retention was developed to simplify complex set-up used for repetitive fed-batch process. At optimal process conditions molar yield of 1.24 mol pyruvate/mol glucose and *STY* higher than 110 g dm⁻³ d⁻¹ were achieved.

To separate pyruvate from fermentation broth fully integrated continuous process has been developed. In this process electro-dialysis was used as a separation unit. Under optimum conditions final (calculated) pyruvate titers higher than 900 mmol dm⁻³ (79 g dm⁻³) were achieved. Additionally, unstructured model for the bioconversion of glucose to pyruvate, as well as model of the electrodialysis process were developed, process parameters were estimated and both models were validated.

Key words: process development, *Escherichia coli*, pyruvate, modeling, *in situ* product recovery

Table of Contents

1. INTRODUCTION.....	1
2. THEORETICAL BACKGROUND.....	5
2.1 Biological background.....	5
2.1.1 Glucose Transport System in <i>Escherichia coli</i>	6
2.1.2 Glycolysis.....	7
2.1.3 Acetate Transport in <i>Escherichia coli</i>	8
2.1.4 The Tricarboxylic Acid Cycle (TCA).....	9
2.2 Bioreactor Concepts.....	11
2.2.1 Mass Balances in the Batch Process.....	12
2.2.2 Mass Balances in the Fed-Batch Process.....	14
2.2.3 Mass Balances in the Continuous Process with Cell Retention.....	15
2.3 Electrodialysis.....	16
2.3.1 Stack Configuration.....	16
2.3.2 Ion Exchange Membranes.....	18
2.3.2 Mass Transfer in Electrodialysis.....	19
3. MATERIALS AND METHODS.....	23
3.1 Biological System.....	23
3.1.1 Strain Storage and Precultivation.....	24
3.2 Medium Composition.....	24
3.2.1 LB-medium.....	24
3.2.2 Synthetic Medium for Preculture.....	24
3.2.3 Synthetic Medium for Fed-batch Fermentation.....	25
3.2.4 Synthetic Medium for Continuous Fermentation.....	25
3.2.5 Trace Elements Solution.....	25
3.2.6 Feed Mediums.....	26
3.2.7 Base.....	26
3.2.8 Antifoam.....	26
3.2.9 Buffer for On-line Measurement of Glucose.....	26
3.2.10 Electrode Rinse Solution.....	27
3.2.11 Solutions for Enzymatic Measurement of Glucose.....	27

3.3 Off-line Analysis	27
3.3.1 Optical Density.....	27
3.3.2 Biomass Dry Weight	27
3.3.3 Glucose.....	28
3.3.3.1 Determination of Glucose by Biosensor Appliance Accutrend®	28
3.3.3.2 Enzymatic Determination of Glucose.....	28
3.3.4 High Performance Liquid Chromatography (HPLC).....	29
3.3.4.1 HPLC for Organic Acids.....	29
3.3.4.2 HPLC for Amino Acids.....	30
3.3.5 Intra-Cellular Pyruvate Concentration	30
3.4 On-Line Analysis	31
3.4.1 pH.....	31
3.4.2 Dissolved Oxygen Concentration	31
3.4.3 Pressure, Temperature, Aeration.....	31
3.4.4 CO ₂ and O ₂ in Exhaust Gas.....	32
3.4.5 Glucose.....	32
3.5 Cultivation.....	35
3.5.1 Fed-Batch Process	35
3.5.2 Repetitive Fed-Batch Process	37
3.5.3 Continuous Process with Cell Retention.....	39
3.5.4 Fully Integrated Continuous Process	39
3.6 Electrodialysis.....	42
3.6.1 Stack Configuration.....	42
3.6.2 ED Operations	43
3.7 Data Acquisition and Process Control	45
3.7.1 Closed-Loop Glucose Control System.....	45
3.7.2 Open-Loop Acetate Control System	47
3.8 Unstructured Model for the Bioconversion of Glucose to Pyruvate	49
3.8.1 Model Theory.....	49
3.8.2 Kinetic Equations	49
3.8.2.1 Simplified Cybernetic Model – Model 1.....	49
3.8.2.2 Multiple-substrate Monod Kinetics – Model 2.....	51
3.8.2.3 Multiple-substrate Monod Kinetics with Variable $Y_{P/G}$ – Model 3.....	52
3.8.3 Mass Balances	53

3.9 Mathematical Model of the Electrodialysis Process	53
3.10 Data Handling.....	54
4. RESULTS AND DISCUSSION.....	55
4.1 Preliminary Investigations	55
4.1.1 Shake Flasks Experiments.....	55
4.1.2 Batch Experiment with Acetate Pulses	57
4.1.3 Fed-batch Experiment	58
4.2 Controlled Fed-batch Process	59
4.2.1 Fed-batch Fermentation of <i>E. coli</i> YYC202	59
4.2.2 Fed-batch Fermentation of <i>E. coli</i> YYC202 <i>ldhA::Kan</i>	61
4.3 Continuous Fermentation with Cell Retention.....	65
4.4 Repetitive Fed-batch	68
4.5 Electrodialysis.....	71
4.5.1 Effect of Current on the Performance of Electrodialysis	71
4.5.2 Effect of Medium Components on the Performance of Electrodialysis.....	73
4.5.3 Iona and Water Transport Modeling in Electrodialysis	75
4.6 <i>In situ</i> Product Recovery (ISPR) Approach with Fully Integrated Electrodialysis	77
4.7 Unstructured Model for the Bioconversion of Glucose to Pyruvate	80
4.7.1 Data Generation.....	80
4.7.2 Estimation of Parameters	83
4.7.3 Validation of the Model	91
5. CONCLUSIONS.....	97
6. LITERATURE	99
7. APPENDIX	109
7.1 List of Symbols	109
7.1.1 List of Abbreviations.....	110
7.1.2 Subscripts	111
7.2 List of Chemicals and Enzymes	112
7.3 List of Equipments	113
7.4 HPLC and LC-MS Parameters.....	114

7.4.1 HPLC for Organic Acids.....	114
7.4.2 HPLC for Amino Acids.....	115
7.4.3 LC-MS.....	115
7.4.4 HPLC Chromatograms.....	116
7.5 Ecological Validation of the Process.....	118
7.6 Economical Validation of the Process	119

CV

Bibliography

1. INTRODUCTION

The commercial demand for pyruvic acid has increased greatly in past decades owing to its various applications, apart from the fact that it plays a central role in energy metabolism in living organisms. Industrially, it is used mainly as a starting material in the biosynthesis of pharmaceuticals such as L-tryptophan, L-tyrosine and alanine, as well as L-dihydroxyphenyl alanine (L-DOPA) by known methods¹⁻⁷. It is also widely used in agrochemical industries in the production of crop protection agents, polymers, cosmetics and food additives⁸. Furthermore calcium pyruvate has a strong effect in reducing fat because it can accelerate the metabolism of fatty acids in the human body^{9,10}. It improves exercise endurance capacity¹¹, serves as a potent antioxidant¹², reduces anoxic injury and free radical formation¹³ and prevents neuronal degeneration associated with ischemia¹⁴.

Due to the importance and the great demand of pyruvate, different processes for the production of pyruvic acid have been developed in the past. They include both, the classical chemical method (pyrolysis) and biotechnological methods.

Pyruvic acid is produced in an industrial scale by the classical method including dehydration and decarboxylation of tartaric acid at 220 °C in the presence of KHSO₄. The crude acid obtained is then distilled under vacuum¹⁵. Also, dehydrations of ethylene glycol¹⁶, bitartratic salts¹⁷, diethyl tartrate¹⁸ and oxidations of lactic acid^{19,20}, propylene glycol^{20,21}, hydroxyacetone²², are common methods for production of pyruvate. All described processes are energy-intensive, environmental incompatible and not cost-effective⁸, therefore, in last two decades, development of environmental friendly and sustainable bioproduction pyruvate processes was intensified. There are basically three methods for biotechnological production of pyruvate⁸:

- the enzymatic methods; pyruvate is produced from D-(-)lactate by the use of permeabilized cells of methylotrophic yeast's *Hansenula polymorpha* or *Pichia pastoris*^{23,24} and cell free oxidation of lactate to pyruvate by the use of immobilized (S)-hydroxyacid-oxidase and catalase²⁵. By both methods high yields and reaction rates were achieved
- the resting cell methods; pyruvate is produced from substrate (1,2-propanediol, fumarate, R-lactate, citrus peel extract) by cells separated from growth medium^{26-31,7}. The main advantage of this method is that the culture time can be reduced
- direct fermentation methods; pyruvate is produced mainly from glucose through glycolysis. By the use of a multi-auxotrophic yeast *Torulopsis glabrata*^{8,33-40} fed-batch

fermentation with the successive addition of glucose resulted in the maximum accumulation of 67 g dm^{-3} of pyruvate in 63 h (yield $0.98 \text{ mol pyruvate/mol glucose}$)³⁶. Similar process using *Escherichia coli TBLA-1*, characteristic lipolic acid auxotrophy *FI-ATPase* deficient^{6,41-43}, with a glucose as carbon source for 24 hours gave 30 g dm^{-3} pyruvate⁴¹. Some other microorganisms are capable to produce pyruvate from glucose, e. g. *Schizophyllum commune*⁴⁴, *Photobacterium mandapamensis*⁴⁵, *Escherichia coli* 518^{46,113}. Except glucose many microorganisms use propane-1,2-diol⁴⁷, glycogen⁴⁸, citrus peel extract⁴⁹, lactic acid⁵⁰, or gluconate^{51,52} as a sole carbon source to accumulate pyruvate but in those fermentation final pyruvate titers are too low to conduct a cost-effective downstream process.

Although the above-mentioned approaches are promising, they have some inherent disadvantages as follows: (i) The maximum theoretical yield of lactate-based pyruvate production is 1 mol mol^{-1} , whereas 2 mol mol^{-1} could be produced theoretically using a C6-molecule like glucose. (ii) Current large-scale market prices of lactate (about 1.5 € kg^{-1}) are approximately five times higher than glucose prices (0.3 € kg^{-1}), not taking into account advantages in atom-economy, as mentioned previously (see (i)). (iii) Following the route of enzymatic synthesis, hydrogen peroxide may be produced, which leads to an unwanted pyruvate decomposition to acetate, carbon dioxide and water, and finally lowers the production yield. (iv) Often, the above-mentioned methods only achieve low titers (about 30 g dm^{-3}), which make the total process development unattractive for an industrial scale-up because of high downstream costs for pyruvate recovery. (v) In the case of the resting cell approach, an expensive multiple step procedure including biomass concentration together with costly waste-water removal is proposed.

In summary, microbial pyruvate production, based on C6 sources like glucose, offers the most promising approach for cost-efficient process development. Among the processes published so far, the approach of Miyata and Yonehara³⁶ achieved the highest titer of 69 g dm^{-3} together with the highest pyruvate/glucose yield of 0.636 g g^{-1} thus offering the best possibilities for further downstream processing. However, the space-time yield of this process was very low ($1.24 \text{ g dm}^{-3} \text{ h}^{-1}$), which significantly hampers its use for scale-up purposes. Thus it is the aim of this study to present an alternative approach that combines high product titers with high pyruvate/substrate yields and also with much higher space-time yields to enable economical process development.

Pyruvate process development therefore started by using the recombinant strain *Escherichia coli* YYC202, which is completely blocked in its ability to convert pyruvate into

acetyl-CoA or acetate. Consequently, acetate is required for growth on glucose minimal medium. Under acetate-limited conditions (non-growing cells) in shake flask experiments at low glucose concentration, a maximum yield of $1.7 \text{ mol}_{\text{pyruvate}}/\text{mol}_{\text{glucose}}$ was achieved⁵³⁻⁵⁴, which could be increased up to $1.9 \text{ mol}_{\text{pyruvate}}/\text{mol}_{\text{glucose}}$ using resuspended cells in buffer. These high yields were not obtained during the growth phase, when glucose is used for biomass production to a significant extent.

Hence, process development had to find an optimal way between highly selective pyruvate formation and necessary biomass production – both at high reaction rates to maximize final space-time yield. It was assumed that acetate represents a key fermentation variable. Therefore, the correlation between acetate consumption rate (*ACR*) and CO₂ production rate (*CTR*) was a matter of detailed analysis to enable an optimal on-line process control via exhaust gas analysis. Additionally, glucose concentrations were controlled on-line. By controlling acetate and glucose feeds, a series of lab-scale fed-batch experiments were performed, which finally lead to an optimized fed-batch process. Furthermore, basic metabolome studies were performed to investigate potential mechanistic limitations of pyruvate-producing strains.

Besides the production process also the product recovery must be taken into account – not only because of its usually high contribution to the total process costs but also on account of the necessity to integrate it on-line into the production process when the product is inhibitory. In the case of pyruvate, some hints were published that high extra-cellular pyruvate concentrations $> 500 \text{ mmol dm}^{-3}$ might cause a significant inhibition of microbial pyruvate synthesis^{40,55}. Hence, pyruvate process development should consider strategies to separate the product and to purify it as well.

Ion exchange and solvent extraction followed by distillation are common methods for pyruvate separation from cell-free fermentation broth⁸. However, the low exchange capacity of resins and the use of concentrated acids as eluents makes the application of ion-exchange for pyruvate isolation very difficult and not attractive in terms of sustainable process development as well as in commercial retrospect.

However, the charge-dependent ion-separation in the electric field of electrodialysis⁵⁶ is regarded as a promising approach for the downstream processing of organic acids from fermentation broth⁵⁷. It has been widely applied for production of table salts, organic acids, amino acids and sugar demineralization as well as for blood treatment and wine stabilization and it represents one of the most important membrane processes for environmentally clean technology in biochemical industries⁵⁸⁻⁶³.

Motivated by the working hypothesis that high extra-cellular pyruvate concentrations might be inhibitory, it was thus the aim of our study to develop a pyruvate production process with integrated product separation using the formerly described production strain *Escherichia coli* YYC202 *ldhA::Kan*⁵⁵. Experimental results of a repetitive fed-batch process, continuous process with cell retention and an *in situ* product recovery (ISPR) approach with fully integrated three-compartment electro dialysis are presented.

A simple unstructured mathematical model for the production of pyruvate from glucose by *Escherichia coli* was developed. The kinetic parameters were developed and the model was able to simulate quite well the dynamic behavior of the batch fermentation. Additionally, mathematical model to represent the ion and water transport behavior of an electro dialysis process for concentrating pyruvic acid under the influence of different current density was developed.

2. THEORETICAL BACKGROUND

2.1 Biological Background

Escherichia coli is a gram negative, facultative, non-sporing procaryotic anaerobe of the *Enterobacteriaceae* family. It is a motile organism that colonies the lower gut of animals. *Escherichia coli* was first described through isolation in the faces of children by the Austrian pediatrician Theodor Escherich in 1885 as "*Bacterium coli comunale*"⁶⁴. These rod-shaped bacteria range in size from 1.0 – 4.0 μm (Figure 2.1).

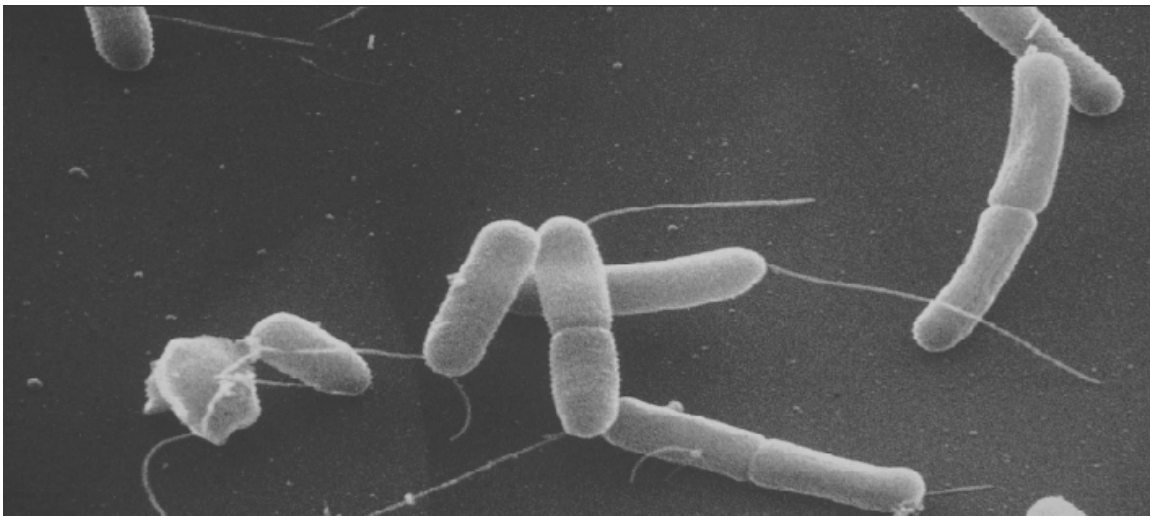


Figure 2.1 *Escherichia coli* cells⁶⁵

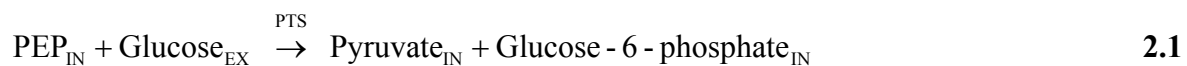
The metabolism is aerobic (oxygen-respiration) or facultative anaerobic (fermentation, nitrate-respiration). In a reach medium under optimal condition, the generation time is 20 minutes at a temperature of 37 °C and a pH between 6.5 and 7.3^{2,2}. Because of its extraordinary position as a preferred model in biochemical genetics, molecular biology and biotechnology, *Escherichia coli* cells

- have a completely sequenced genome as in the case of *Escherichia coli* K12 with 4,639,221 base pair sequence⁶⁶;
- are easy to handle in the laboratory because of their rapid growth rate and simple nutrient requirements, which can be met with a minimal medium;
- are successfully used in industrial production process for the production of recombinant proteins and fine chemicals e. g. for insulin, interferon, enzymes such as asparaginase and penicillin acylase, amino acids, vitamins, and nucleotides⁶⁷;

- are prokaryotes and as a result are normally considered by scientists to be simple organisms having a relatively simple structure;
- have been widely analyzed genetically and microbiologically by many research groups and used for many decades around the world, making *Escherichia coli* an organism with the largest available knowledge⁶⁶;
- are used in research purposes for the control of metabolic fluxes⁶⁸.

2.1.1 Glucose Transport System in *Escherichia coli*

The transport of substrates into the cell through the cytoplasmic membrane is catalyzed by a variety of specific transport systems. Most bacteria can also be adapted to their continuously changing surroundings in order to effectively compete with other organisms for limiting nutrients. The substrates are usually in form of sugars e.g. glucose, fructose, mannose etc⁶⁵. *E. coli* uses glucose as energy and carbon source. The glucose uptake system in *E. coli* is achieved through the phosphoenolpyruvate (PEP) – dependent phosphotransferase systems (PTSs). There are about 16 phosphotransferase systems known up until now in *E. coli*, which are not only responsible for the transport and phosphorylation of substrate in cells but also in the movement of cells towards the carbon sources, and in the regulation of a number of metabolic pathways. The overall process of the PTS catalyzed reaction for glucose is as follows:



Glucose phosphorylation is coupled to its translocation across the cytoplasmic membrane, the energy for these processes being provided by the "energy-rich" glycolytic intermediate PEP.

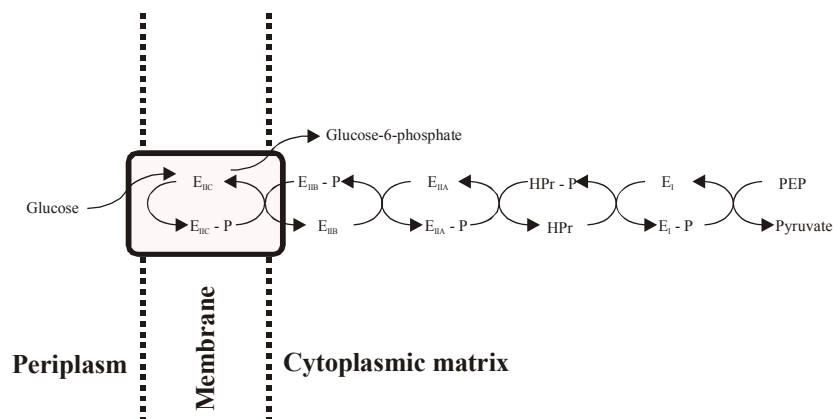


Figure 2.2 PEP-dependent phosphotransferase system for glucose

The phosphate group is transferred from PEP to the sugar via obligatory phospho intermediates of, HPr, E_{IIA}, and E_{IIB}. Enzyme I (E_I) and histidine protein (HPr) are soluble cytoplasmic non-sugar specific proteins that are generally called PTS proteins. The E_{IIS} are sugar specific and consist of three domains (A, B, C). Enzyme IIA (E_{IIA}) contains the first phosphorylation site (P-His), and enzyme IIB (E_{IIB}) contains the second phosphorylation site (either a Cys or a His residue). Enzyme IIC (E_{IIC}) has the membrane-bound hydrophobic domain and contains the sugar binding site (Figure 2.2). In glucose PTS of *E. coli*, the phosphate group from PEP is not directly transferred onto the sugar but through the soluble E_I and HPr to the first phosphorylation site of E_{IIA}, which in turn transfers the phosphate group to the phosphorylation site of E_{IIB}. The E_{IIB} domain transfers the phosphate group from E_{IIA} onto the sugar, which already binds to the sugar binding site of the membrane bound E_{IIC}.

The glucose taken up by the cells (under aerobic conditions) is catabolised to 70 % through the glycolytic pathway and to approximately 30 % through the pentose phosphate (phosphogluconate) pathway (PPP). The 2-keto-3-deoxy-6-phosphogluconate pathway plays a minimum role⁶⁹.

The pentose phosphate pathway generates essential pentose intermediates, particularly riboses which are used in the biosynthesis of nucleic acid, and also in the production of NADPH which is a carrier of chemical energy in the form of reducing power needed for the biosynthesis of fatty acids⁷⁰. The catabolism of glucose through the glycolytic pathway (Figure 2.3) under aerobic condition leads to the tricarboxylic acid (TCA) cycle (Figure 2.5).

2.1.2 Glycolysis

The glycolytic or Embden-Meyerhof pathway is the most common pathway for glucose degradation to pyruvate in the stage two of catabolism. It is found in all major groups of microorganisms and functions in the presence or absence of oxygen. Glycolysis (Greek *glyco*, sweet, and *lysis*, a loosening) is located in the cytoplasmic matrix when present in eucaryotic microorganisms.

The glycolytic pathway degrades one glucose to two pyruvates by the sequence of reactions (Figure 2.3)⁷¹. ATP and NADH are also produced. The yields of ATP and NADH may be calculated by considering the two stages separately. In the six-carbon stage two ATPs are used to form fructose-1,6-bisphosphate. For each glyceraldehyde 3-phosphate transformed into pyruvate, one NADH and two ATPs are formed. Because two glyceraldehyde 3-phosphates arise from a single glucose (one by way of dihydroxyacetone phosphate), the three-carbon stage generates four ATPs and two NADHs per glucose. Subtraction of the ATP

used in the six-carbon stage from that produced in the three-carbon stage gives a net yield of two ATPs per glucose.

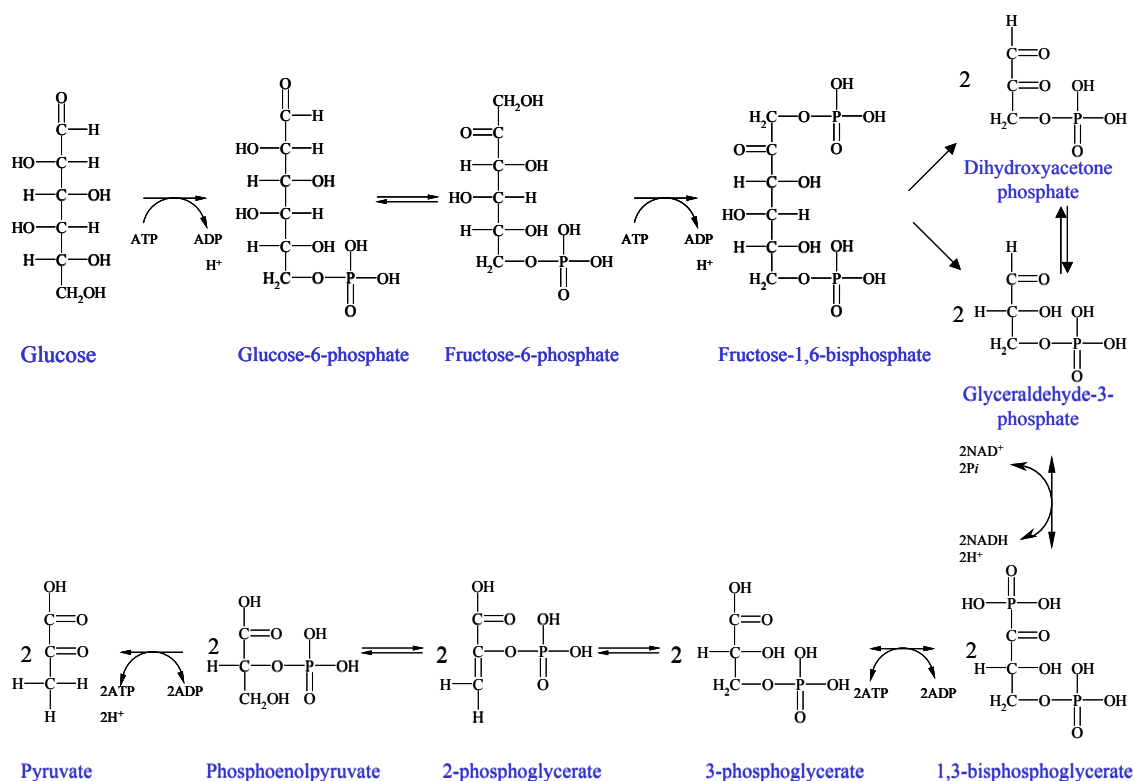
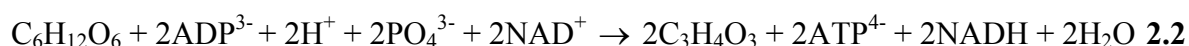


Figure 2.3 The glycolytic pathway for the breakdown of glucose to pyruvate

Thus the catabolism of glucose to pyruvate in glycolysis can be represented by the following overall equation:



2.1.3 Acetate Transport in *Escherichia coli*

Experiments with vesicles of *E. coli* membrane have provided evidence that specific transport system for acetate does not exist in this organism⁷². The strong inhibitory effect of acetate on bacterial growth has been linked to collapse of the trans-membrane pH gradient. This finding, along with a study of the independence of growth inhibition on acetate concentration, has provided support for the long-held view that acetic acid is one of a group of weak acids, called uncoupling agents, that catalytically dissipate the proton-motive force, Δp (defined as the proton electrochemical potential difference across the cytoplasmic membrane; Figure 2.4 illustrates the mechanism of dissipation).

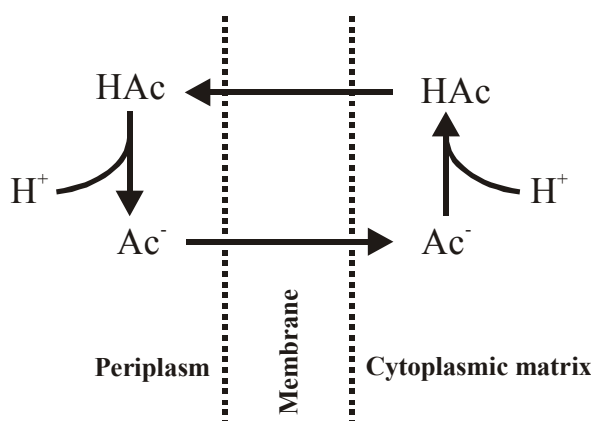
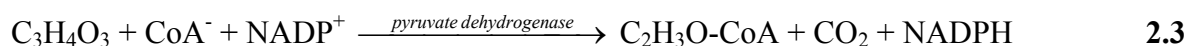


Figure 2.4 Generally accepted mechanism of uncoupling by acetic acid. HAc represents the un-dissociated acetic acid

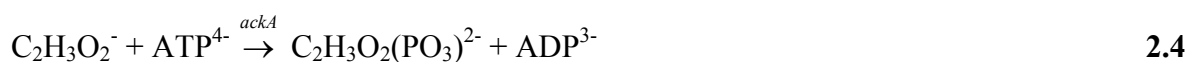
However, acetate transport is generally thought to occur by simple diffusion through bi-layer because transport-deficient mutants have not been isolated and because the saturation behavior typical of protein-dependent transport has not been observed⁷³.

2.1.4 The Tricarboxylic Acid (TCA) Cycle

Although some energy is obtained from the breakdown of glucose to pyruvate by the pathways previously described, much more is released when pyruvate is degraded aerobically to CO₂ in the TCA cycle. The multi-enzyme system called the pyruvate dehydrogenase complex first oxidizes pyruvate to form CO₂ and acetyl coenzyme A (Ac-CoA, C₂H₃O-CoA), an energy-rich molecule composed of coenzyme A (CoA) and acetic acid joined by a high-energy thiol ester bond (Equation 2.3).

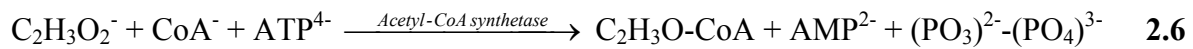


Also, Ac-CoA arises from the catabolism of acetate. There are basically two mechanisms for the conversion of acetate into Ac-CoA in *E. coli*. Acetate might be converted by acetate kinase (*ackA*) phosphorylates to acetyl phosphate (Equation 2.4) and phosphotransacetylase (*pta*) transfers the acetyl moiety from acetyl phosphate to CoA to form Ac-CoA (Equation 2.5).



These two enzymes might vary in amount due to different carbon sources, and they are neither induced by acetate or catabolite repressed by glucose.

Apart from the above mention process, acetate is converted by Ac-CoA synthetase, which is an enzyme lacking in glucose grown cells (glucose repressed). Ac-CoA synthetase ligates acetate and CoA in the presence of ATP to form Ac-CoA (Equation 2.6).



The substrate for the tricarboxylic acid (TCA) cycle, citric acid cycle, or Krebs cycle is Ac-CoA. In the first reaction Ac-CoA is condensed with a four-carbon intermediate, oxaloacetate, to form citrate and to begin the six-carbon stage.

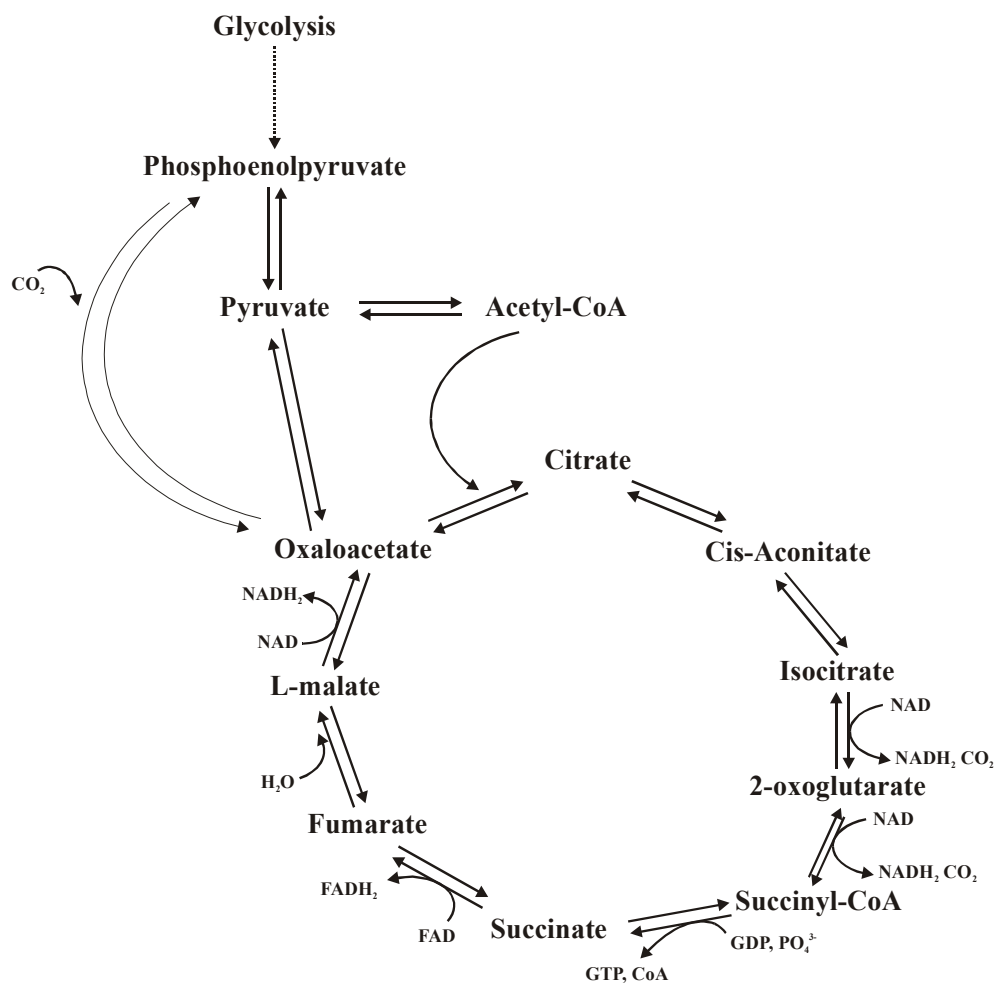


Figure 2.5 The TCA cycle

Citrate (a tertiary alcohol) is rearranged to give iso-citrate, a more readily oxidized secondary alcohol. Iso-citrate is subsequently oxidized and decarboxylated twice to yield α -ketoglutarate, then succinyl-CoA. At this point two NADHs are formed and two carbons were added as acetyl-CoA at the start, balance is maintained and no net carbon is lost. The cycle

now enters the four carbon stage during which two oxidation steps yield one FADH_2 and one NADH per acetyl-CoA. In addition, GTP (a high energy molecule equivalent to ATP) is produced from succinyl-CoA by substrate level phosphorylation. Eventually oxaloacetate is reformed and ready to join with another acetyl-CoA. Figure 2.5 shows that the TCA cycle generates two CO_2 , three NADH , one FADH_2 , and one GTP for each acetyl-CoA molecule oxidized.

The TCA cycle appears to be functional in many aerobic bacteria, free-living protozoa, and most algae and fungi. However, the facultative anaerobe *E. coli* does not use the complete TCA cycle under anaerobic conditions or when the glucose concentration is high but does at other times.

2.2 Bioreactor Concepts

Bioreactors are used for the production of biomass, for the production of bioproducts by microorganisms or by mammalian cells, and for biotransformation of products by cells or enzymes. A bioreactor has to be optimized for mass transfer, heat transfer, power consumption, product yield and product quality. The optimal type, size and instrumentation of a bioreactor for an industrial production are finally determined by economic parameters, e.g. by the production costs of the product. Bioreactors can be classified as stirred-tank reactors, bubble-column reactors, loop reactors and fixed-bed reactors⁷⁴⁻⁷⁶.

The basic bioreactor concepts of stirred-tank reactors, i.e., the batch, the fed-batch and the continuous flow stirred-tank reactors (CSTR), together with the mass balances will be described in this section.

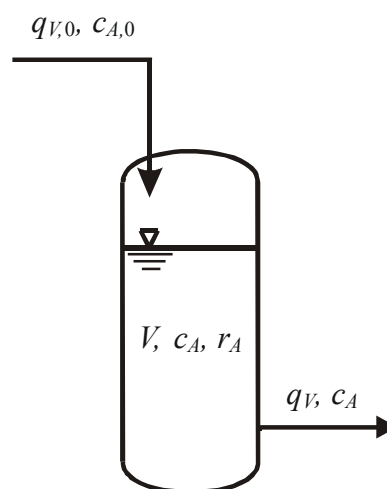


Figure 2.6 The mass balance over the bioreactor. Accumulation = IN – OUT + Production

In order to describe bioreactors concepts and macro-kinetic behaviors in bioreactors a mass balance over the bioreactor should be drawn up (Figure 2.6, Equation 2.7)⁷⁶. The accumulation of a compound A in the reactor, with the concentration c_A , is equal to the amount of A that comes in, minus the amount that goes out, and augmented by the amount that is produced:

$$\frac{d(V \cdot c_A)}{dt} = q_{V,0} \cdot c_{A,0} - q_V \cdot c_A + r_A \cdot V \quad 2.7$$

where V is the liquid volume in the bioreactor, respectively, t is time, $q_{V,0}$ and q_V the volumetric flow of the in and outgoing stream, respectively, and r_A the production rate per unit volume. The subscripts 0 refer to the concentration and volumetric flow of influent.

2.2.1 Mass Balances in the Batch Process

The most-prominent characteristic of the batch reactor is the fact that there are not in- and outgoing flow (Figure 2.7).

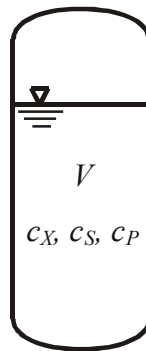


Figure 2.7 The batch reactor. Accumulation = Production

This means that all that is produced is accumulated. The mass balance (Equation 2.7) thus simplifies to assuming ideal mixing:

$$\frac{d(V \cdot c_A)}{dt} = r_A \cdot V \quad 2.8$$

When the volume V remains constant, Equation 2.8 further simplifies to:

$$\frac{dc_A}{dt} = r_A \quad 2.9$$

The Equation 2.10 describes mass balances equation for biomass in the batch bioreactor of complete mixing:

$$\frac{dc_X}{dt} = \mu \cdot c_X \quad 2.10$$

where c_X is biomass concentration and μ is specific growth rate. To express μ , and to relate it with substrate concentration, c_S , Monod's empirical equation (Equation 2.11) has been commonly used:

$$\mu = \mu_{MAX} \cdot \frac{c_S}{K_S + c_S} \quad 2.11$$

where μ_{MAX} is maximum specific growth rate achievable when $c_S \gg K_S$ and the concentration of all other essential nutrients is unchanged, and K_S is Monod constant. The Monod equation consequently may break down if growth is rapid, or if specific growth rate is inhibited by medium constituents such as substrate or product. Additionally, it has often been observed that below some low threshold value of substrate, cells do not proliferate and/or the desired product does not appear in the fermentation. This phenomenon may be due to a maintenance process wherein the cell must consume substrate at a small but finite rate just to survive. The general form of the specific growth rate including maintenance, m , is

$$\mu = \mu_{MAX} \cdot \frac{c_S}{K_S + c_S} - m \quad 2.12$$

Additionally, mass balances for substrate (Equation 2.13) and product (Equation 2.14) in the batch process assuming ideal mixing and constant volume, if substrate is used for both, biomass and product formation, are given as:

$$\frac{dc_S}{dt} = -\frac{1}{Y_{X/S}} r_X - Y_{P/S} \cdot r_S \cdot c_X \quad 2.13$$

$$\frac{dc_P}{dt} = Y_{P/S} \cdot r_S \cdot c_X \quad 2.14$$

where $Y_{X/S}$ is molar yield biomass/substrate, $Y_{P/S}$ is molar yield product/substrate, r_X is the rate of biomass formation (Equation 2.10), and r_S is the rate of substrate consumption. The rate of substrate consumption (product formation) for a simple kinetic is described by Michaelis-Menten equation (Equation 2.15) and is given as:

$$r_S = v_{MAX} \cdot \frac{c_S}{K_m + c_S} \quad 2.15$$

where v_{MAX} is maximum rate of reaction, and K_m Michaelis-Menten constant. Michaelis-Menten equation is analogous to Monod equation, but this one has been derived theoretically. Often, even an apparent single-step enzyme system does not follow Michaelis-Menten behavior. Two common types of inhibition, those occur in the systems and break down the

Michaelis-Menten equation, are competitive or substrate analog inhibition, and reversible noncompetitive inhibition.

2.2.2 Mass Balances in the Fed-Batch Process

A fed-batch culture is a batch culture, which is fed continuously, or sequentially, with medium, without the removal of culture fluid, except for normal sampling. Thus, the volume of the culture increases with time. The systematic feeding is done in order to add precursors for desired products, or to add regulating compounds such as inducers at a desired point in the batch operation, to maintain low nutrient levels to minimize catabolite repression, or to extend the stationary phase by nutrient addition to obtain additional product.

Fed-batch cultivation is a useful technique not only for cultivation of microorganisms showing substrate inhibition or catabolite expression, but also for achieving high biomass densities within short cultivation time. For feeding nutrients into the bioreactor, various techniques have been developed. Feeding techniques includes constant feeding, exponential feeding, and feeding with the respiratory quotient or pH as the control indicator as well as various other strategies⁷⁷.

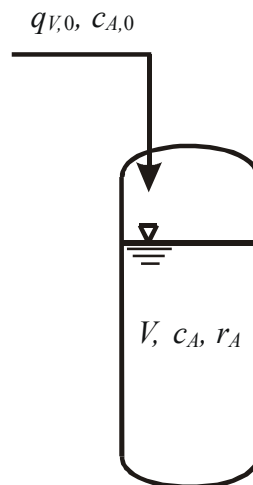


Figure 2.8 The fed-batch reactor. Accumulation = IN + Production

The distinguishing feature of the fed-batch reactor is that there is only an ingoing flow and no outgoing flow (Figure 2.8). Assuming ideal mixing Equation 2.7 thus becomes:

$$\frac{d(V \cdot c_A)}{dt} = q_{V,0} \cdot c_{A,0} + r_A \cdot V \quad 2.16$$

Application of the general mass balance equation for a fed-batch culture (Equation 2.16) on the biomass (Equation 2.17), limiting substrate (Equation 2.18) and product (Equation 2.19) results in the following mass balance equations:

$$\frac{1}{V} \frac{d(V \cdot c_X)}{dt} = \mu \cdot c_X \quad 2.17$$

$$\frac{1}{V} \frac{d(V \cdot c_S)}{dt} = \frac{q_{V,0}}{V} \cdot c_{S,0} - \frac{1}{Y} r_X - Y_{P/S} \cdot r_S \cdot c_X \quad 2.18$$

$$\frac{1}{V} \frac{d(V \cdot c_P)}{dt} = Y_{P/S} \cdot r_S \cdot c_X \quad 2.19$$

2.2.3 Mass Balances in the Continuous Process with Cell Retention

An interesting consideration is the case of single vessel with reuse and recycle of the microbial mass (Figure 2.9).

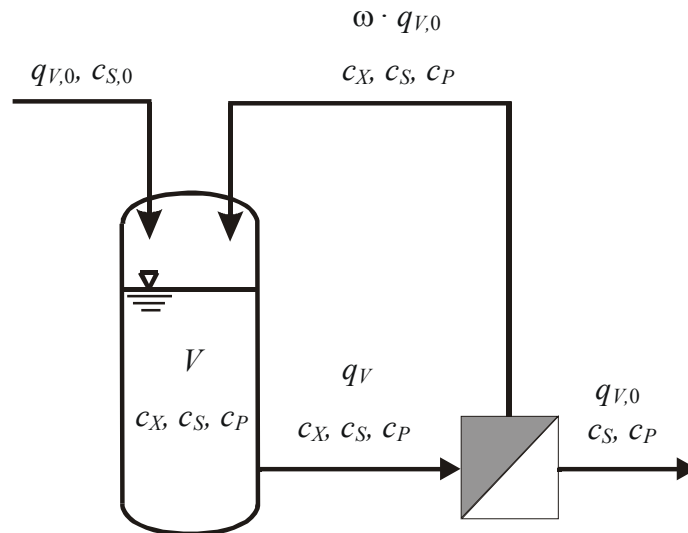


Figure 2.9 The continuous reactor with recycling

It is evident from the figure that

$$q_V = (1 + \omega) \cdot q_{V,0} \quad 2.20$$

$$q_{V,0} = q_{V,P} \quad 2.21$$

where q_V is volumetric flow rate of the cell suspension from reactor, $q_{V,0}$ is volumetric flow rate of the fresh medium, $q_{V,P}$ is volumetric flow rate of cell free fermentation solution, and ω is recycle ratio. Mass balances equation for biomass in the reactor of complete mixing in Figure 2.9 is (if fresh medium stream to a continuous culture consist only of sterile nutrient):

$$V \cdot \frac{dc_X}{dt} = c_X \cdot \omega \cdot q_{V,0} - c_X \cdot q_V + V \cdot r_X \quad 2.22$$

where c_X is biomass concentration in reactor, and r_X is rate of biomass formation. At the steady-state:

$$\frac{1}{c_X} \cdot r_X = \frac{q_V}{V} - \frac{\omega \cdot q_{V,0}}{V} \quad 2.23$$

From Equations 2.20 and 2.23,

$$\mu = (1 + \omega) \cdot D - \omega \cdot D = D \quad 2.24$$

provided

$$D = \frac{q_{V,0}}{V}, \quad 2.25$$

$$\mu = \frac{1}{c_X} \cdot r_X \quad 2.26$$

where D is dilution rate (equal to the number of tank volumes which pass through the vessel per unit time). Additionally, mass balances for substrate (Equation 2.27) and product (Equation 2.28) in the reactor of complete mixing with recycling in the steady-state if substrate is used for both, biomass and product formation, are given as:

$$D(c_{S,0} - c_S) - \frac{1}{Y} r_X - Y_{P/S} \cdot r_S \cdot c_X = 0 \quad 2.27$$

$$-D \cdot c_P + Y_{P/S} \cdot r_S \cdot c_X = 0 \quad 2.28$$

2.3 Electrodialysis

The principal transport process that is used in electrodialysis is the migration of charged species in electric fields. The electrolyte and membranes are subjected to an electric field, and a transport of current by ionic conduction is induced. In the membrane that is dominated by migration, whereas in the electrolyte solution this transport is complemented by diffusion and convection processes⁷⁸⁻⁸³.

2.3.1 Stack Configuration

A unit cell from an electrodialysis (mono-polar electrodialysis) stack⁸¹ is shown in Figure 2.10. An anion selective membrane is placed facing the anode, while the cation selective membrane faces the cathode. The respective ions were forced through the membrane by the imposed electric field. Desalination takes place in the channel center where electroneutrality is present. In most applications, multiple anion and cation exchange

membranes are arranged in an alternating pattern between an anode and a cathode to form series of concentrating and diluting cells in the stack (between 5 and 500 cell pairs, typically more than 100).

Bi-polar membrane electro dialysis⁸¹ also referred to as water splitting electro dialysis, can convert aqueous salt solutions into acids and bases (see section 3.5.1). A water splitting stack is similar to a conventional (mono-polar) electro dialysis stack but incorporates a third type of membrane, the bi-polar membrane, which is composed of a cation and anion membrane layers laminated together.

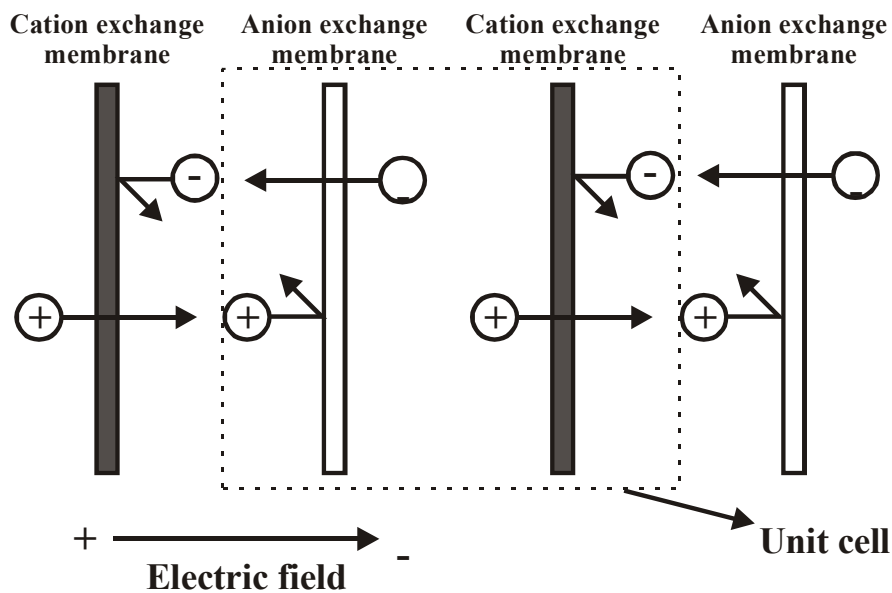


Figure 2.10 Principle of electro dialysis – the electric field forces the anions and cations to migrate in the opposite directions, while the cation and anion selective membranes restrict their movement through the different compartments

The performance of an electro dialysis process can be determined by calculating so called current efficiency (CE) of a given run. Current efficiency gives the efficiency of current utilization in transporting salts from the diluting stream to the concentrate stream. Current efficiency was calculated based on the following relation⁸¹:

$$CE = \frac{N \cdot F}{i} \quad 2.30$$

where i is the current density [$A \text{ m}^{-2}$], F is the Faraday's constant (96487 C mol^{-1}) and N is the mole flux [$\text{mol m}^{-2} \text{ s}^{-1}$]. The current density is calculated from the Equation 2.31, where I is current, and A [m^2] is the total effective area installed. The parameter N is calculated from the

Equation 2.32, where V [m³] is volume of concentrate solution, c_{Salt} [mol m⁻³] is the salt concentration in the concentrate solution and t is the time of operation.

$$i = \frac{I}{A} \quad 2.31$$

$$N = \frac{V}{A} \cdot \frac{dc_{Salt}}{dt} \quad 2.32$$

2.3.2 Ion Exchange Membranes

The membrane works through the principle of electro neutrality. In the membrane charged, ionic groups are attached at regular intervals along the polymer chains, which form the skeleton of the membranes (Figure 2.11). These groups are positively charge in anion selective membranes, which promote content with a high concentration of anions, while repelling cations. In addition, the structure and distribution of ionic groups can be engineered, for example, to allow higher concentrations of mono-ionic species, as opposed to species with greater charges. In this case this results in the selective transport of mono-ionic species, from a mono- and di-ionic containing electrolyte⁸⁰.

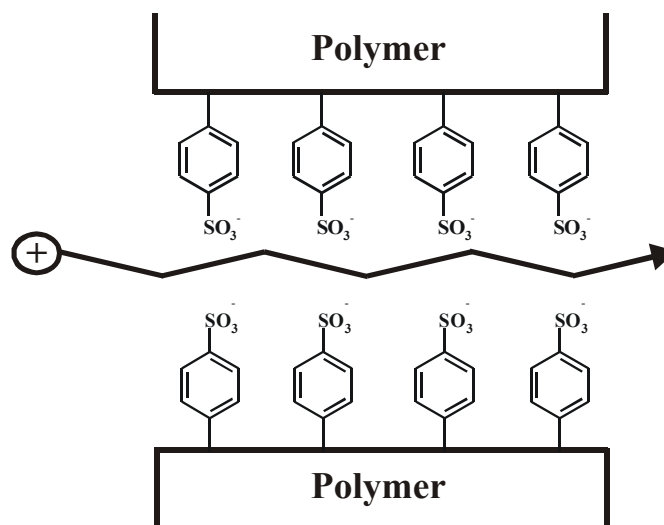


Figure 2.11 A typical cation exchange membrane

The most important characteristics of perm-selective membranes used for electrodialysis are low electrical resistance, good perm-selective qualities for cations and anions, good mechanical properties, good form stability, and high chemical stability. The use of electrodialysis is generally restricted to small ions because the electrochemical properties

of perm-selective membranes are changed upon their association with large ions. When these ions are present in the solution, the electrical conductivity and perm-selectivity of the membranes decreases. If large ions are transferred by an electrical current into perm-selective membranes, they may become blocked there, poisoning the membrane⁸⁴. Materials that cause fouling and poisoning can be classified into three categories:

- (1) organic anions, proteins, and microorganisms that are too large to penetrate the membrane and accumulate on its surface,
- (2) organic anions that are small enough to penetrate the membranes but whose electro-mobility is too low that they remain inside the membrane, causing considerable increase of resistance, and
- (3) organic anions that are smaller than those of category (2), but still cause a certain increase in electrical resistance of the membrane.

2.3.3 Mass Transfer in Electrodialysis^{78,79,82,85-89}

Mass transfer through membranes consists of two steps (Figure 2.12):

- (1) the reduction of salt concentration in the solution by electro-transport of ions from the boundary layer near the membrane, and
- (2) the diffusion of ions to the partially desalinated boundary layer.

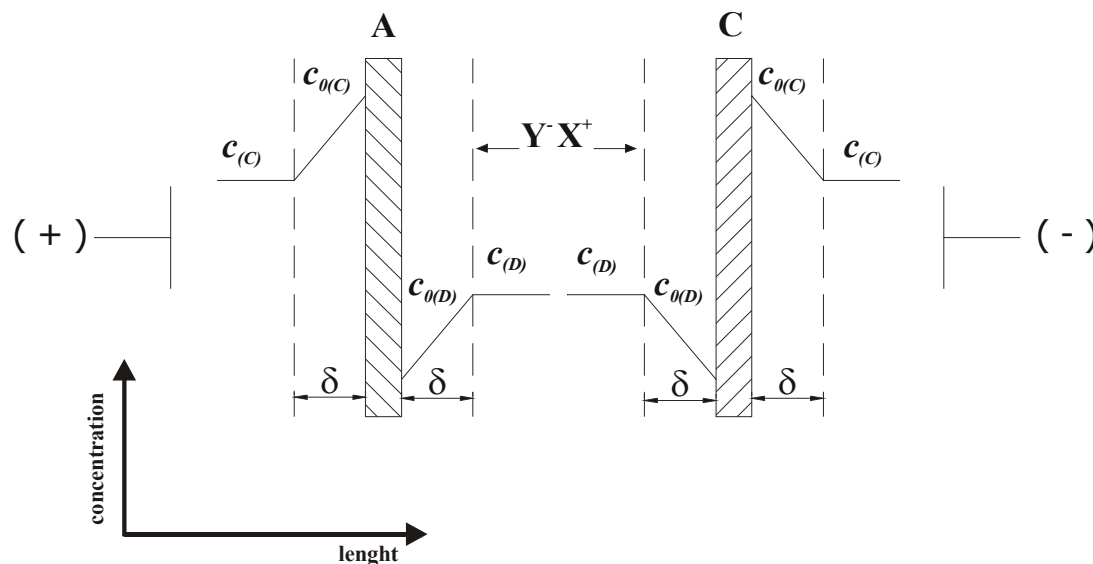


Figure 2.12 Mass transfer in electro-dialysis. A – anion exchange membrane; C – cation exchange membrane; c – concentration in the bulk, c_0 – concentration in the boundary layer near the membrane; (D) – the diluate stream of the electro-dialysis unit; (A) – the concentrate stream of the electro-dialysis unit⁸²

The kinetics of the first step is given by the Nernst equation:

$$N_E = \frac{(\bar{t}_m - t_s) \cdot i}{F} \quad 2.32$$

where N_E is the mole flux of ions by electro-transport, t_s the transport number in solution, and \bar{t}_m transport number in membrane. The second step is given by Fick's first law:

$$N_D = \frac{D \cdot (c - c_0)}{\delta} \quad 2.33$$

where N_D is mole flux of ions by diffusion, D the diffusion coefficient [$\text{m}^2 \text{s}^{-1}$], c the concentration of the solution, c_0 the concentration of the solution at the boundary layer, and δ the thickness of the boundary layer [m]. The thickness of the boundary layer is δ is a function of the linear velocity of the solution in the cell and the geometry of the spacer. Under steady-state conditions,

$$N_E = N_D \quad 2.34$$

From Equations 2.32 – 2.34, the following can be derived:

$$i = \frac{D \cdot F \cdot (c - c_0)}{\delta \cdot (\bar{t}_m - t_s)} \quad 2.35$$

Increasing the voltage of the stack raises the current density. The flux of ions by electro-transport is also increased until the concentration of the solution in the boundary layer approaches zero ($c_0 \cong 0$). Under these conditions the mole flux of ions by diffusion is maximal:

$$N_{D,max} = \frac{D \cdot c}{\delta} \quad 2.36$$

and

$$i_{max} = \frac{D \cdot F \cdot c}{\delta \cdot (\bar{t}_m - t_s)} \quad 2.37$$

A further increase of N_D can be achieved only by decreasing δ . This can be achieved by raising the linear velocity of the solution in the cell to a level at which the pressure drop across the cells will not cause internal leakage. When

$$N_E = N_{D,max} \quad 2.38$$

the ED unit is operating at the highest value of mass transfer. A further increase in the stack voltage will raise the current density. Most of this additional current, however, will cause dissociation of water rather than mass transfer from the diluate to the concentrate.

When the concentration of the solution in the boundary layers decreases, the electrical resistance of the cell pair increases. When the concentration in the boundary layers is low, the water dissociates, causing scaling and fouling on the anion-exchange membranes. Therefore, it is important that the current density be prevented from approaching the limiting current-density value.

Water transport through membranes from the diluate to the concentrate can occur in one of the two ways⁸²:

- (1) by the transport of water molecules together with ions through the membranes – the flux is proportional to the electric current and is called electroosmosis, or
- (2) by osmosis caused by difference in concentration across the membrane.

$$q_{V,W} = \frac{t_w \cdot V_M \cdot i \cdot A}{F} + J_w \quad \mathbf{2.39}$$

where, $q_{V,W}$ is the water flow rate through a membrane, t_w is the transport number of water, V_M is the water molar volume and J_w is the osmotic water transport. Usually, both ion diffusion and osmotic water transfer are negligible with respect to other fluxes⁷⁹ (in particular, that is true for the commercial membranes).

3. MATERIALS AND METHODS

3.1 Biological System

The strains used were *Escherichia coli* YYC202 and *Escherichia coli* YYC202 *ldhA::Kan* constructed in Institute of Biotechnology 2, Forschungszentrum Juelich⁵³⁻⁵⁵. Both strains are completely blocked in their ability to convert pyruvate into acetyl-CoA, phosphoenolpyruvate (PEP) or acetate, which was realized by the complete chromosomal deletion of genes coding for pyruvate dehydrogenase (*aceEF*), pyruvate formate lyase (*pflB*), pyruvate oxidase (*poxB*) and PEP synthetase (*pps*). Thus, the strains were acetate auxotrophic (Figure 3.1). In the strain *Escherichia coli* YYC202 *ldhA::Kan*, the lactate dehydrogenase (*ldhA*), responsible for the conversion of pyruvate into lactate, is inactivated. The *ldhA* mutation was performed by P1 vir transduction⁹⁰ using *Escherichia coli* NZN117⁹¹ as a donor.

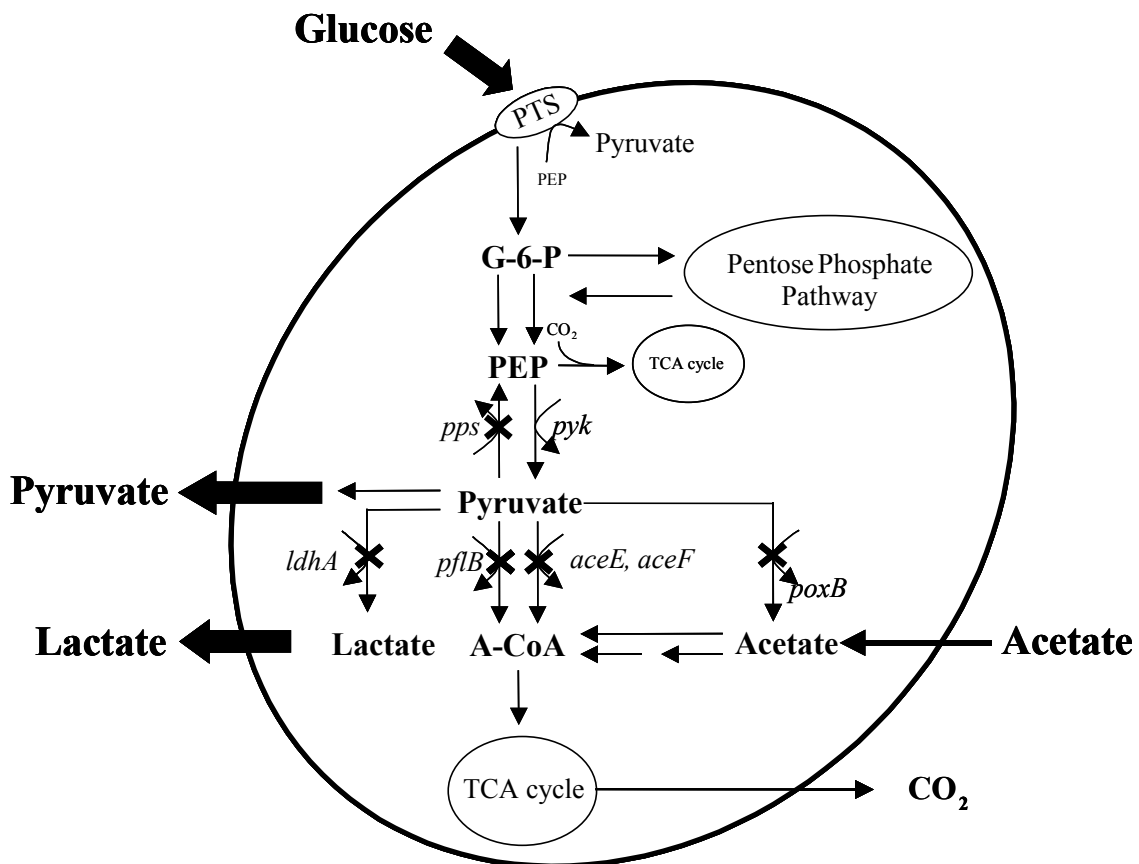


Figure 3.1 Metabolism of glucose and pyruvate in *Escherichia coli* YYC202 *ldhA::Kan*

3.1.1 Strain Storage and Precultivation

For the preparation of cryoculture 1L flask containing 100 cm³ of Luria-Bertani (LB) medium (section 3.2.1) was inoculated from agar plate culture. Flask was incubated in the rotation shaker (3033, GFL GmbH) at 37 °C and 150 rpm for 10 hours. At the end of cultivation ($OD_{600} = 2 - 3$) 100 cm³ of sterile glycerol was added in the culture. Culture samples were stored in cryogenic vials at – 80 °C.

Precultivation was carried out in 1L flasks containing 200 cm³ medium (section 3.2.2). Flasks were inoculated with 0.75 cm³ of cryoculture, and incubated in the rotation shaker at 37 °C and 160 rpm for 15 hours.

3.2 Medium Composition

3.2.1 LB-medium

Tryptone, yeast extract and NaCl were dissolved in distilled water and pH was adjusted to 7.2 with 45 % NaOH. Medium was sterilized at 121 °C for 20 minutes. Tetracycline and kanamycin were prepared separately (dissolved in ethanol and sterilized by filtration).

Table 3.1 Composition of the LB-medium

Compound	Concentration [g dm⁻³]
tryptone	10.00
yeast extract	5.00
NaCl	5.00
tetracycline	0.01
kanamycin	0.01

3.2.2 Synthetic Medium for Preculture

All components were dissolved in distilled water. MgSO₄ solution, CaCl₂ solution and glucose solution were prepared and sterilized separately in order to prevent a non-enzymatic browning of reduced sugar through reaction with the amino groups and the crystallization of MgNH₄PO₄ (Mailand reaction). pH of salts solution was adjusted to 7.2 with 45 % NaOH. All solutions were sterilized at 121 °C for 20 minutes.

Table 3.2 Composition of the synthetic medium for preculture

Compound	Concentration [g dm⁻³]
Na ₂ HPO ₄	6.00
KH ₂ PO ₄	3.00
NaCl	0.50
NH ₄ Cl	1.00
MgSO ₄	0.05
CaCl ₂	0.01
glucose monohydrate	2.00
potassium acetate	0.20

3.2.3 Synthetic Medium for Fed-batch Fermentation

All components were dissolved in distilled water. MgSO₄ solution and glucose solution were prepared and sterilized separately. pH of salts solution was adjusted to 7.2 with 45 % NaOH. All solutions were sterilized at 121 °C for 20 minutes. Additionally, trace elements solution was prepared separately (see section 3.2.5).

Table 3.3 Composition of the synthetic medium for fed-batch fermentation

Compound	Concentration [g dm⁻³]
NaH ₂ PO ₄ · H ₂ O	1.50
KH ₂ PO ₄	3.25
K ₂ HPO ₄	2.50
NH ₄ Cl	0.20
(NH ₄) ₂ SO ₄	2.00
MgSO ₄	0.50
trace elements	1.00 cm ³ dm ⁻³
glucose monohydrate	11.00
potassium acetate	0.78

3.2.4 Synthetic Medium for Continuous Fermentation

Composition of the synthetic medium for continuous fermentation was same as is described in the section 3.2.3 except 1 cm³ dm⁻³ of antifoam solution (see section 3.2.8) was added. Additionally, acetate concentration in the feed medium was varied according to the experimental plan (0, 20 and 40 g dm⁻³ of potassium acetate).

3.2.5 Trace Elements Solution

The components of the trace elements solution were dissolved in 5 N hydrochloric solution (245 cm³ of 32 % HCl and 500 cm³ distilled water).

Table 3.4 Composition of trace elements solution

Compound	Concentration [g dm⁻³]
CaCl ₂ · 2H ₂ O	10.00
ZnSO ₄ · 7H ₂ O	0.50
CuCl ₂ · 2H ₂ O	0.25
MnSO ₄ · H ₂ O	2.50
CoCl ₂ · 6H ₂ O	1.75
H ₃ BO ₃	0.12
AlCl ₃ · 6H ₂ O	2.50
Na ₂ MoO ₄ · 2H ₂ O	0.50
FeSO ₄ · 7H ₂ O	10.00

3.2.6 Feed Mediums

Glucose feed solution and acetate feed solution were separately dissolved in water and sterilized at 121 °C for 20 minutes.

Table 3.5 Composition of glucose and acetate feed solutions

Compound	Concentration [g dm⁻³]
glucose monohydrate	700
potassium acetate	109

3.2.7 Base

25 % NH₄OH solution was used for pH regulation.

3.2.8 Antifoam

Antifoam S 289 was sterilized at 121 °C and it was used undiluted.

3.2.9 Buffer for On-line Measurement of Glucose

Compounds were dissolved in distilled water. pH was adjusted to 7.35 – 7.45 with 32 % HCl. Finally 1 cm³ dm⁻³ of TWEEN 20 was added.

Table 3.6 Composition of the buffer for on-line glucose measurement

Compound	Concentration [g dm⁻³]
(NH ₄) ₂ SO ₄	8.36
KH ₂ PO ₄	2.28
NaCl	5.84

3.2.10 Electrode Rinse Solution

0.5 mol dm⁻³ Na₂SO₄ solution was used as an electrode rinse solution.

3.2.11 Solutions for Enzymatic Measurement of Glucose

Compounds of tris-maleic buffer were dissolved in distilled water and pH was adjusted to 6.8 with 45 % NaOH. MgCl₂ · 6H₂O solution was dissolved in the water. NAD, ATP and MgCl₂ solution were dissolved in tris-maleic buffer. NAD/ATP solution was stored at -4 °C. The glucose standard solutions were made from glucose-monohydrate, and dissolved in the water to the following concentrations 0.05 g dm⁻³, 0.10 g dm⁻³, 0.20 g dm⁻³, 0.25 g dm⁻³, 0.30 g dm⁻³, 0.35 g dm⁻³, 0.40 g dm⁻³ and 0.50 g dm⁻³. The glucose standard solutions were stored at -4 °C.

Table 3.7 Composition of solutions for on-line glucose measurement

Tris-maleic buffer pH = 6.8	
Compound	Concentration [g dm⁻³]
tris-(hydroxymethyl)-aminomethane	1.12
maleic acid	1.16
MgCl₂ solution	
Compound	Concentration [g dm⁻³]
MgCl ₂ · 6H ₂ O	20.34
NAD/ATP-mix solution	
Compound	Concentration [g dm⁻³]
NAD	0.80
ATP	0.61
MgCl ₂ solution	42 cm ³ dm ⁻³

3.3 Off-Line Analysis

3.3.1 Optical Density

The optical density (OD_{600}) was measured in a double-beam spectrophotometer (UV-160, Shimadzu) at 600 nm against water after appropriate dilution of samples with water.

3.3.2 Biomass Dry Weight

Biomass dry weight (DW) was measured by filtration of 2.5 cm³ fermentation broth using pre-weighted micro filters (0.2 µm cut-off, Schleicher & Schuell). After drying for 48 h

at 80 °C, the filters were cooled down in an exicator for an additional 48 h. After filter was weighed the cell dry mass was calculated.

3.3.3 Glucose

3.3.3.1 Determination of Glucose by Biosensor Appliance Accutrend®

Determination of glucose concentration was carried out with the use of an enzyme-based biosensor appliance Accutrend® (Roche Diagnostic) consisted of Accutrend® test strips and Accutrend® analyzer. The enzyme glucose oxidase, which is immobilized on the test strip, oxidizes glucose in the presence of oxygen to equimolar amount of gluconolactone and hydrogen peroxide. On such a way formed hydrogen peroxide is measured amperometrically.

The measurement window of the Accutrend® biosensor appliance is between 0.1 – 6.0 g dm⁻³. After appropriate dilution of fermentation sample with water, 10 mm³ of sample was injected onto a cavity of the Accutrend® test strip. After 30 seconds, a reading is shown on the display of the Accutrend® analyzer.

3.3.3.2 Enzymatic Determination of Glucose

Enzymatic determination of glucose is based on the photometric measurement of NADH formed in the series of enzymatic reactions starting from glucose. In excess of ATP, NAD, hexokinase and glucose-6-phosphate (G6P) dehydrogenase, glucose is completely converted in 6-phosphogluconate. The amount of NADH formed is stoichiometric with the amount of glucose.

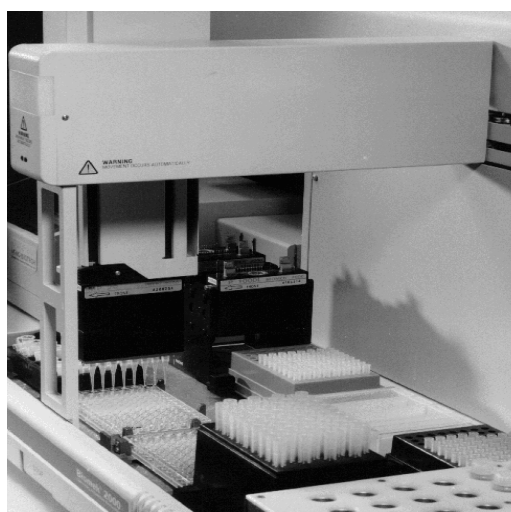


Figure 3.2 Automatic pipetting station

The automatic pipetting station (Figure 3.2) consist of a laboratory robot (Biomek 2000, Beckman Instrument) was used for enzymatic determination of glucose. The robot can pipette and dispense sample volumes between 1 – 1000 mm³. The pipetting station was furnished with a robot arm, which was capable of executing single working steps. The reservoirs, pipette tips, micro-titer plates and pipetting modules had their respective positions at the base of robot.

The measurement was carried out using a micro-titer plate with 96 wells. By the help of the automatic pipetting station micro-titer plate was filled with solutions according to Table 3.8. Initial extinctions for glucose standards and samples (E_0) at 340 nm were measured on a micro-titer plate reader (Thermomax, Molecular Devices). Plate was incubated on a shaker (Titrimax 100, Heidolph) for 90 minutes at room temperature. After incubation the extinctions (E_1) for both, glucose standards and samples, were measured.

The extinction differences of glucose standards ($\Delta E = E_1 - E_0$) were calculated and linearly correlated with concentrations of glucose standards. The unknown glucose concentrations of samples were calculated from the extinction differences measured and estimated slope of regression line.

Table 3.8 Pipetted volume of solutions per well

Compound	Standard [mm ³]	Sample [mm ³]
NAD/ATP-mix	220	220
Glucose standard	40	-
Sample	-	40
G6P dehydrogenase	20	20
Hexokinase	20	20

3.3.4 High Performance Liquid Chromatography (HPLC)

After centrifugation of the fermentation samples at 13,000 rpm for 10 minutes (Biofuge pico, Heraeus), the supernatants were diluted using a dilutor (Micro LAB 1000, Hamilton). Both the samples for organic and amino acids were diluted with the dilution ratio 1:100.

3.3.4.1 HPLC for Organic Acids

The concentrations of pyruvate, acetate and lactate in the fermentation supernatant were measured using an HPLC. Determination of the organic acid concentration involves the use of two Aminex HPX-87H (Biorad) columns in series. The separation was performed with

5 mmol dm⁻³ H₂SO₄ solution at a flow rate of 0.5 cm³ min⁻¹ (pump S1000, Sykam) and the detection was at a wavelength of $\lambda = 254$ nm (Diode Array Detector, DAD). The signal was analyzed with an integrator (C-R3A, Sykam) and the sample volume used was 100 mm³.

3.3.4.2 HPLC for Amino Acids

The concentrations of alanine, glutamate and aspartate in the fermentation supernatant were measured using an HPLC (Sykam). The column used for the detection of amino acids was Lichrospher 100 RP 18-5 EC (Merck). The gradient separation (section 7.5.2) was performed with a flow rate of 0.9 cm³ min⁻¹ at a temperature of 40 °C. The sample injection volume was 10 mm³. The detection was at extinction of 330 nm and absorbance of 450 nm (fluorescence detector, RF-535, Shimadzu).

3.3.5 Intra-Cellular Pyruvate Concentration

Fermentation broth was sampled in 15 cm³ of quenching solution (60 %, w/w, aqueous methanol containing 70 mmol dm⁻³ 2-[4-(2-hydroxyethyl)-1-piperazinyl]ethanesulfonic acid (HEPES)) which was maintained at - 50 °C. Sampling volume was calculated by linear extrapolation taking for a referable value 5 cm³ of sample if *OD* was 25.

The quenched bacterial suspension was centrifuged (Avanti 30, Beckmann) at 10,300 g for 5 minutes at - 20 °C. The supernatant was removed and the remaining cell pellets were resuspended in 2 cm³ of 43.8 % w/w perchloric acid at - 18 °C. In order to ensure complete extraction the samples were homogenized and stored at - 80 °C. After one freeze-thaw cycle the samples were ultra-centrifuged at 42,000 g for 30 minutes at 4 °C.

The clear supernatant was neutralized to a pH = 7 with saturated potassium carbonate solution at - 2 °C. The perchlorate precipitate was ultra-centrifuged at 42,000 g for 30 minutes at 4 °C. The supernatant was used for measurement of pyruvate intra-cellular concentration by the use of LC-MS. Quenching, extraction and calculation of intra-cellular pyruvate concentrations was realized as described in Buchholz et al⁹².

Intra-cellular pyruvate concentration was measured by the use of LC-MS (HPLC Gynkotek Model 480, Germany; MS Thermo Finnigan, Germany). A beta-Nucleodes-OH (Marchery-Nagel, Germany) was used and the gradient separation was performed (section 7.5.3).

Intra-cellular concentrations were calculated by multiplying the concentrations determined in cell extracts with a dilution factor. The dilution of the sample (Equation 3.1) is

a function of intra-cellular volume V_I , volume of extraction V_E , neutralizing reagents V_N , and inter-cellular volume in the centrifuged pellets⁹².

$$Dilution = \frac{V_I + V_E + V_N + V_X}{V_I} \quad 3.1$$

Intra-cellular volume, V_I , was calculated approximately as described in Pramanik and Keasling¹⁰⁹ (Equation 3.2):

$$V_I = \rho_X \cdot V_S \cdot K_E \quad 3.2$$

where ρ_X is cell density, V_S sample volume, and K_E specific cell volume.

3.4 On-Line Analysis

3.4.1 pH

Gel-pH-electrode (F-615-B130-DH, Broadley James) was used for on-line measurement of pH in fermentation processes. The electrode was calibrated before sterilization at two points (buffers pH = 4.01 and pH = 7.00, room temperature) and afterwards sterilized together with bioreactor. Determine pH value was transferred to process control system over the measuring amplifier. An integrated PID-controller connected with peristaltic pump was used for control of pH value.

3.4.2 Dissolved Oxygen Concentration

pO₂ electrode (12 mm OxyProbe, Broadley James) was used for on-line measurement of dissolved oxygen concentration (oxygen partial pressure) in the fermentation processes. The electrode was calibrated after sterilization at 37° C, 1800 rpm, 0.25 bar overpressure and gas-flow rate of 1 dm³ min⁻¹ with nitrogen (0 %) and air (100 %, saturation). Determined pO₂ value was transferred to process control system by the measuring amplifier.

3.4.3 Pressure, Temperature, Aeration

Pressure, temperature and aeration were measured by the use of corresponding sensors. Calibration of those sensors was not necessary prior to every fermentation. Measured values were transferred to process control system over the measuring amplifier. Integrated PID-controllers were used for control of those parameters.

3.4.4 CO₂ and O₂ in the Exhaust Gas

CO₂ and O₂ content in exhaust gas were measured by the use of the gas analyzer (Binos 100 2M Fisher-Rosemount). CO₂ was monitored using an infrared photometer. Paramagnetic sensor was used for measurement of O₂ in exhaust gas. The pump, which keeps the gas-flow constant (1 dm³ min⁻¹), was integrated in the gas analyzer.

The gas analyzer was calibrated immediately prior to inoculation. Nitrogen was used for calibration of zero point. O₂-set point (20.95 %) was calibrated with air. Defined mixture of gases (10 % CO₂, 15 % O₂, 75 % N₂) was used for calibration of CO₂-set point.

3.4.5 Glucose

Three peristaltic pumps (U 501 and U 101, Watson & Marlow) were used to ensure continuous sampling of permeate from the bioreactor (Figure 3.3). The first pump was integrated in the small by-pass (approximately 20 cm³ internal volume) connected to the bioreactor.

To avoid oxygen limitation, fermentation broth was pumped at a high flow rate (approximately 1 dm³ min⁻¹) through a cross-flow hollow-fibre ultra-filtration unit (cut-off 500 kDa, filtration area 23 cm², Schleicher & Schuell) installed in the by-pass. Thus, a mean by-pass residence time of approximately 2 s was achieved.

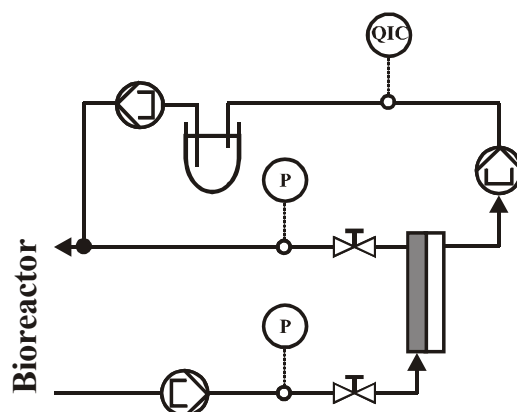


Figure 3.3 Scheme of the set-up used for continuous sampling of permeate from the bioreactor

The first pump was integrated in the small by-pass (approximately 20 cm³ internal volume) connected to the bioreactor. To avoid oxygen limitation, fermentation broth was pumped at a high flow rate (approximately 1 dm³ min⁻¹) through a cross-flow hollow-fibre

ultrafiltration unit (cut-off 500 kDa, filtration area 23 cm², Schleicher & Schuell) installed in the by-pass. Thus, a mean by-pass residence time of approximately 2 s was achieved.

1 – 2 cm³ min⁻¹ cell free permeate was supplied and pumped by the second pump into a flask for pressure compensation while passing through the manifold of the on-line glucose measuring system. With the third pump, unused permeate was pumped back from the flask for pressure compensation into the bioreactor. The whole sampling system was sterilized with 1 mol dm⁻³ NaOH at room temperature for 3 hours. A picture of the set-up used for continuous sampling of permeate from the bioreactor is shown in Figure 3.3.

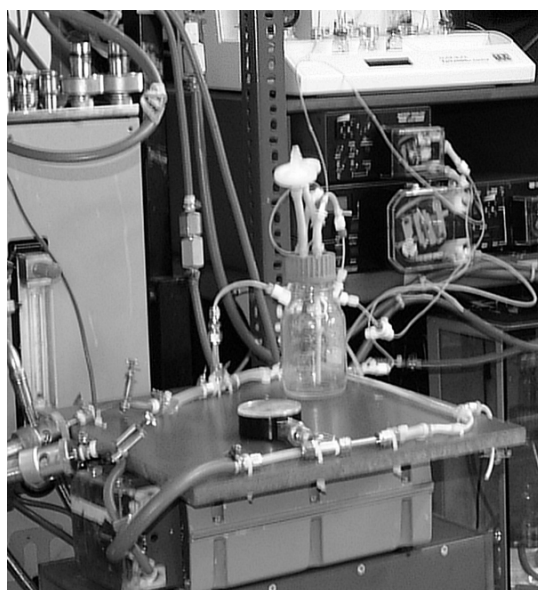


Figure 3.4 Picture of the set-up used for continuous sampling of permeate from the bioreactor

The On-Line General Analyzer (OLGA GL2b, IBA GmbH) based on SIA (sequential injection analysis) technique was used for on-line measurement of glucose⁹³. Glucose samples were automatically taken with the help of predescribed system. Every 120 s 10 mm³ sample was taken from cell free permeate stream and analyzed for glucose concentration.

Before each fermentation new biosensor strip (SensLab²) was inserted in the measuring cell of device. The enzyme glucose oxidase, which is immobilized on the biosensor strip, oxidizes glucose in the presence of oxygen to equimolar amount of gluconolactone and hydrogen peroxide. On such a way formed hydrogen peroxide was measured by amperometric detection. Measured values (electric current) were transferred to

process control system over the measuring amplifier. OLGA Windows™ software was used for evaluation, re-calculation and acquisition of measured values. Two points calibration were performed automatically in 60 – 90 minutes intervals with 2 g dm^{-3} and 10 g dm^{-3} glucose standard solution (dissolved in OLGA buffer). OLGA buffer (section 3.2.9) was used as well for different rinse and dilution steps, which were automatically taken by the device.

The liquid handling system of OLGA is shown in Figure 3.5. Dead time of complete system from sampling to calculation of unknown concentration was approximately 2 minutes.

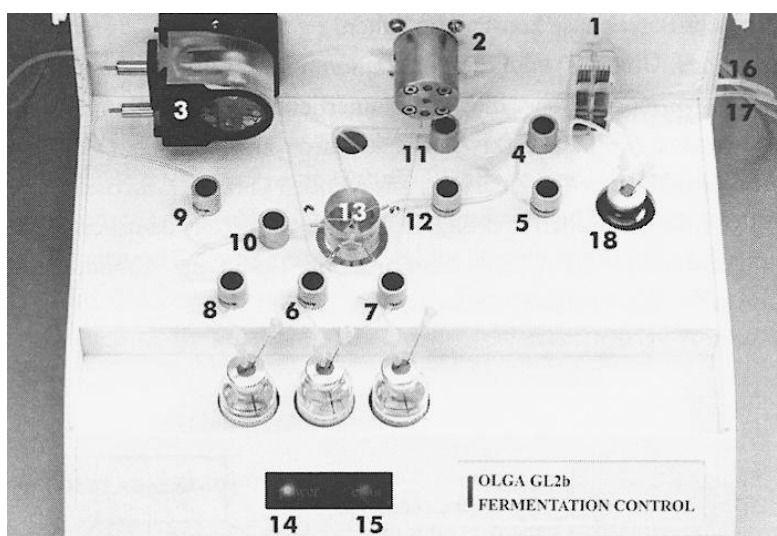


Figure 3.5 The liquid handling system of OLGA GL2b. 1 - measuring cell; 2 - micro dosing pump; 3 - peristaltic pump; 4 – 12 valves; 13 - manifold; 14 and 15 - control lights; 16 - tube guide for waste; 17 - tube guide for running buffer; 18 - isopropyl

Glucose concentration was controlled in most fermentation at 5 g dm^{-3} . For this glucose concentration level following OLGA parameters were used:

Measuring area:	$1 - 30 \text{ mmol dm}^{-3}$
Calibration solution 1:	2 g dm^{-3}
Calibration solution 2:	10 g dm^{-3}
General:	
injection per sample:	1
injection per standard:	2
analysis and calculation:	height of peak
cycles before re-calibration:	30

	cycles before isopropyl:	60	
Standard injection cycle:	rinsing:	20 s	25 mm ³ s ⁻¹
	injection:	2 s	10 mm ³ s ⁻¹
	rinsing of the measuring cell:	10 s	30 mm ³ s ⁻¹
	injection break:	3 s	3 mm ³ s ⁻¹
	measuring cycle break:	3 s	3 mm ³ s ⁻¹
	rinsing with isopropyl:	5 s	25 mm ³ s ⁻¹
	rinsing:	60 s	25 mm ³ s ⁻¹
Bioreactor:	inlet:	10 s	25 mm ³ s ⁻¹
	rinsing:	15 s	25 mm ³ s ⁻¹
Calibration:	inlet:	5 s	15 mm ³ s ⁻¹
	rinsing:	8 s	20 mm ³ s ⁻¹

3.5 Cultivation

All experiments were carried out in a 7.5 dm³ bioreactor (INFORS, Switzerland) containing 2.25 dm³ starting medium (section 3.2.3), which was equipped with standard control units for pH, pressure, temperature, aeration, stirrer speed etc.

After sterilization of the bioreactor and peripheral equipment, fermentation medium was filled into the bioreactor through a sterile microfiltration-unit (0.2 µm cut-off, Sartobran, Sartorius) and pH was adjusted to 7.0 by 25 % ammonia titration, also during the latter fermentation process. All experiments were carried out at the temperature of 37 °C. Sufficient aeration ($pO_2 \geq 40\%$) was obtained by vigorous stirring (200 – 1800 rpm), air-flow rate (1 – 10 dm³ min⁻¹) and reactor overpressure (0.2 – 0.8 bar). The outlet gas stream was condensed by a reflux cooler. The condensate was returned to the medium. Exhaust gases were analyzed by the gas analyzer (Binos 100 2 M, Rosemont). The bioreactor was inoculated with 10 % of the working volume of a preculture.

3.5.1 Fed-Batch Process

A schematic diagram of the fermentation set-up is shown in Figure 3.6. Glucose feeding was started when the concentration was about 5 g dm⁻³. This level was controlled until the end of the fermentation by help of automated glucose feed adjustment (section 3.7.1) which was realized using a Kalman filter combined with a minimal covariance controller (MV3), both implemented in MEDUSA, a process control software.

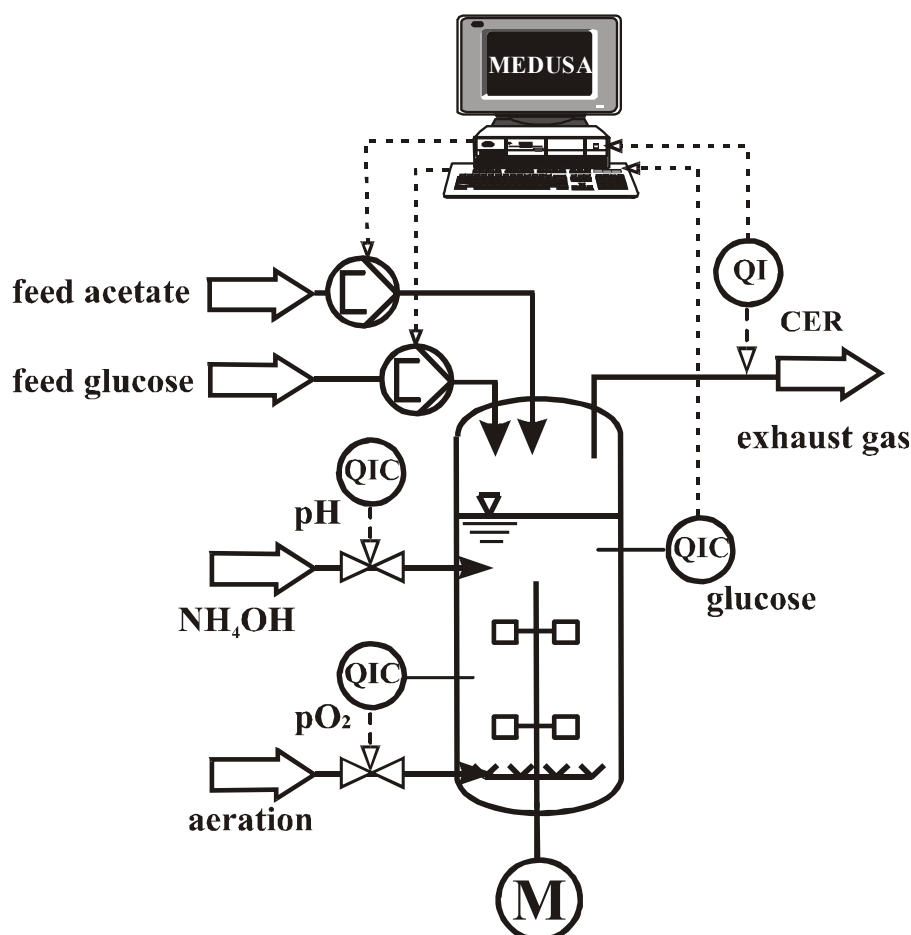


Figure 3.6 Schematic diagram of the experimental and controller set-up used for fed-batch fermentation; — mass flow; ----- signal flow

An acetate feed, according to a developed feeding strategy (section 3.7.2), was started, after the depletion of the initial batch amount, which was indicated on-line by decreasing carbon dioxide emission rates. The acetate feed was stopped after biomass concentration kept constant for 3 hours time interval. The fermentation was stopped after 35 hours. Picture of the fermentation set-up is shown in the Figure 3.7. 20 cm³ samples from bioreactor were taken in a predetermined schedule (1 – 2 h intervals) for analysis of organic acids, amino acids, *OD*, biomass dry weight, pH, glucose and intracellular pyruvate concentration (in fully integrated approach, see section 3.5.4).

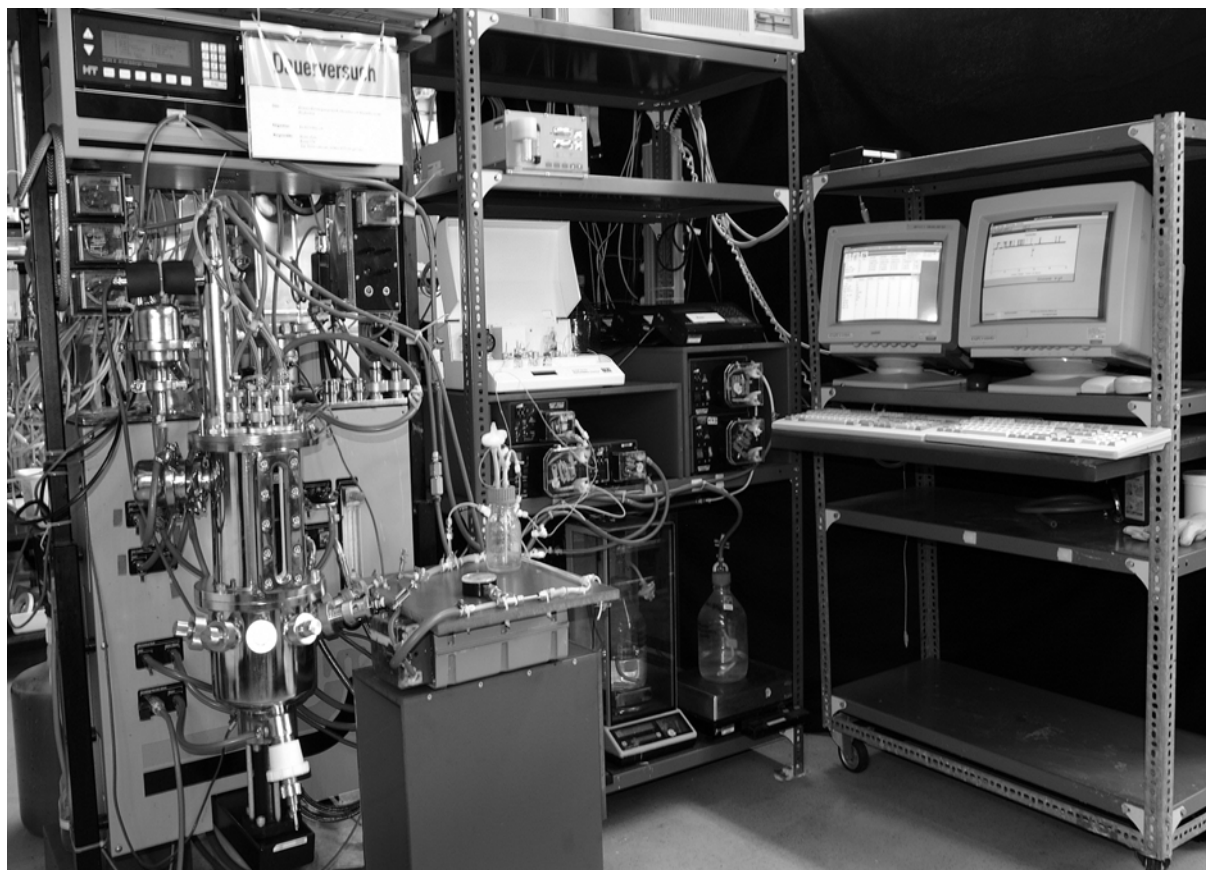


Figure 3.7 Picture of the fermentation set-up used in the fed-batch fermentation process

3.5.2 Repetitive Fed-Batch Process

Process was started and carried out as fed-batch process. After biomass concentration was constant for 3 hours time interval acetate feed was stopped and fermentation medium was pumped through by-pass consisted of a cross-flow hollow-fibre ultrafiltration module (area 0.98 m^2 , cut-off 500 kDa, Schleicher & Schuell) and a peristaltic pump (621 F/L, Watson-Marlow).

Before making use of the by-pass unit it was sterilized with 1 M NaOH for three hours. Biomass was retained in the system (bioreactor-diafiltration unit) and cell free permeate was pumped out. When 60 % of fermentation medium was pumped out of the system, in the form of permeate, equal volume of fresh fermentation medium (section 3.2.3) was added in the bioreactor through diafiltration unit to prevent disposal of the fermentation broth in the by-pass.

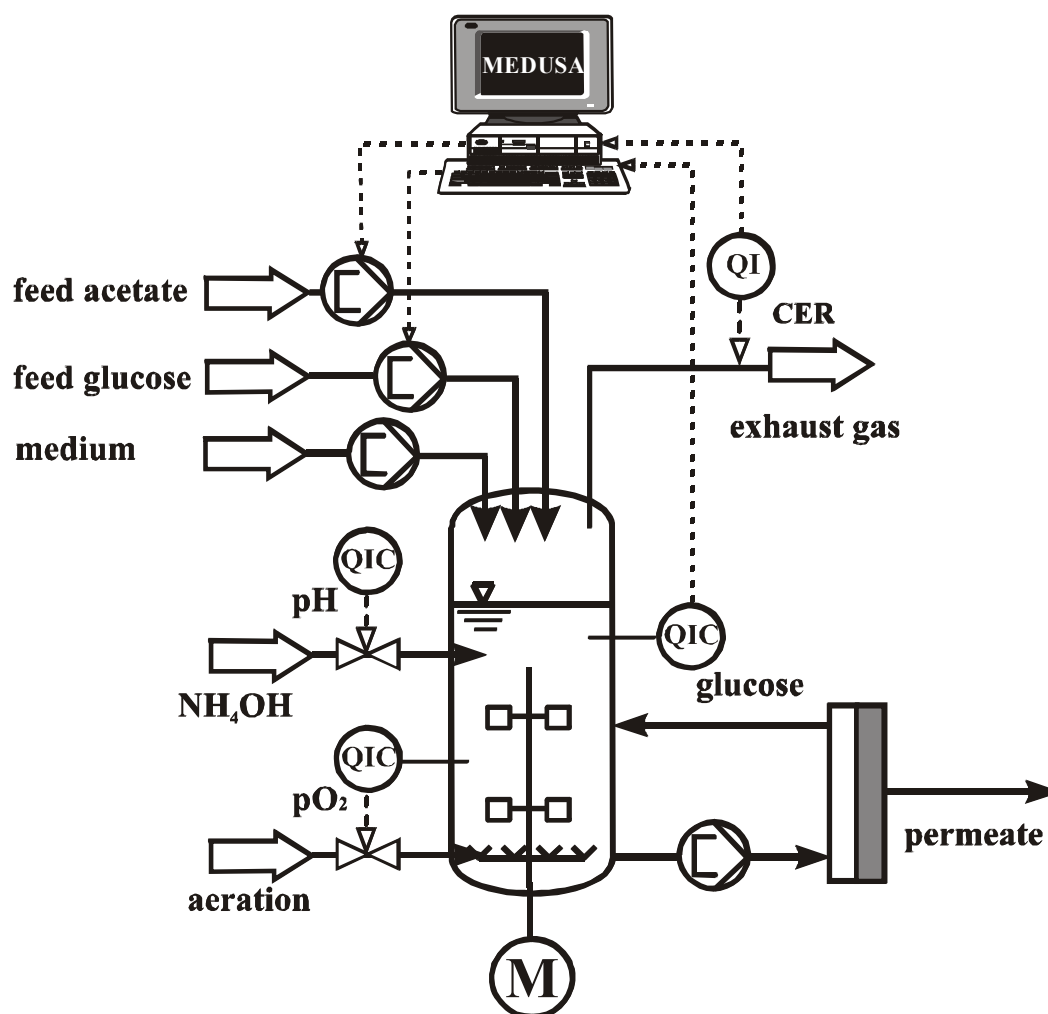


Figure 3.8 Schematic diagram of the experimental and controller set-up used for repetitive fed-batch process; — mass flow; - - - signal flow

Glucose concentration level was controlled between $1 - 5 \text{ g dm}^{-3}$ by the use of described system (section 3.7.1). New cycle biomass retention-medium dilution was started after calculated glucose feed rate was lower than 10 g h^{-1} . A schematic diagram of the experimental and controller set-up used for repetitive fed-batch process is shown in Figure 3.8.

20 cm^3 samples from bioreactor were taken in a predetermined schedule (1 – 2 h intervals) for analysis of organic acids, amino acids, *OD*, biomass dry weight, pH and glucose. 2 cm^3 of cell free permeate from diafiltration were taken at the start and at the end of the cycle for analysis of organic acids, amino acids and glucose.

3.5.3 Continuous Process with Cell Retention

Process was started and carried out as fed-batch process. When the maximal optical density in fed-batch fermentation was achieved, acetate feed was stopped and continuous process with cell retention was started as follows.

Biomass was retained in the system: bioreactor-diafiltration unit. Permeate generated in the ultrafiltration unit was transported to the CFB tank by the peristaltic pump with a constant flow rate of 0.35. By-pass construction was the same as in repetitive fed-batch experiment. For permeate generation a cross-flow hollow-fibre module of 0.15 m² filtration area and a cut-off of 500 kDa (Schleicher & Schuell) was used.

All processes were carried out with a dilution rate of approximately 0.1 h⁻¹. Glucose flow was kept constant in the range of 60-80 cm³ h⁻¹ depending on acetate concentration in the fresh feed medium. Fresh medium was fed in the bioreactor at a constant flow rate of 0.27 – 0.29 dm³ h⁻¹.

20 cm³ samples from bioreactor were taken in a predetermined schedule (1 – 2 h intervals) for analysis of organic acids, amino acids, *OD*, biomass dry weight, pH and glucose. 2 cm³ of cell free permeate from diafiltration were taken at the start and at the end of the cycle for analysis of organic acids, amino acids and glucose.

3.5.4 Fully Integrated Continuous Process

Process consists of four main steps: (a) continuous fermentation with cell recycle by ultrafiltration (see section 3.5.3); (b) protein separation by nanofiltration; (c) product recovery by electrodialysis (see section 3.6.2) and (d) sterilization of depleted fermentation broth by microfiltration. Schematic diagram of the experimental set-up used for fully integrated continuous process is shown in the Figure 3.9.

Four peristaltic pumps (U 501 and U 504, Watson & Marlow) were used to ensure continuous generation of cell and protein free fermentation broth (CPF_B) required for electrodialysis. Scheme of the set-up used for continuous generation of CPF_B permeate is shown in the Figure 3.10.

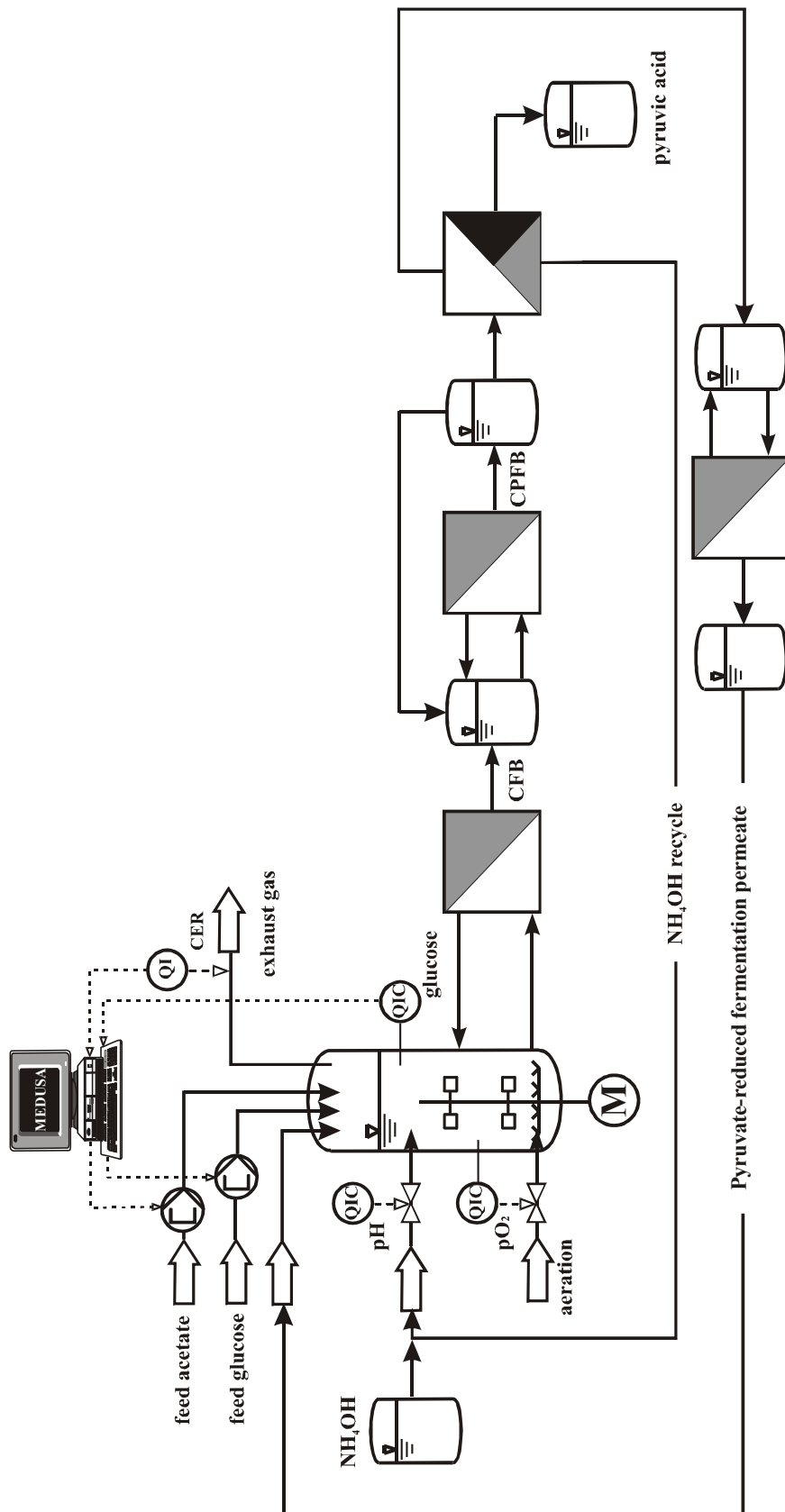


Figure 3.9 Schematic diagram of the experimental set-up used for fully integrated continuous process

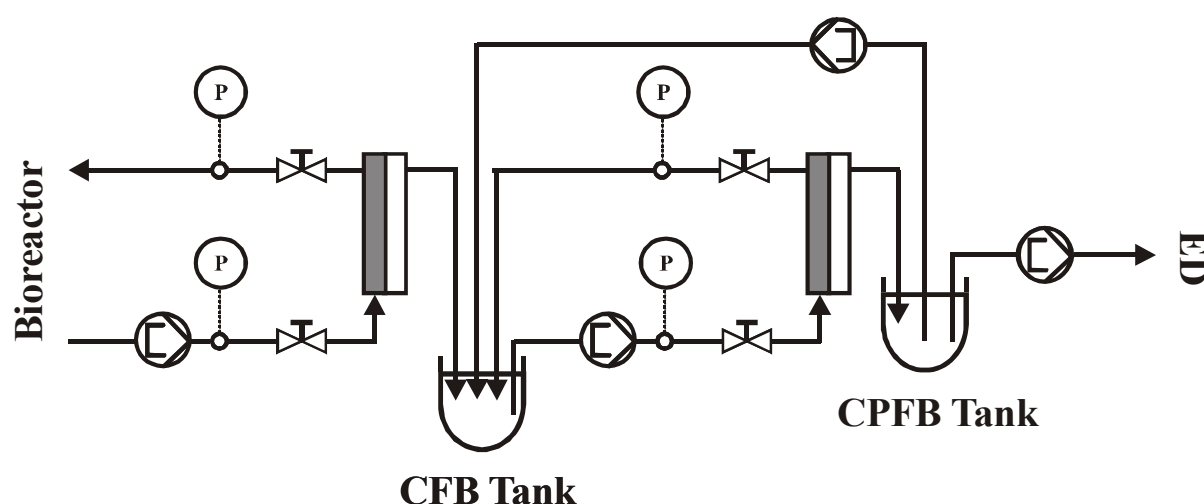


Figure 3.10 Scheme of the set-up used for continuous generation of CPF B permeate

Cell free fermentation broth (CFB) generated in ultrafiltration unit (see section 3.5.3) was transported to the CFB tank by the first peristaltic pump with a pump rate of $0.4 \text{ dm}^3 \text{ h}^{-1}$. The second pump was integrated in the by-pass connected to the CFB tank. CFB broth was pumped at a high flow rate (approximately $2 \text{ dm}^3 \text{ min}^{-1}$) through planar module (ULTRAN, Schleicher & Schuell, Germany) consist of four cassettes with pore size of 10 kDa installed in the by-pass. $2 - 3 \text{ dm}^3 \text{ h}^{-1}$ CPF B permeate was generated in the nanofiltration unit and collected in the CPF B tank. $0.4 \text{ dm}^3 \text{ h}^{-1}$ of CPF B permeate was pumped into the feed tank of the ED unit by the third pump. With the fourth pump, unused CPF B permeate was pumped back from the CPF B tank into the CFB tank. Picture of the ultra- and nano-filtration set-up used in the fully integrated continuous process is shown in the Figure 3.11.

ED was carried out as is described in section 3.6.2. The power supply was set at a constant current. During the first hour I was set at 5 A, and in the remaining part of the process to 2 A, respectively. Depleted CPF B broth was pumped back from the feed tank of the ED unit into the bioreactor through a sterile microfiltration-unit ($0.2 \mu\text{m}$ cut-off, Sartobran, Satorius) with a flow rate of $0.32 \text{ dm}^3 \text{ h}^{-1}$ to prevent possible contamination of the bioreactor. NH_4OH produced in the electrodialysis was pumped from the base tank into the bioreactor at constant flow of $0.01 \text{ dm}^3 \text{ h}^{-1}$.

Process was started and carried out as continuous process with cell retention. When 4 dm^3 of CPF B were generated fully integrated continuous process was started and carried out as it was previously described.

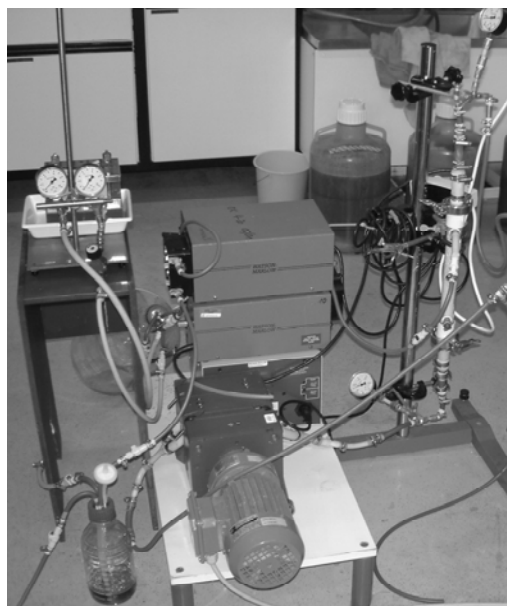


Figure 3.11 Picture of the ultra- and nano-filtration set-up

20 cm³ samples from bioreactor were taken in a predetermined schedule (1 – 2 h intervals) for analysis of organic acids, amino acids, *OD*, biomass dry weight, pH and glucose. 2 cm³ of cell free permeate generated in the ultrafiltration unit were taken for analysis of organic acids, amino acids and glucose. At the same time point 2 cm³ of sample was taken from the feed, the acid and the base tank of the ED unit for analysis of organic acids, amino acids, pH, glucose and inorganic materials.

3.6 Electrodialysis

3.6.1 Stack Configuration

One-stage experiments were performed using three compartments ED stack with the principle being represented in the Figure 3.12. The three compartments ED stack consisted of anion-exchange (A), cation-exchange (C), and bipolar (aBc) membranes to allow three streams to flow, i.e. acid, base, and feed streams. The electrodes were kept from directly contacting the base solution by a cation-exchange membrane.

Pyruvate ions and sodium ions in the feed compartment simultaneously moved into the acid and the base compartment through anion- and cation-exchange membranes, respectively, during ED operation. Free pyruvic acid was formed by combination of pyruvate ions and hydrogen ions generated on the cation-exchange layer of the bi-polar membrane. Sodium

hydroxide was simultaneously generated by the combination of sodium ions and hydroxyl ions formed on the anion-exchange side of the bi-polar membrane.

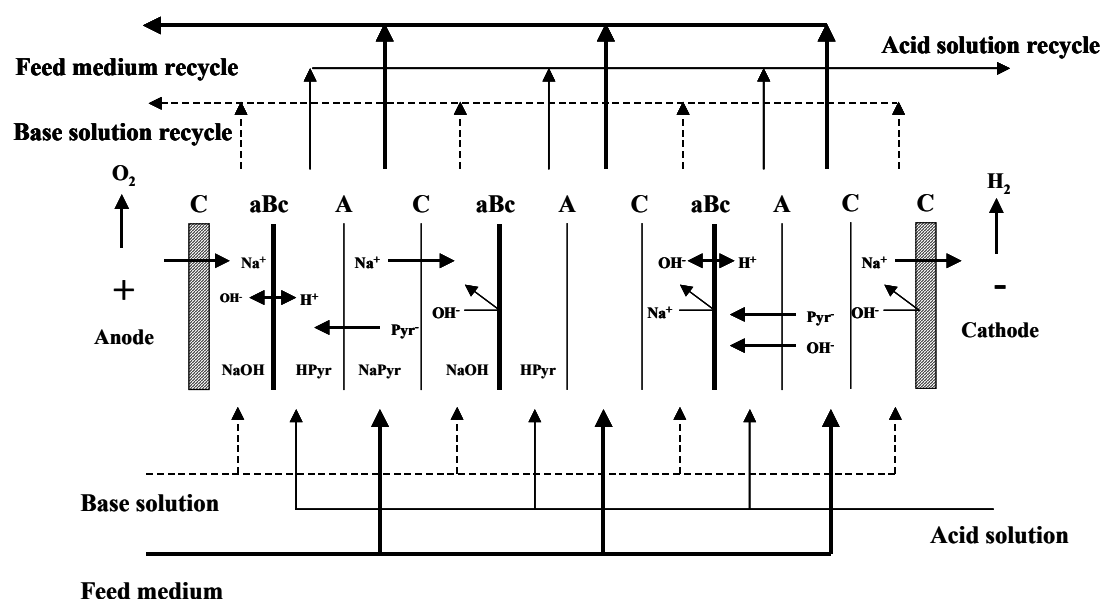


Figure 3.12 Principle of three compartment electrodiolysis

The electrolyte solution was circulated continuously to transfer the electric current and to remove gases (O₂ and H₂) produced by the electrode reaction during the operation of the ED.

3.6.2 ED Operations

The experimental equipment for ED used three-compartment electrodiolysis (WSED) unit (Goema, Figure 3.12) with a membrane stack having four cells pairs. The three-compartment ED stack consisted of anion-exchange, cation-exchange and bi-polar membrane produced by Tokuyama Co. The effective area of membranes was 0.56 m². Picture of experimental set-up is shown in Figure 3.13.

Electric power was supplied to the ED stack by a power unit (NGRE 100/10, Rohde & Schwarz). The power supply was set at a constant current in the range of 2 - 10 A. ED could not be operated with higher current due to the low mechanical strength of membranes in adjacent strong basic solution throughout several experiments. All experiments were started in a constant current mode and switched to a constant voltage mode when the stack voltage exceeded the maximum voltage of the membranes and power supply (40 V) because of the high ohmic resistance of very dilute pyruvate solution.

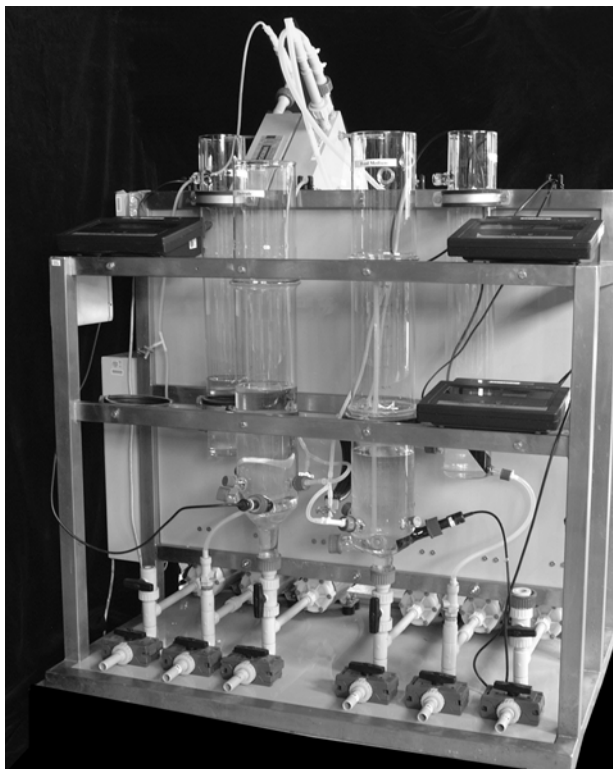


Figure 3.13 Picture of the electrodesalination unit

The ED configuration was composed of four solution tanks holding the acid, the base, the feed and the electrode rinse solution. The initial concentration of pyruvate in the model solution was 40 g dm^{-3} , and in the fermentation broth varied between $35 - 60 \text{ g dm}^{-3}$. $0.5 \text{ mol dm}^{-3} \text{ Na}_2\text{SO}_4$ was used as the electrode rinse solution in all experiments. Initially the acid and the base compartments were filled with demineralized water. All streams were circulated through the acid, the base, the feed and the electrode rinse solution compartment, respectively, and then recycled to the reservoir for 5 minutes before electric power was supplied to the ED stack. Solutions were circulated in the system by the use of centrifugal pumps (Iwaki Co.) with a flow rate of approximately $1 \text{ dm}^3 \text{ h}^{-1}$.

The voltage drop in the system was measured by voltmeter. The pH and conductivity (LF537, WTW) of the acid, the base and the feed solutions were measured using pH meters (632, Methrom) and conductivity meters, respectively. From each compartment, 2 cm^3 samples were taken in a predetermined schedule for analysis of pyruvic acid, pH, glucose (in ED experiments with fermentation broth) and inorganic materials (in fully integrated approach).

Before the start of an experiment a standardized cleaning-in-place procedure was performed using water (10 min), 1% (w/w) NaOH and 1% (w/w) NaCl (30 min), water (10 min) two fold, 1 % (w/w) HCl (30 min) and water (10 min) two fold.

3.7 Data Acquisition and Process Control

Control of process parameters was performed with devices developed by Infors. For total process control, altogether three PCs were used. One PC for OLGA control and acquisition of on-line measured glucose concentrations (PC-1), another for LabView (National Instruments process control software, USA) based total process data management (PC-2) and a third PC with MEDUSA software for the control of glucose and acetate supply (PC-3).

3.7.1 Closed-Loop Glucose Control System^{94,110,112}

For the control of the glucose in the fed-batch process a control strategy was developed and implemented on a process computer (PC-3) to overcome the problems: non-linearity of the control system, noisy and time delayed (and often discrete-time) measurement outputs. The principle scheme of the approach is shown in Figure 3.14. The model based adaptive control strategy with on-line bioreactor identification was used.

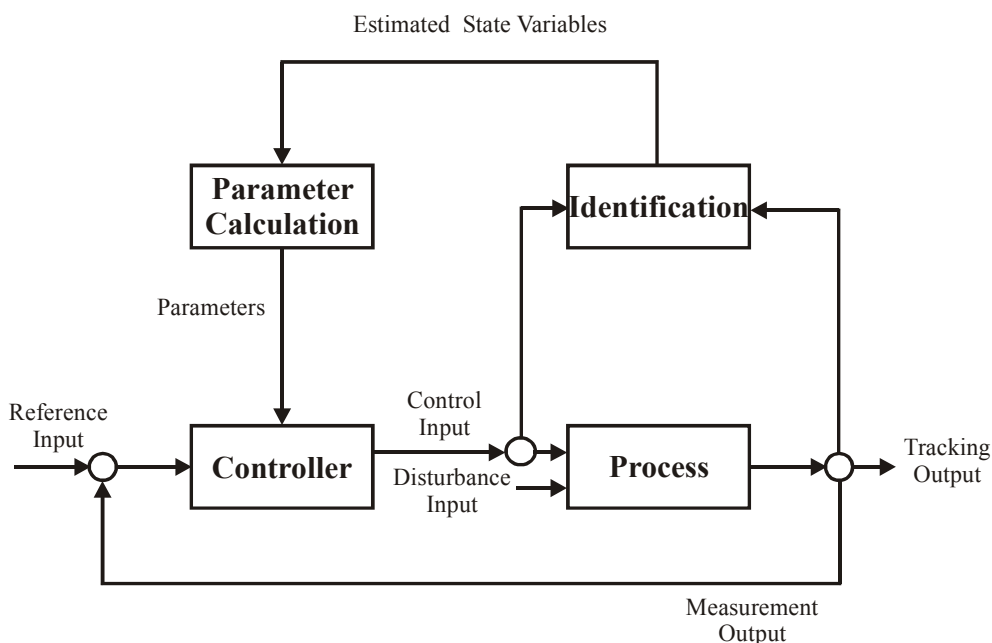


Figure 3.14 Principle scheme for glucose control in the fed-batch process based on adaptive control system

The commonly used feedback control system (measurement output = tracking output) is coupled with process identification to get real time and smoothed state variables. These discrete-time estimated state variables are used to determine the parameters of a suitable controller. Thus controller can be adapted to a changing dynamic behavior of the bioprocess.

A minimum variance controller, MV3¹⁰¹, proved to be suitable for substrate (glucose) control of fermentation processes: minimum variance controllers try to minimize a function $F_{(t+1)}$ which is given by the sum of the square of the tracking output difference from the reference input ($c_{G,\infty} - c_G$) at the discrete time $t + 1$, s_{t+1}^2 , and the square of the control input difference from the operating point ($q_{V,G,\infty} - q_{V,G}$) at the discrete time t , v_t^2 (Equation 3.3):

$$F_{(t+1)} = \{s_{(t+1)}^2 + u \cdot q_{V,(t)}^2\} \quad 3.3$$

The variable u is used as a weighting factor for control input difference. The tracking output difference $s_{(t+1)}$, is single mass balance for the substrate (Equation 2.18). That means the minimum variance controller needs not only real time estimated glucose concentration, \hat{c}_G , but also an estimation of the real time volumetric glucose consumption rate, \hat{Q}_S (Equation 3.4):

$$\hat{Q}_S = r_S \cdot c_X \quad 3.4$$

For real time estimation of these state variables a semi continuous extended Kalman filter was used⁹⁵⁻¹⁰⁰. The extended Kalman filter minimizes the variance of the estimation error of the state variables at the discrete time t when a time delayed measurement output is received. Real time estimation of the glucose concentration and the volumetric glucose consumption is then possible by solving the differential equations of state (Equations 3.5 – 3.7) and the measurement equation (Equation 3.8) up to real time:

$$\frac{d\hat{c}_G}{dt} = \frac{q_V \cdot (c_{G,0} - c_G)}{V_R} - \hat{Q}_G + g_{1,(t)} \quad 3.5$$

$$\frac{d\hat{Q}_G}{dt} = b + g_{2,(t)} \quad 3.6$$

$$\frac{db}{dt} = b \cdot \frac{q_V}{V_R} + g_{3,(t)} \quad 3.7$$

The added state variable, b , is the time dependent change in volumetric glucose consumption, $g_{1,(t)}$, $g_{2,(t)}$ and $g_{3,(t)}$ are random disturbances, q_V is volumetric flow rate, and V_R is reaction (medium) volume. Equation 3.5 allows the description of exponential glucose consumption in a fed-batch operated bioreactor. Measurement equation using $M_{(t)}$ as random error:

$$c_{G,ms} = c_G + M_{(t)}$$

3.8

The real time estimated glucose concentration and volumetric glucose consumption are used for parameter adaptation of the minimum variance controller (Figure 3.14). For the regulation of glucose concentration in the fed-batch experiments following parameter values were used:

g_1 [g dm ⁻³ h ⁻¹]:	0.5 absolute, 10 % relative
g_2 [g dm ⁻³ h ⁻¹]:	0.5 absolute, 10 % relative
g_3 [g dm ⁻³ h ⁻¹]:	0.5 absolute, 10 % relative
u [-]:	13
$c_{G,\infty}$ [g dm ⁻³]:	5
$q_{V,\infty}$ [dm ³ h ⁻¹]:	average value of ten last pump rates

3.7.2 Open-Loop Acetate Control System⁵⁵

The open-loop acetate control system was based on the correlation between volume-specific CO₂ transfer rate (CTR [mmol dm⁻³ h⁻¹]) and acetate consumption rate (ACR [mmol dm⁻³ h⁻¹]). CTR was calculated on-line using exhaust gas analysis data (for CO₂ and O₂), which were referred to the current reactor content (estimated by weight measurement) and which considered the actual airflow rate.

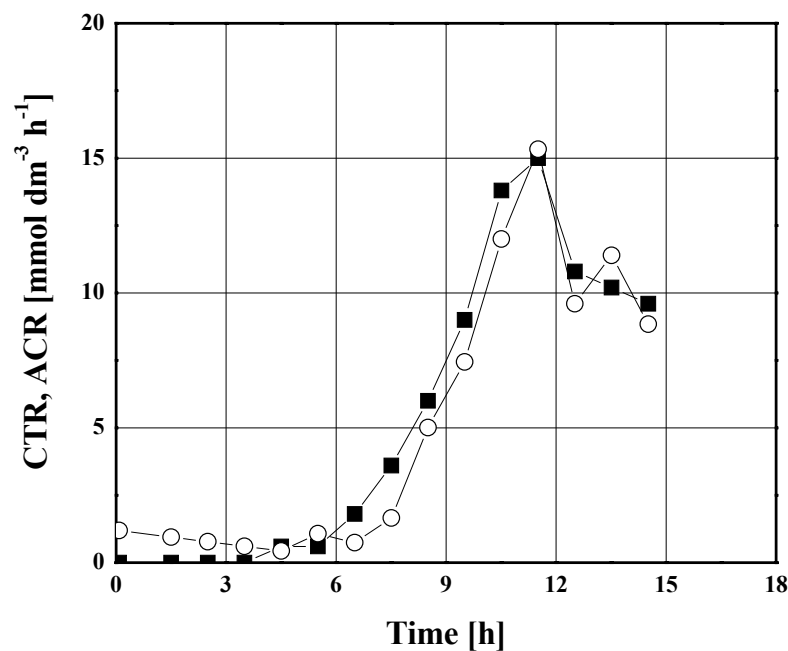


Figure 3.15 Correlation between ACR (○) and CTR (■)

According to a heuristic approach, the acetate feed was calculated depending on the estimated CTR using a feed solution (109 g dm^{-3} potassium acetate), which was fed into the bioreactor by a feeding system (YFC 01Z, Sartorius AG). As an outcome of experimental studies, a “simple” correlation between ACR and CTR was found (Figure 3.15, Equation 3.9).

$$ACR = CTR \quad 3.9$$

An optimum equal molar ratio was identified. Based on this correlation, the following feeding profile was empirically formulated (Equation 3.10):

$$q_M = \frac{M \cdot \rho \cdot CTR \cdot V_R}{c_A \cdot f} \quad 3.10$$

where $q_M [\text{g h}^{-1}]$ is acetate flow rate, $M [\text{g mol}^{-1}]$ is molecular weight of potassium acetate, $\rho [\text{g dm}^{-3}]$ is density of potassium acetate feed solution (approximately 1000 g dm^{-3}), $c_A [\text{g dm}^{-3}]$ is concentration of potassium acetate in the feed solution and $V_R [\text{dm}^3]$ is fermentation broth volume.

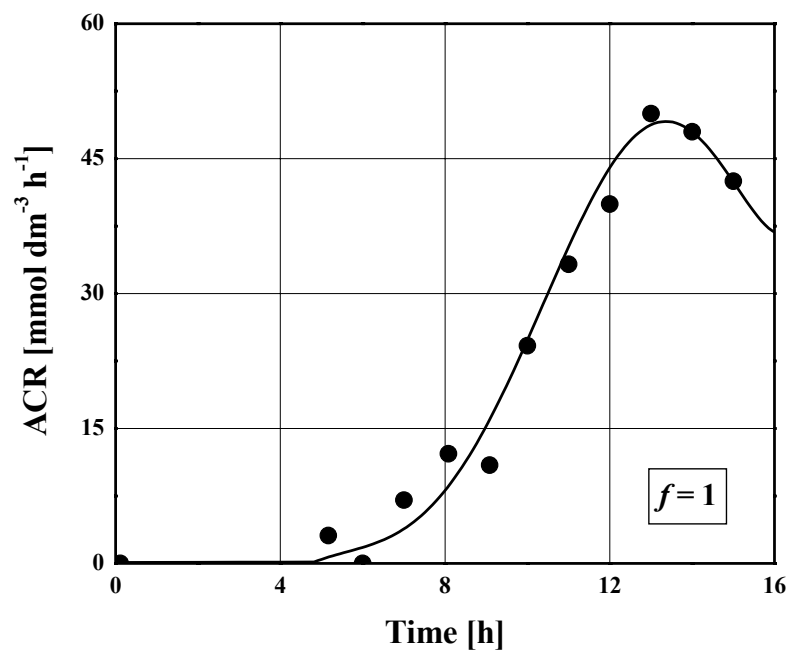


Figure 3.16 Comparison between ACR calculated on-line (—) and ACR calculated off-line (○) for saturated concentration of acetate ($f=1$)

This correlation was used to carry out a process under acetate limitation, saturation and accumulation by changing just parameter f . If parameter f was lower than 1, acetate was fed in an accumulation manner. If parameter f was equal to 1, acetate was fed in a saturation

manner, and if parameter f was higher than 1, acetate was fed in a limitation manner. A comparison of ACR calculated on-line (Equation 3.9) and ACR calculated off-line (on the basis of HPLC results for acetate concentrations and amount of acetate fed in bioreactor) for acetate saturating conditions ($f = 1$) is shown in Figure 3.16.

3.8 Unstructured Model for the Bioconversion of Glucose to Pyruvate

3.8.1 Model Theory

The mathematical models were derived based on the following assumptions:

- a) Glucose and acetate were only limiting substrates, all other nutrients like nitrogen, phosphate, and growth factors are in excess supply;
- b) There was no oxygen effect on biomass growth and bioconversion of glucose to pyruvate;
- c) Glucose and acetate were utilized simultaneously for biomass growth;
- d) Product formation was non-associated to the microbial growth
- e) Bioconversion of glucose to pyruvate was an overall one step enzymatic reaction;
- f) Pyruvate production was inhibited by high pyruvate concentrations.

3.8.2 Kinetic Equations

Three different models were developed. The mathematical descriptions of biomass growth, substrate consumption, and product formation, for the bioconversion of glucose to pyruvate by *E. coli* YYC202 *ldhA::Kan* strain, were taken into account. In Model 1 biomass formation was described as simplified modification of cybernetic model^{114-117,125,126}. Multiple substrate Monod kinetics was used for description of biomass growth in Model 2^{74,118,119}. In both models, Model 1 and Model 2, pyruvate formation was presented with modified Michaelis-Menten equation for noncompetitive inhibition with product¹²⁰. In Model 3 biomass growth was described with multiple substrate Monod kinetics. In this model pyruvate formation was presented by simple Michaelis-Menten enzyme kinetic¹²¹. Yield coefficient pyruvate/glucose in Model 3 was assumed to be time dependent and function of pyruvate concentration.

3.8.2.1 Simplified Cybernetic Model – Model 1

The total rate of biomass production was assumed to be the sum (Equation 3.13) of contributions of individual substrates, glucose (Equation 3.11) and acetate (Equation 3.12):

$$\mu_G = \mu_{MAX,G} \cdot \frac{c_G}{K_S^G + c_G} \quad 3.11$$

$$\mu_A = \mu_{MAX,A} \cdot \frac{c_A}{K_S^A + c_A} \quad 3.12$$

$$\mu = \mu_G + \mu_A \quad 3.13$$

The biomass dependent substrate consumption rates are expressed in Equations 3.14 and 3.15.

$$r_G = \frac{\mu_G}{Y_{X/G}} \quad 3.14$$

$$r_A = \frac{\mu_A}{Y_{X/A}} \quad 3.15$$

Modified Michaelis-Menten equation for noncompetitive inhibition with product¹²⁰ can be expressed as

$$r_P = V_{MAX} \cdot \frac{c_G}{K_m^G + c_G} \cdot \left(1 - \frac{c_P}{c_{P,MAX}} \right) \quad 3.16$$

where $c_{P,MAX}$ is critical pyruvate concentration above which reaction stops. The specific substrate consumption rates (r_G and r_A) includes a growth linked parts ($\mu/Y_{X/G,MAX}$ and $\mu/Y_{X/A,MAX}$) and a non-growing linked parts (m_G and m_A), which takes into account the maintenance energy demand^{74,121,122}. As the result of maintenance metabolism the apparent values for the yield coefficients ($Y_{X/G}$, $Y_{X/A}$) are lower than the maximum theoretical values ($Y_{X/G,MAX}$, $Y_{X/A,MAX}$).

Four different sub-models, namely 1a (Equations 3.17 and 3.18), 1b (Equations 3.19 and 3.20), 1c (Equations 3.21 and 3.22), and 1d (Equations 3.23 and 3.24), were developed, assuming dependency and independency of yield coefficients on biomass growth and maintenance energy demand.

Model 1a:

$$Y_{X/G} = \frac{Y_{X/G,MAX} \cdot \mu}{Y_{X/G,MAX} \cdot m_G + \mu} \quad 3.17$$

$$Y_{X/A} = \frac{Y_{X/A,MAX} \cdot \mu}{Y_{X/A,MAX} \cdot m_A + \mu} \quad 3.18$$

Model 1b:

$$Y_{X/G} = const. \quad 3.19$$

$$Y_{X/A} = \frac{Y_{X/A,MAX} \cdot \mu}{Y_{X/A,MAX} \cdot m_A + \mu} \quad 3.20$$

Model 1c:

$$Y_{X/G} = \frac{Y_{X/G,MAX} \cdot \mu}{Y_{X/G,MAX} \cdot m_G + \mu} \quad 3.21$$

$$Y_{X/A} = \text{const.} \quad 3.22$$

Model 1d:

$$Y_{X/G} = \text{const.} \quad 3.23$$

$$Y_{X/A} = \text{const.} \quad 3.24$$

3.8.2.2 Multiple-substrate Monod Kinetics – Model 2

The multiple substrate Monod kinetic^{119,123} (multiplicative Monod Kinetic) is frequently used to describe the effects of dual limitation on cell growth. The multiple substrate Monod kinetic assumes that, if two essential substrates are present at sub-saturating concentrations, both directly limit the overall growth rate (μ_{MAX}), and the limitation effects are multiplicative (Equation 3.25).

$$\mu = \mu_{MAX} \cdot \frac{c_G}{K_S^G + c_G} \cdot \frac{c_A}{K_S^A + c_A} \quad 3.25$$

$$r_G = \frac{\mu}{Y_{X/G}} \quad 3.26$$

$$r_A = \frac{\mu}{Y_{X/A}} \quad 3.27$$

$$r_P = V_{MAX} \cdot \frac{c_G}{K_m^G + c_G} \cdot \left(1 - \frac{c_P}{c_{P,MAX}} \right) \quad 3.28$$

In this approach pyruvate formation is equal to that one used in Model 1. Additionally, four different sub-models, namely 2a (Equations 3.29 and 3.230), 1b (Equations 3.31 and 3.32), 1c (Equations 3.33 and 3.34), and 1 d (Equations 3.35 and 3.36), are developed, assuming dependency and independency of yield coefficients on biomass growth and maintenance energy demand.

Model 2a:

$$Y_{X/G} = \frac{Y_{X/G,MAX} \cdot \mu}{Y_{X/G,MAX} \cdot m_G + \mu} \quad 3.29$$

$$Y_{X/A} = \frac{Y_{X/A,MAX} \cdot \mu}{Y_{X/A,MAX} \cdot m_A + \mu} \quad 3.30$$

Model 2b:

$$Y_{X/G} = const. \quad 3.31$$

$$Y_{X/A} = \frac{Y_{X/A,MAX} \cdot \mu}{Y_{X/A,MAX} \cdot m_A + \mu} \quad 3.32$$

Model 2c:

$$Y_{X/G} = \frac{Y_{X/G,MAX} \cdot \mu}{Y_{X/G,MAX} \cdot m_G + \mu} \quad 3.33$$

$$Y_{X/A} = const. \quad 3.34$$

Model 2d:

$$Y_{X/G} = const. \quad 3.35$$

$$Y_{X/A} = const. \quad 3.36$$

3.8.2.3 Multiple-substrate Monod Kinetics with Variable $Y_{P/G}$ – Model 3

Basically, Model 3 (Equations 3.37 – 3.43) is Model 2b, simplified in bioconversion part. Simple Michaelis-Menten kinetics (Equation 3.40) was used in this model approach. Yield coefficient $Y_{P/G}$ was assumed to be function of pyruvate extra cellular concentration and time dependent.

$$\mu = \mu_{MAX} \cdot \frac{c_G}{K_S^G + c_G} \cdot \frac{c_A}{K_S^A + c_A} \quad 3.37$$

$$r_G = \frac{\mu}{Y_{X/G}} \quad 3.38$$

$$r_A = \frac{\mu}{Y_{X/A}} \quad 3.39$$

$$r_P = V_{MAX} \cdot \frac{c_G}{K_m^G + c_G} \quad 3.40$$

with

$$Y_{X/G} = \text{const.} \quad 3.41$$

$$Y_{X/A} = \frac{Y_{X/A,MAX} \cdot \mu}{Y_{X/A,MAX} \cdot m_A + \mu} \quad 3.42$$

$$Y_{P/G} = Y_{P/G,MAX} \cdot \left(1 - \frac{c_P}{c_{P,MAX}} \right) \quad 3.43$$

3.8.3 Mass Balances

The mathematical model (Equations 3.44 – 3.48) based on the mass balance of the components in a fed-batch reactor is represented by the following differential equations:

$$\frac{dc_X}{dt} = -\frac{q_V}{V} \cdot c_X + \mu \cdot c_X \quad 3.44$$

$$\frac{dc_G}{dt} = -\frac{q_V}{V} \cdot c_G + \frac{q_{V,G}}{V} c_{G,0} - r_G \cdot c_X - r_P \cdot c_X \quad 3.45$$

$$\frac{dc_A}{dt} = -\frac{q_V}{V} \cdot c_A + \frac{q_{V,A}}{V} c_{A,0} - r_A \cdot c_X \quad 3.46$$

$$\frac{dc_P}{dt} = -\frac{q_V}{V} \cdot c_P + r_P \cdot c_X \cdot Y_{P/G} \quad 3.47$$

$$\frac{dV}{dt} = q_{V,G} + q_{V,A} = q_V \quad 3.48$$

where V is the reactor volume, q_V is overall volumetric flow rate in the time t , $q_{V,G}$ and $q_{V,A}$ are volumetric flow rates of substrates (glucose and acetate) in the time t , and $c_{G,0}$ and $c_{A,0}$ are glucose and acetate concentration in the feed.

The fed-batch reactor experiments (see section 3.6.1) were performed under different conditions, concerning glucose-feeding profile (it was kept constant during experiment at three different levels: 10 g h⁻¹, 20 g h⁻¹ and 30 g h⁻¹), to generate experimental data for parameter estimation of assumed models. Acetate was fed according to developed acetate control system under acetate saturating conditions (see section 3.7.2).

3.9 Mathematical Model of the Electrodialysis Process

A simple mathematical model representing the ion and water transport behavior of the electrodialysis process to concentrate pyruvic acid under the influence of different current (current density) was developed. It was assumed that the amount of the water transferred from the feed compartment (FC) to acid compartment (AC) is directly proportional to the current

density applied. The water transport trend from the FC to the AC is expressed in the form of Equation 3.49:

$$V_{AC}^t = V_{AC}^0 + \Delta V_{AC} \quad 3.49$$

where V_A^t is the volume of AC at time t , V_A^0 the initial volume of AC and ΔV_A the volume of water being transported from the FC to AC. The term ΔV_A could be replaced by the term $(\alpha + \beta \cdot i) \cdot t$ represents the amount of the water being transferred from the FC to the AC (Equation 3.50). Both α and β terms are called phenomenological coefficients⁸⁸, and i is current density (Equation 2.31).

$$V_{AC}^t = V_{AC}^0 + (\alpha + \beta \cdot i) \cdot t \quad 3.50$$

The rate of ion transport was determined by evaluating the pyruvate concentration in the AC at any time t (Equation 3.51)⁸⁸.

$$c_{AC}^t = \frac{(A + B \cdot c_{FC}^0) \cdot I \cdot t + c_{AC}^0 \cdot V_{AC}^0 \cdot F}{V_{AC}^t \cdot F + (\alpha + \beta \cdot i) \cdot t \cdot F + B \cdot I \cdot t} \quad 3.51$$

where A and B are ion transport rate constants, c_{FC}^0 is initial pyruvate concentration in the FC, I is current, c_{AC}^0 is initial pyruvate concentration in the AC, V_{AC}^0 is the initial volume of the AC, and F is Faraday constant. Equation 3.51 is derived from the different equations for calculation of current efficiency (Equations 3.52 and 3.53)⁸⁸.

$$CE = \frac{(c_{AC}^t \cdot V_{AC}^t - c_{AC}^0 \cdot V_{AC}^0) \cdot F}{I \cdot t} \quad 3.52$$

$$CE = A - B \cdot (c_{AC}^t - c_{FC}^0) \quad 3.53$$

3.10 Data Handling

The model parameters were estimated by the non-linear regression analysis. The associated model parameters have been identified by the non-linear optimization using the Nelder-Mead method¹¹¹. The numerical value of the parameters were evaluated by fitting the model to the experimental data with "Scientist"¹²⁴ computer programme which performed the non-linear regression analysis. The model equations were solved numerically by the fourth order Runge-Kutta algorithm. The set of optimum parameters was used for the simulation. The simulation data were compared with the obtained experimental data. The "Episode" algorithm for stiff system of differential equations, implemented in the "Scientist" software package, was used for the simulations.

4. RESULTS AND DISCUSSION

4.1 Preliminary Investigations

4.1.1 Shake Flasks Experiments

Shake flask experiments were performed in order to collect preliminary knowledge about pyruvate production process from glucose by *Escherichia coli* YYC202 strain. Because of the strain genotype (see section 3.1) glucose and acetate consumption were assumed to be key process parameters. Three process conditions, concerning starting concentrations of glucose and acetate were analyzed, (1) "low" glucose and acetate concentration ($c_G = 4 \text{ mmol dm}^{-3}$, $c_{Ac} = 2 \text{ mmol dm}^{-3}$); (2) "high" glucose concentration and "low" acetate concentration ($c_G = 20 \text{ mmol dm}^{-3}$, $c_{Ac} = 2 \text{ mmol dm}^{-3}$); and (3) "high" glucose concentration and "high" acetate concentration ($c_G = 20 \text{ mmol dm}^{-3}$, $c_{Ac} = 20 \text{ mmol dm}^{-3}$).

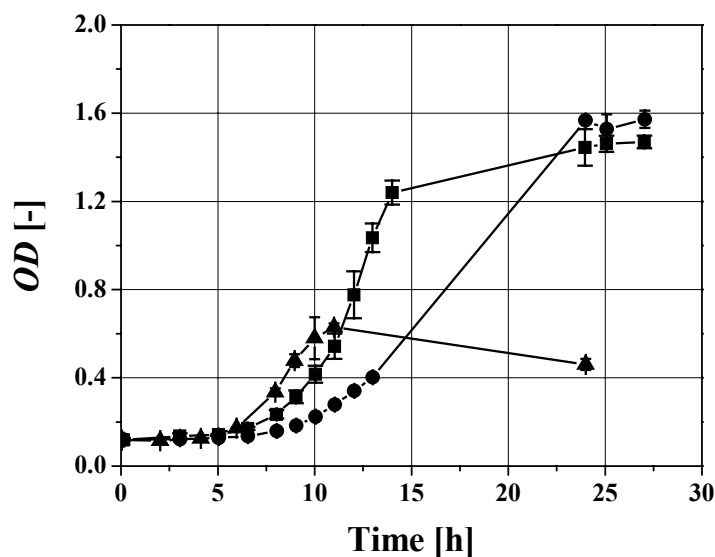


Figure 4.1 Effect of glucose and acetate starting concentrations on biomass growth (OD) in shake flask experiments using *Escherichia coli* YYC202. (1) - ▲; (2) - ■; (3) - ●

Significant inhibiting effect on the biomass growth (Figure 4.1, Table 4.1) and on the glucose consumption (Figure 4.2) was observed in the experiment at the higher acetate starting concentration (process conditions (3)). These results were compared with the experiments at lower acetate starting concentration (process conditions (1) and (2)). Such

result was expected because of known acetate inhibiting effect on other *E. coli* strains¹⁰⁴. In No negative effect of glucose on biomass growth rate (Figure 4.1, Table 4.1) was observed at the investigated range of glucose starting concentrations (2 – 20 mmol dm⁻³).

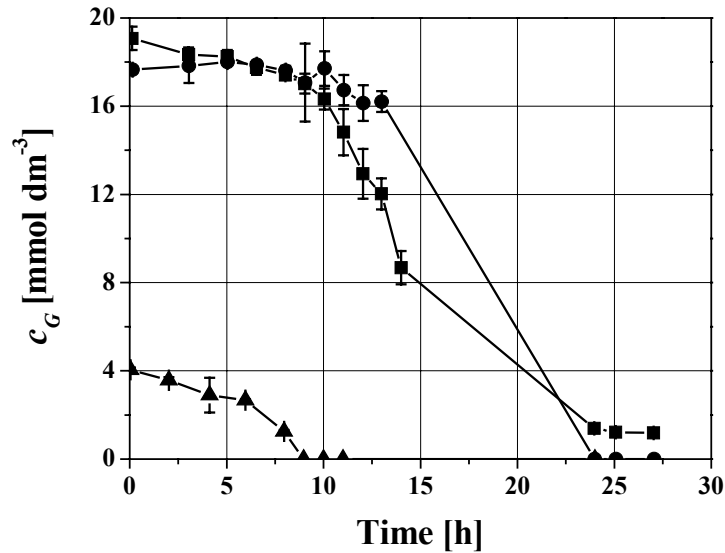


Figure 4.2 Effect of glucose and acetate starting concentrations on glucose concentration (c_G) profiles in shake flask experiments using *Escherichia coli* YYC202. (1) - \blacktriangle ; (2) - \blacksquare ; (3) - \bullet

Table 4.1 Effect of glucose and acetate starting concentrations on μ_{MAX} , $Y_{P/G}$, STY and final c_P for acetate controlled fed-batch fermentations using *Escherichia coli* YYC202 *ldhA::Kan* strain.

	(1)	(2)	(3)
μ_{MAX} [h ⁻¹]	0.35	0.35	0.22
$Y_{P/G}$ [mol mol ⁻¹]	1.75	1.85	1.86
STY [g dm ⁻³ d ⁻¹]	1.8	2.8	3.0

Additionally, molar yield pyruvate/glucose ($Y_{P/G}$) achieved in performed experiments (Table 4.1) is closed to the maximum theoretical yield of glucose-based pyruvate production (2 mol pyruvate/mol glucose). Low space-time yield (STY) obtained (Table 4.1) in the shake flask experiments was expected because of low biomass concentration achieved at low starting concentration of substrates. In the shake flasks experiment pH was not

controlled. Hence pH decreases significantly during the experiments. Final pH approximately 5 was achieved at all process conditions. This value is outside of optimal range for biomass growth and pyruvate production ($\text{pH} \approx 7.0$)⁵³. Furthermore, there was no oxygen supply (strain is aerobic) and experiments were performed on complex medium.

4.1.2 Batch Experiment with Acetate Pulses

To eliminate negative influence of low pH on process, and to ensure oxygen supply in the experiment, cultivation was performed in the bioreactor, equipped with standard control units of pH, pressure, temperature, aeration, stirrer speed (see section 3.5). Limitation by high acetate concentration in the medium was avoided by performing the experiment at low acetate concentration. Every time when the acetate was consumed, indicating an increase of dissolved oxygen concentration level (pO_2), new fresh acetate was added (5 mmol dm⁻³) in the bioreactor (Figure 4.3). Experiment was realized as a batch process concerning glucose.

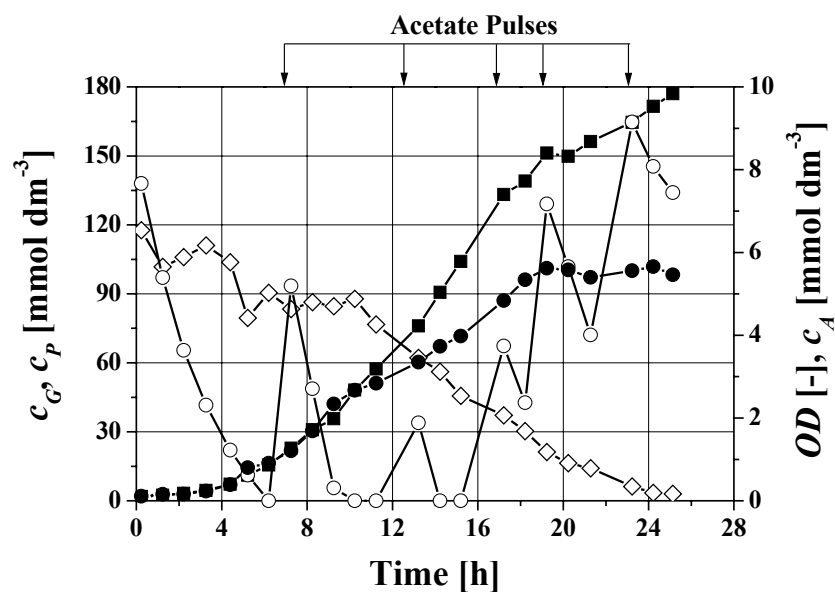


Figure 4.3 Influence of acetate pulses on biomass growth, glucose consumption and pyruvate production in batch process using *E. coli* YYC202 strain. Biomass - ●; glucose - ◇; acetate - ○; pyruvate - ■

As was expected, final biomass and final pyruvate concentration were higher than in the shake flasks experiment, because of higher starting glucose concentration. Integral STY of 14.95 g dm⁻³ d⁻¹ obtained in the batch experiment with acetate pulses was 5 fold higher than

the best one achieved in the shake flasks experiment. Contrary, integral $Y_{P/G}$ was significantly higher in the shake flasks experiments (Table 4.1) than in the experiment with acetate pulses ($Y_{P/G} = 1.49 \text{ mol mol}^{-1}$). Probably because the larger part of glucose flux was used for biomass growth.

Integral $Y_{P/G}$ achieved in the batch experiment with acetate pulses was close to the best one published so far (1.6 mol mol^{-1})¹⁰⁶. However, integral STY and final c_P of this process were very low ($14.95 \text{ g dm}^{-3} \text{ h}^{-1}$; 180 mmol dm^{-3}), which significantly hampers its use for scale-up purposes.

4.1.3 Fed-batch Experiment

Average acetate consumption rate was calculated to be $1.6 \text{ mmol dm}^{-3} \text{ h}^{-1}$ from batch experiment with acetate pulses. Fed-batch experimental set-up was developed and acetate was fed into bioreactor with constant rate calculated from previously identified average acetate consumption rate. Starting glucose concentration was equal as in the batch experiment at acetate pulses, and glucose was not fed into bioreactor. Experimental results are summarized in the Figure 4.4.

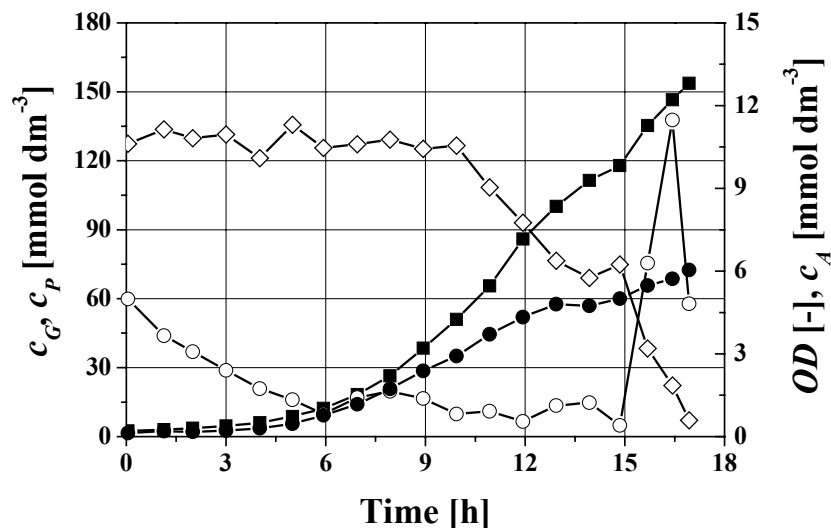


Figure 4.4 Influence of acetate feed rate on biomass growth, glucose consumption and pyruvate production in fed-batch process using *E. coli* YYC202 strain. Biomass - ●; glucose - ◇; acetate - ○; pyruvate - ■

Integral STY in the fed-batch experiment was improved 25 % up to $19.17 \text{ g dm}^{-3} \text{ d}^{-1}$ comparing it with integral STY achieved in the batch experiment with acetate pulses.

Unfortunately final c_P (154 mmol dm⁻³) and integral $Y_{P/G}$ (1.28 mol mol⁻¹) were lower than in the batch experiment with acetate pulses.

The correlation between acetate consumption rate (ACR) and CO₂ transfer rate (CTR) was founded and open loop acetate control system based on on-line measurement of O₂ and CO₂ amount in exhaust gases was established (see section 3.7.2). This control system was used in the acetate controlled (designed for optimization of model parameters and validation of models) and controlled fed-batch processes.

4.2 Controlled Fed-batch Process

Fermentations were realized as a two-stage fed-batch process. During the first phase (cell growth and early pyruvate production stage) glucose and acetate were fed according to the process control developed (see sections 3.7.1 and 3.7.2). After biomass concentration remained constant for 3 hours, the second phase (high-selectively pyruvate production stage) was started by stopping the acetate feed so that only glucose was fed to the culture.

4.2.1 Fed-batch Fermentation of *E. coli* YYC202

A fed-batch fermentation set-up was used to study the effects of different acetate feeding strategies (limitation $f = 1.5$, saturation $f = 1$, and accumulation $f = 0.8$) on molar pyruvate/glucose ($Y_{P/G}$) yield, integral space-time yield (STY) and final pyruvate titer c_P ⁵⁵. Acetate influence was investigated at constant glucose concentration of 5 ± 1 g dm⁻³. This glucose level was chosen to ensure saturating conditions for glucose uptake (the K_S value for the glucose-specific phosphoenolpyruvate:carbohydrate phosphotransferase system (PTSG) is known to be half-saturated at 3 to 10 μmol dm⁻³, and that of the mannose-specific (PTSM) at 1.3 mmol dm⁻³ ^{102,103}). Figures 4.5 and 4.6 indicate that the limiting acetate supply caused lower maximal biomass and pyruvate titers compared to saturating or accumulating acetate feeding strategies.

This result can be explained by the strain's acetate auxotrophy demanding a sufficient external acetate supply for cell growth and maintenance, which obviously was not achieved using the acetate-limiting feeding procedure ($f = 1.5$). As a consequence, lower $Y_{P/G}$ and STY were observed in the experiment (Table 4.2).

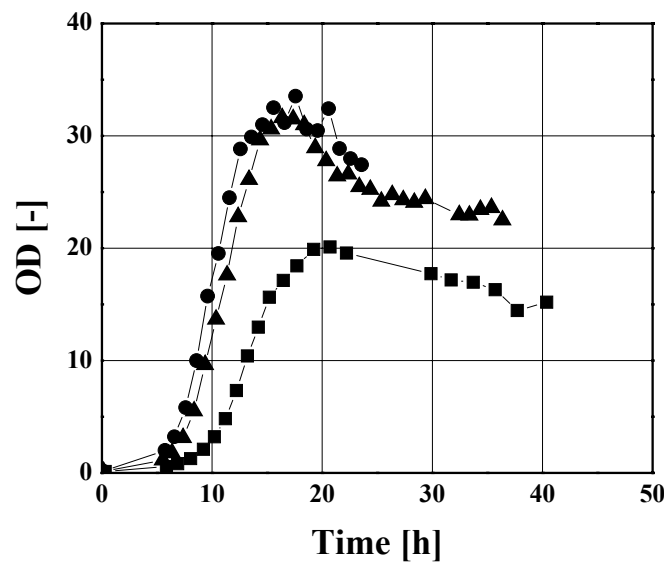


Figure 4.5 Effect of acetate feeding strategies on biomass concentration in fed-batch process using *Escherichia coli* YYC202 strain; acetate limitation ($f = 1.5$) - ■; acetate saturation ($f = 1.0$) - ●; acetate accumulation ($f = 0.8$) - ▲

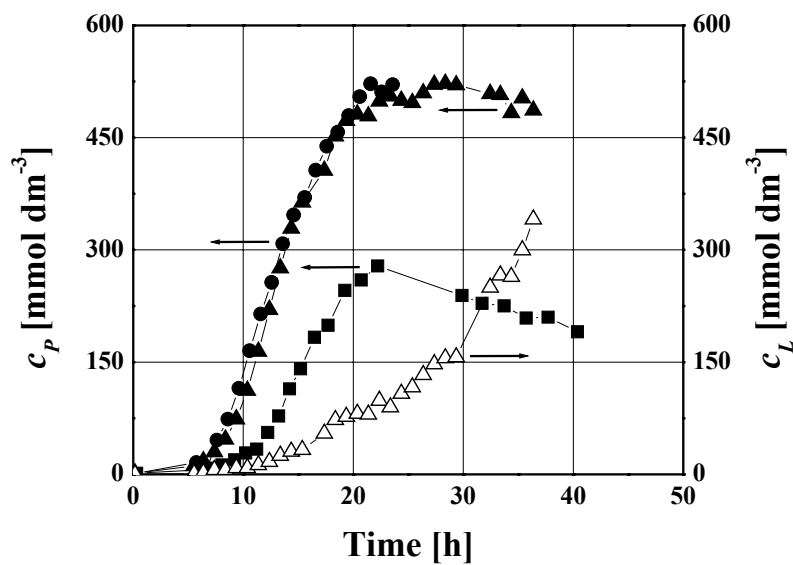


Figure 4.6 Effect of acetate feeding strategies on pyruvate concentration (c_p) in fed-batch process using *Escherichia coli* YYC202 strain; acetate limitation ($f = 1.5$) - ■; acetate saturation ($f = 1.0$) - ●; acetate accumulation ($f = 0.8$) - ▲. Lactate concentration (c_L) in experiment with acetate accumulation - Δ

Table 4.2 Influence of different acetate feeding strategies on $Y_{P/G}$, STY and final c_P for fed-batch fermentations using *Escherichia coli* YYC202 strain.

*Calculated for 24 h of process time (normal fermentation time 35 h)

	$f = 1.5$	$f = 1.0^*$	$f = 0.8$
$Y_{P/G}$ [mol mol ⁻¹]	0.34	0.86	0.80
STY [g dm ⁻³ d ⁻¹]	12.3	46.5	30.0
c_P [mmol dm ⁻³] ([g dm ⁻³])	209 (18.4)	521 (45.8)	500 (44.0)

Acetate maintenance demands as well as additional carbon and energy requirements for cell growth strongly decrease the maximal achievable pyruvate/glucose yields. On the other hand, no negative effect of acetate accumulation on pyruvate production and biomass growth was observed. This seems to be in contrast to preliminary investigations in the shake flask experiments and previously published results focusing on other *E. coli* strains, where inhibiting acetate concentrations were identified at about 5 to 10 g dm⁻³ ¹⁰⁴. In the case of *E. coli* YYC202 acetate concentrations even higher than 20 g dm⁻³ were still tolerated. Maximal c_P was limited to concentrations of about 500 ± 20 mmol dm⁻³, irrespective of whether saturating or accumulating acetate feeds were used. At optimal process conditions (accumulated concentration of acetate) a final c_P of about 500 mmol dm⁻³ (44 g dm⁻³), $Y_{P/G}$ of 0.80 mol mol⁻¹ and an integral STY of 30 g dm⁻³ d⁻¹ were obtained. Unfortunately, strong co-production of lactate (final lactate concentration higher than 300 mmol dm⁻³ (26 g dm⁻³)) was observed in each experiment. Interestingly, a significant increase of lactate production was observed after the final pyruvate concentration reached its maximal value of about 500 mmol dm⁻³.

Hence, we concluded that co-production of lactate cannot be suppressed by process engineering means and that the construction of a new genotype is advantageous. As a consequence, a new production strain *Escherichia coli* YYC202 *ldhA::Kan* was constructed, in which the gene *ldhA* encoding for lactate dehydrogenase was mutated so the conversion of pyruvate to lactate was inactivated⁵⁴.

4.2.2 Fed-batch Fermentation of *E. coli* YYC202 *ldhA::Kan*

A new series of fed-batch experiments was performed with the new strain using the same process control as described above. The effects of different acetate feeding strategies at

constant glucose concentration of 5 g dm^{-3} were analyzed^{55, 105}. As a result, the same acetate limiting effect on biomass growth (Figure 4.7) and on pyruvate production (Figure 4.8) was observed, but lactate was not produced at all. In analogy to the experimental results using *E. coli* YYC202, acetate limitation subsequently caused lower biomass growth and pyruvate production. There was no significant difference between the effect of saturated or accumulated concentration of acetate on pyruvate production.

It should be stressed that the long lag-phase during the acetate accumulating experiment was caused by technical pH control problems and is not characteristic of the "normal" process. From Figure 4.7 we conclude that the proper selection of factor f of Equation 3.10 clearly influences the optimal fermentation performance (see also Table 4.3). As a result, a final c_P higher than 700 mmol dm^{-3} (62 g dm^{-3}), $Y_{P/G}$ of $1.11 \text{ mol mol}^{-1}$ and an integral STY of $42 \text{ g dm}^{-3} \text{ d}^{-1}$ were achieved under the best conditions, which means with f set at 0.8.

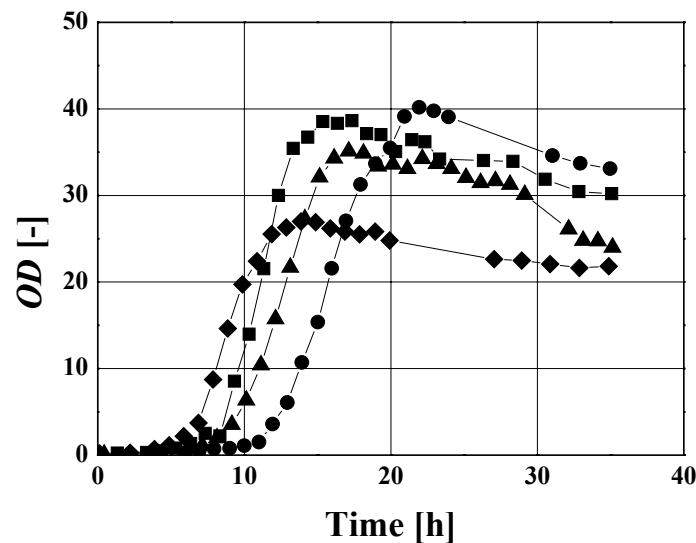


Figure 4.7 Effect of acetate feeding strategies on biomass concentration in fed-batch process using *Escherichia coli* YYC202 *ldhA::Kan* strain; acetate limitation ($f = 2.0$) - \blacklozenge ; acetate limitation ($f = 1.5$) - \blacksquare ; acetate saturation ($f = 1.0$) - \bullet ; acetate accumulation ($f = 0.8$) - \blacktriangle

Comparing these results with those of *E. coli* YYC202, a 40 % increase of the final pyruvate titer can be stated together with a 39 % increase of integral pyruvate/glucose yield. The final titer and (to a certain extent) also the final yield are comparable to the best results of Li et al.¹⁰⁶ using *Torulopsis glabrata*. However, it should be noticed that the space-time yield

of the *E. coli* process is much higher. Here $42 \text{ g dm}^{-3} \text{ d}^{-1}$ is produced, which is more than 40 % higher than in the yeast process, which needs 56 h compared to only 30 h using the *E. coli* strain.

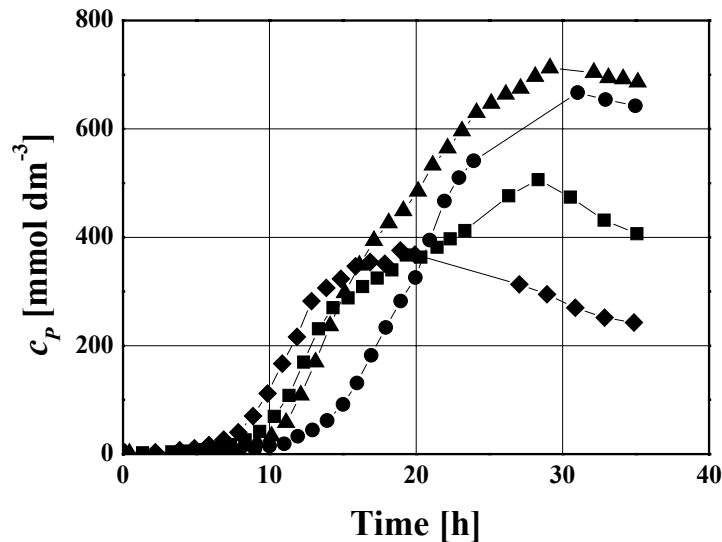


Figure 4.8 Effect of acetate feeding strategies on pyruvate concentration (c_P) in fed-batch process using *Escherichia coli* YYC202 *ldhA::Kan* strain; acetate limitation ($f = 2.0$) - \blacklozenge ; acetate limitation ($f = 1.5$) - \blacksquare ; acetate saturation ($f = 1.0$) - \bullet ; acetate accumulation ($f = 0.8$) - \blacktriangle

Table 4.3 Influence of different acetate feeding strategies on $Y_{P/G}$, STY and final c_P for fed-batch fermentations using *Escherichia coli* YYC202 *ldhA::Kan* strain

	$f = 2.0$	$f = 1.5$	$f = 1.0$	$f = 0.8$
$Y_{P/G} [\text{mol mol}^{-1}]$	0.42	0.68	0.96	1.11
$STY [\text{g dm}^{-3} \text{ d}^{-1}]$	14.7	24.4	36.0	42.0
$c_P [\text{mmol dm}^{-3}] ([\text{g dm}^{-3}])$	242 (21.3)	406 (35.7)	633 (55.7)	704 (62.0)

However, when pyruvate curves, given in Figure 4.8, are studied the question arises: "Why the maximum titer of about 700 mmol dm^{-3} cannot be increased?". To elucidate the problem Figure 4.9 indicates that pyruvate production rates (r_P) strongly decrease with increasing extracellular pyruvate concentrations. This rate is equal to zero at the end of fed-batch fermentation (in the last 5 hours of fermentation there was no pyruvate production at

all). Hence, we concluded that high extracellular pyruvate titers might have an inhibiting effect.

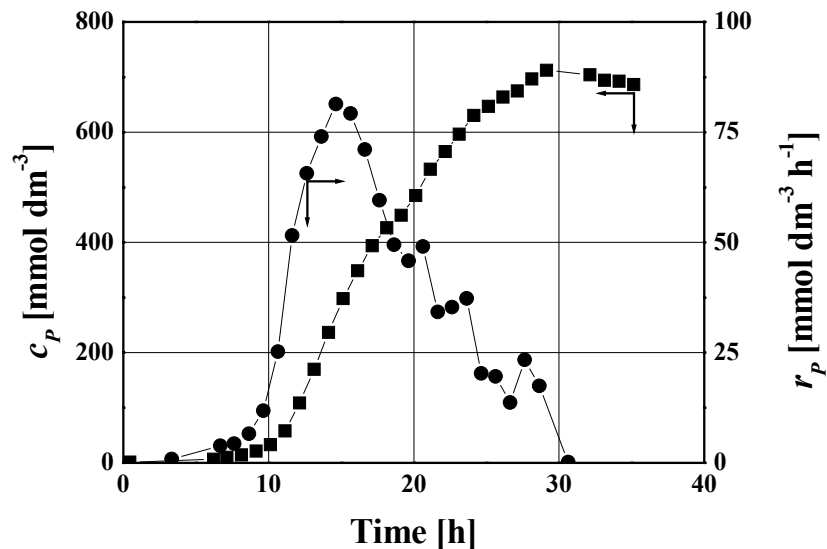


Figure 4.9 Effect of pyruvate extra-cellular concentrations (■) on pyruvate production rate (●). Results obtained in the experiment with acetate accumulation ($f = 0.8$) for *E. coli* *YYC202 ldhA::Kan* strain. Specific pyruvate production rate was calculated differentially.

The experiments were performed to test the hypothesis. For instance, cell samples were taken after the end of the fed-batch fermentation (at high pyruvate concentrations), washed several times in physiological solution (to avoid any inhibiting effect of pyruvate), resuspended in a buffer solution without any nutrient except glucose and cultivated on the shaker. The treated biomass was capable of converting glucose into pyruvate almost stoichiometrically (data not shown), which sustained our hypothesis.

Additionally, cell samples, taken during lab-scale fed-batch pyruvate production, were used to determine their intracellular pyruvate concentrations (Figure 4.10), for which purpose the method and the devices described in section 3.3.5 were used⁹². As shown, intra- and extracellular pyruvate concentrations were compared. The results showed that extra-cellular pyruvate concentrations are about 10^2 -fold higher than the intra-cellular counterparts. We can conclude that active pyruvate transport is most likely to export pyruvate into the supernatant, contrary to our original assumption of pyruvate transport by diffusion. Additionally, intracellular ATP levels were determined (again using the method of Bucholz et al.⁹²), which

appeared to be very low (in the range of 0.5 mmol dm^{-3}). This might be an indication of an energy-coupled pyruvate export that becomes limited at high external pyruvate concentrations.

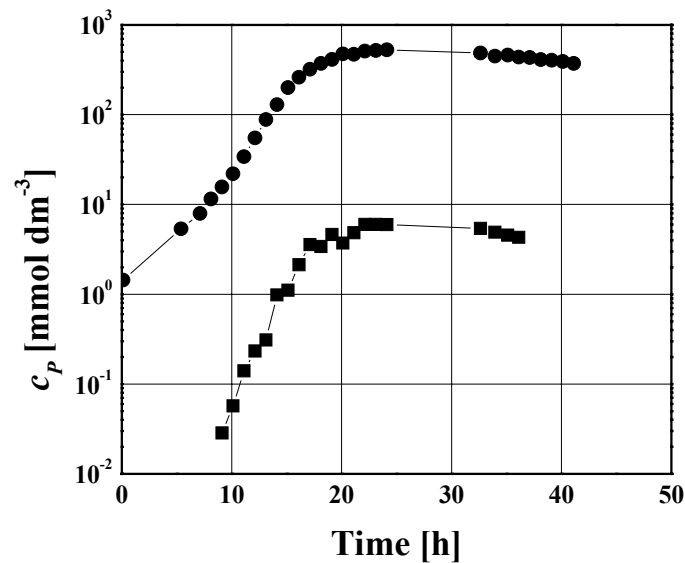


Figure 4.10 Comparison between intra- (■) and extra-cellular (●) concentration of pyruvate (c_P) in fed-batch experiment. Results obtained in the experiment with acetate accumulation ($f = 0.8$) for *E. coli* YYC202 strain

4.3 Continuous Fermentation with Cell Retention

Fed-batch experiments^{55, 105} already indicated that a high pyruvate/glucose yield could only be achieved when non-growing cells were used for the biotransformation of glucose. Otherwise, glucose together with the auxotrophic substrate acetate is consumed in significant amounts for cell growth. These studies lead to the conclusion that the high extra-cellular pyruvate titers "somehow" inhibit the microbial product synthesis. Maybe a futile cycling takes place but it is not identified until now.

Motivated by these findings a continuous fermentation with cell retention was investigated that should allow a high-selective pyruvate production with non-growing, retained cells in the presence of diluted extra-cellular pyruvate concentrations. As indicated in the section 3.6.3 above, a dilution rate of $D = 0.1 \text{ h}^{-1}$ was realized after a maximum cell density ($OD = 30$) was achieved at the end of the initial glucose- and acetate-controlled fed-batch period (about 14 h after inoculation, end of phase I, Figure 4.11). The glucose

containing feed of the following period also contained 0, 20 and 40 g dm⁻³ acetate in a series of three subsequent experiments.

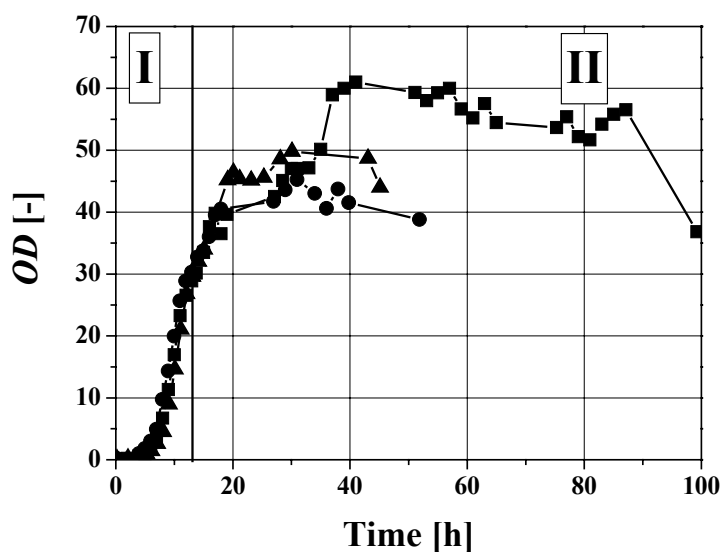


Figure 4.11 Effect of acetate concentrations (0 g dm⁻³ - ■; 20 g dm⁻³ - ▲; 40 g dm⁻³ - ●) in the glucose containing feed on biomass concentration and strain stability in the continuous fermentation with cell retention. Phase I – fed-batch period, Phase II – continuous period

Surprisingly, we observed that only the acetate-free feed enabled a continuous process lasting more than 80 h process time. Relatively high pyruvate concentrations (Figure 4.12) of about 600 mmol dm⁻³ were achieved in all experiments which caused a significant drop of the biomass specific pyruvate production rate (Figure 4.13) from about 6 (at the end of the fed-batch period) down to 2.0 – 2.5 mmol g_{CDW}⁻¹ h⁻¹ in the presence of pyruvate titers > 500 mmol dm⁻³ (in the continuous period).

Thus, maximum space-time-yields of 104 – 117 g dm⁻³ d⁻¹ were achieved together with low pyruvate/glucose yields of 1.10 – 1.24 mol mol⁻¹ (Table 4.4). From these results we concluded that an increase of dilution rate would be advantageous to maintain pyruvate formation on a high level. However, we qualified the long-term stability of the strain and the achievable product/substrate yields as non-sufficient. Hence other process alternatives were studied.

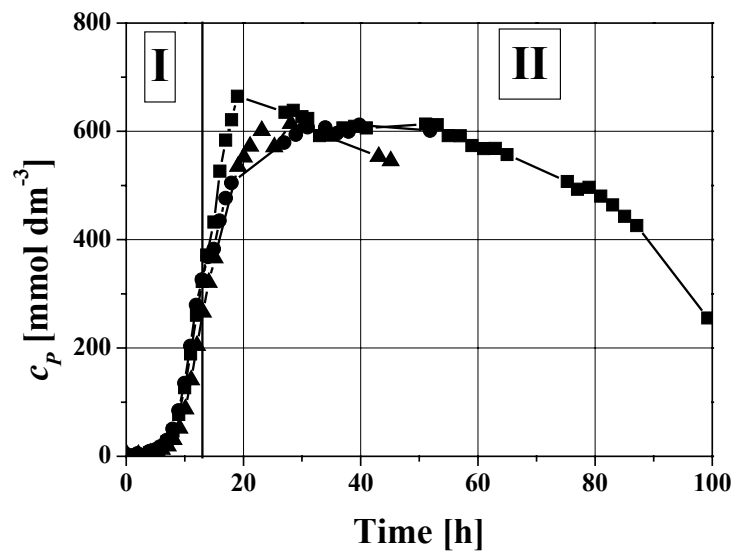


Figure 4.12 Effect of acetate concentrations (0 g dm^{-3} - ■; 20 g dm^{-3} - ▲; 40 g dm^{-3} - ●) in the glucose containing feed on the pyruvate concentrations in the continuous fermentation with cell retention. Phase I – fed-batch period, Phase II – continuous period

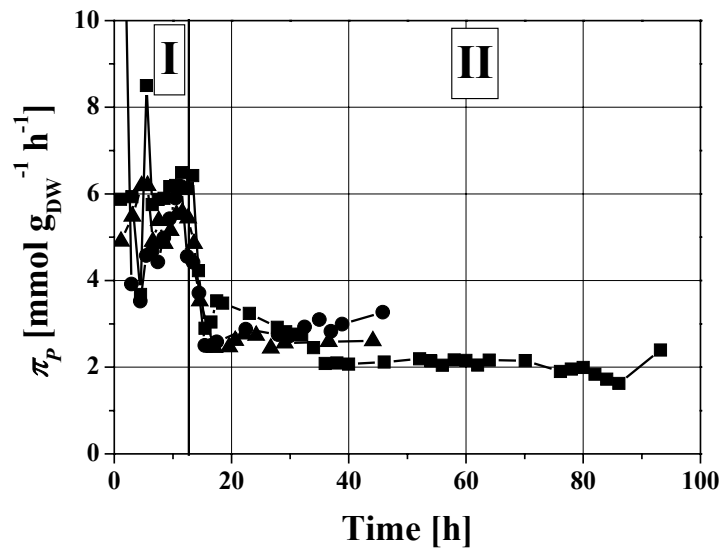


Figure 4.13 Effect of acetate concentrations (0 g dm^{-3} - ■; 20 g dm^{-3} - ▲; 40 g dm^{-3} - ●) in the glucose containing feed on the biomass specific pyruvate production rate (π_p) in the continuous fermentation with cell retention. Phase I – fed-batch period, Phase II – continuous period. Biomass specific pyruvate production rate was calculated differentially.

Table 4.4 Effect of acetate concentrations (0 g dm^{-3} - ■; 20 g dm^{-3} - ▲; 40 g dm^{-3} - ●) in the glucose containing feed on the $Y_{P/G}$ and STY in the continuous period of the fermentation with cell retention.

Acetate concentration	$Y_{P/G}$ [mol mol ⁻¹]	STY [g dm ⁻³ d ⁻¹]
0 g dm^{-3}	0.42	0.68
20 g dm^{-3}	14.7	24.4
40 g dm^{-3}	242 (21.3)	406 (35.7)

4.4 Repetitive Fed-batch

Because of the problems observed during the continuous experiments, the repetitive fed-batch alternative with cell retention was studied. The following (heuristic) guidelines were formulated in order to achieve an optimized process development:

- (i) the process time should not extend the "critical" value of approximately 40 h to prevent strain instability,
- (ii) product formation should most presumably occur with non-growing cells to enable a highly selective glucose conversion to pyruvate,
- (iii) a series of multiple production cycles should be realized to increase space-time yield and to minimize the production period with high extra-cellular pyruvate titers.

As indicated in Figure 4.14, altogether four production cycles (II-V) were realized in a repetitive fed-batch experiment with cell retention after the strain was cultivated for biomass production in phase I. Figure 4.14 shows the changes in biomass concentration, pyruvate concentration and specific pyruvate production rate during the experiment. Furthermore, the integral molar yield pyruvate/glucose ($Y_{P/G}$) and integral space-time yield (STY) were calculated for each cycle (Table 4.5).

In general the experiment can be divided in two parts. Part I (cycle I) characterized by cell growth, enabled pyruvate and biomass production at the same time. The Part I was glucose and acetate controlled. Part II (cycles II – V) enabled highly-selective pyruvate production with non-growing cells. The highest STY of $145 \text{ g dm}^{-3} \text{ d}^{-1}$ was observed in the second cycle (non-growing pyruvate production phase), which represents a more than 3 fold increase compared to the best *E. coli* fed-batch results ($42 \text{ g dm}^{-3} \text{ d}^{-1}$). The pyruvate/glucose

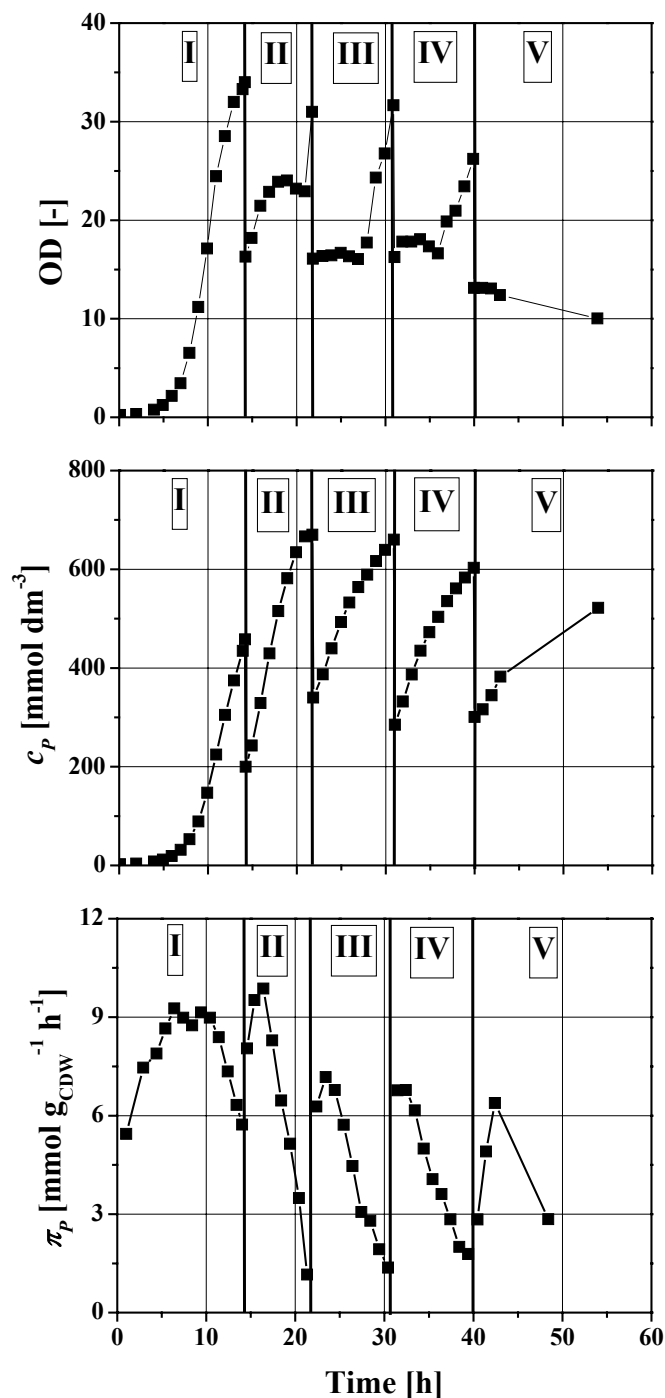


Figure 4.14 Biomass concentration, pyruvate concentration (c_p) and specific pyruvate production rate (π_p) in the repetitive fed-batch experiment. Specific pyruvate production rate was calculated differentially.

yield $Y_{P/G}$ achieved in cycles II, III and IV were higher than 1.70 mol mol⁻¹ (0.83 g g⁻¹) which is significantly better than the best fed-batch results of 1.11 mol mol⁻¹ and is well comparable to the results using non-growing cells in shaking flasks with low external pyruvate titers^{53,54}.

The final pyruvate titers in cycles II-IV are comparable to the best results of Li et al.¹⁰⁶ using *Torulopsis glabrata*. However it should be noticed that the *STY* and $Y_{P/G}$ of the *E. coli* process are significantly improved. Using *E. coli* the *STY* is more than 5 fold higher leading to $145 \text{ g dm}^{-3} \text{ d}^{-1}$, which coincides, with even more efficient pyruvate/glucose yields $Y_{P/G}$ up to $1.78 \text{ mol mol}^{-1}$ (0.87 g g^{-1}) compared to the best value of 0.80 g g^{-1} published so far (Li et al.¹⁰⁶).

Figure 4.14 also indicates a close correlation between decreasing specific pyruvate formation rates and increasing pyruvate concentrations during each cycle. We concluded that there is obviously an inhibition of pyruvate production caused by high extra-cellular pyruvate concentrations. If the cell concentration curves (Figure 4.14) are analyzed, one might wonder about the increase of biomass concentration at the beginning of the second cycle.

Table 4.5 Integral yield pyruvate/glucose ($Y_{P/G}$) and integral space-time yield (*STY*) obtained in the repetitive fed-batch experiment and calculated separately for each cycle

	$Y_{P/G}$ [mol mol ⁻¹]	<i>STY</i> [g dm ⁻³ d ⁻¹]
Cycle I	1.46	68
Cycle II	1.71	145
Cycle III	1.72	82
Cycle IV	1.78	80
Cycle V	1.21	39

However, we would like to point out that the production of pyruvate was not growth dependent. Increase of the biomass concentration is due to the apparently slow cell recycling from the ultra-filtration unit back into the bioreactor. In analogy, no cell growth occurred at the end of the cycles (II-IV). Because of bio-fouling effects in the ultra-filtration unit the membrane permeability reduced (as indicated by extended filtration periods) which might also caused the sequential decreases of $Y_{P/G}$ and *STY* from one cycle to the next (Table 4.5).

4.5 Electrodialysis

While the continuous and the repetitive fed-batch experiments with cell retention aimed at the non-selective separation of the potentially inhibiting product pyruvate from the fermentation suspension, an *in situ* product recovery (ISPR) approach would additionally allow the concentration of the product in a separate liquid phase which fortunately reduces the amount of water to be handled during downstream processing. As indicated earlier, electrodialysis was considered for fully integrated pyruvate separation and concentration.

4.5.1 Effect of Current on the Performance of Electrodialysis

Preliminary experiments using a synthetic solution (25 g dm⁻³ pyruvate in water) were performed in order to study the effect of current on the performance of the electrodialysis process (Figures 3.12, 4.15). Experimental results are summarized in Table 4.6.

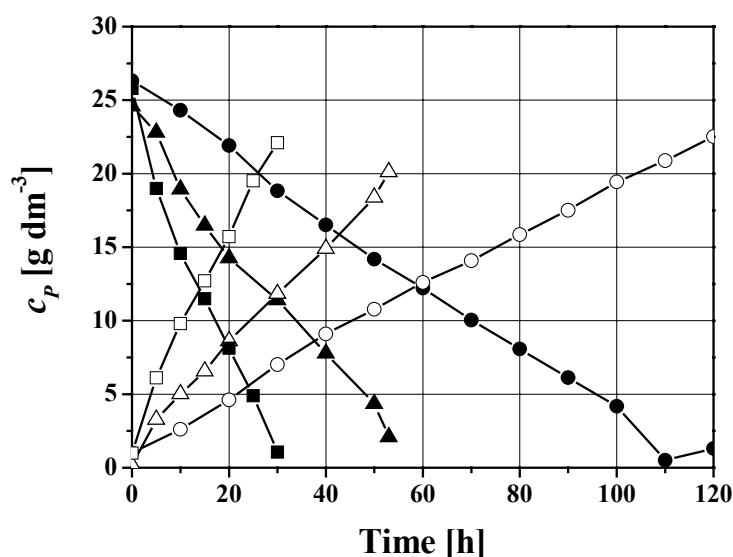


Figure 4.15 Pyruvate concentration (c_P) in the electrodialysis experiments for different currents; 2 A - ●, 5 A - ▲, and 10 A - ■ (closed symbols – pyruvate concentrations in the feed compartment; open symbols – pyruvate concentration in the acid compartment)

The power supply was set at a constant current in the range of 2 – 10 A. Experiments were terminated when the conductivity of the feed solution was 1 mS cm⁻¹. Current efficiencies higher than 91 % and pyruvate recovery higher than 91 % were achieved in each experiment. The lowest current efficiency was observed in the experiment at constant current

of 10 A. If the electrodialysis is operated at a current density beyond the limiting value, the current efficiency significantly decreases, and excessive energy is also dissipated for splitting water. However, in the range tested up to 10 A no limiting current could be found, and there was no sudden change observed in resistance at 25 g dm⁻³ of pyruvate as shown in Figure 4.16. Anyhow, lower current efficiency in the experiment at a constant current of 10 A cannot be explained by limiting current⁸⁵.

Table 4.6 Comparison of results for electrodialysis of pyruvate model solution, for different currents

Current [A]	Pyruvic acid recovery [%]	Current efficiency [%]	Energy consumption [kWh kg ⁻¹]	Volumetric productivity [g dm ⁻³ h ⁻¹]
2	95.0	97.0	1.3	11.8
5	91.5	96.3	1.4	22.5
10	94.4	91.3	1.7	45.2

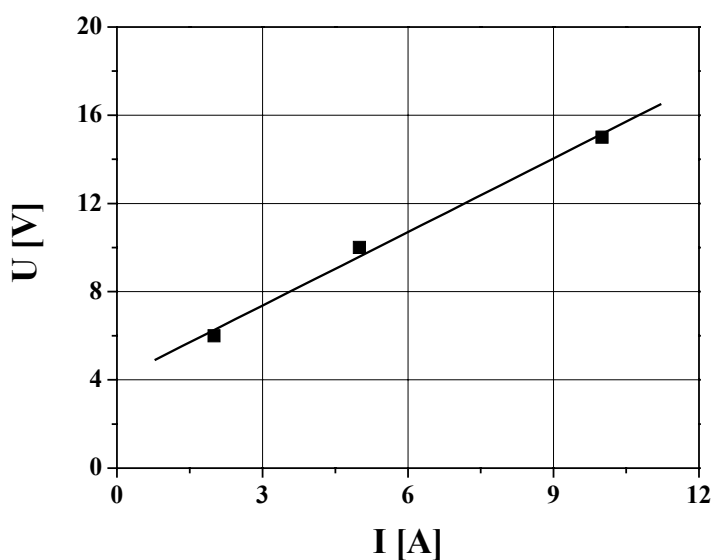


Figure 4.16 Identification of limiting current

High current efficiency leads to a reduction in the membrane area, and low energy consumption to a reduction in the operating costs. 20 % higher energy consumption for

recovery of 1 kg of pyruvic acid in the experiment at a constant current of 10 A was a reason for performing of further experiments at lower constant current even volumetric productivity was approximately 2 fold higher (Table 4.6).

4.5.2 Effect of Medium Components on the Performance of Electrodialysis

Preliminary experiments using a synthetic solution (48.0 g dm^{-3} pyruvate in water) and fermentation broth (42 g dm^{-3} pyruvate) were performed in order to study the effect of medium components on the performance of the electrodialysis process (Figures 3.12, 4.17). Experimental results are summarized in Table 4.7.

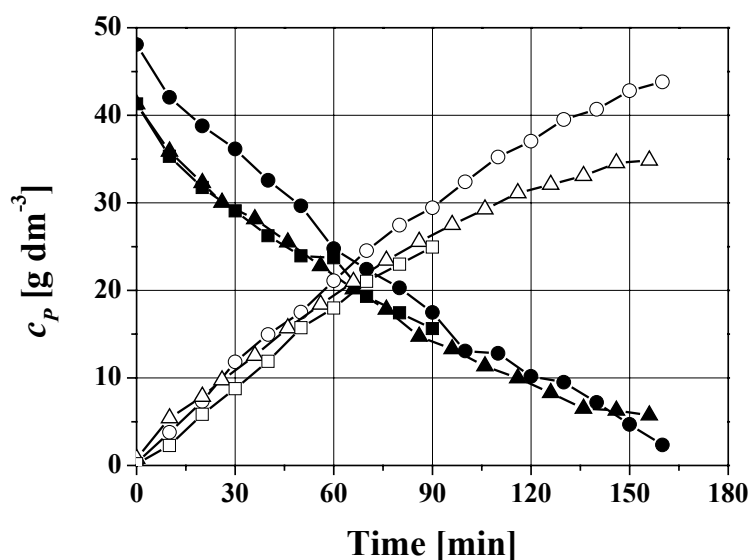


Figure 4.17 Pyruvate concentration (c_P) in the electrodialysis experiments for pyruvate model solution - ●, cell-free fermentation broth (CFB) - ▲, and cell- and protein-free fermentation broth CPF - ■ (closed symbols – pyruvate concentrations in the feed compartment; open symbols – pyruvate concentration in the acid compartment)

Experiments were carried out at a fixed current (5 A) for the whole period. Each experiment was stopped when the stack voltage increased to a maximum value of 40 V to prevent a possible membrane rupture. Current efficiencies higher than 99 % and 91 % pyruvate recovery were achieved in the experiment with the model solution. Compared to the best result 30 % recovery decrease was observed by the use of cell-free fermentation broth (CFB) with a similar current efficiency.

Table 4.7 Comparison of results for electrodialysis of pyruvate model solution, cell-free fermentation broth and cell- and protein-free fermentation broth

	Feed medium initial pyruvate [g L ⁻¹]	Acid medium final pyruvate [g L ⁻¹]	Pyruvic acid recovery [%]	Current efficiency [%]
Model solution	48.0	43.8	91.2	99.4
CFB	41.3	24.9	60.2	99.8
CPF	41.3	34.8	84.3	95.6

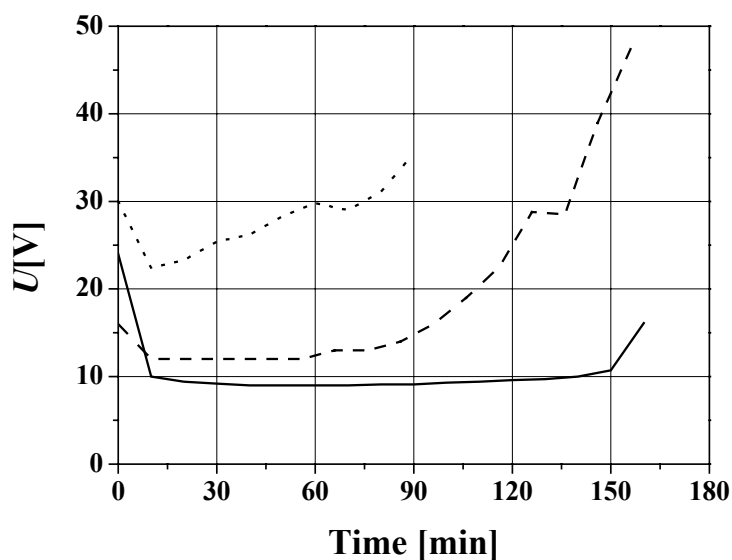


Figure 4.18 Voltage (U) levels in the electrodialysis experiments for pyruvate model solution - —, cell-free fermentation broth CFB - ·····, and cell- and protein-free fermentation broth CPF - - - - -

However, when fermentation broth was used, higher voltage levels and an accelerated voltage increase were measured (Figure 4.18), indicating membrane fouling by high-molecular medium components like proteins, cell debris etc. Hence, an ultra-filtration step (cut-off 10 kDa) was installed for protein separation, which resulted in an 84 % pyruvate recovery achieving 90 % current efficiency. We concluded that cell- and protein-free broth (CPF) should be used for electrodialysis. However, slightly reduced pyruvate recovery and current efficiency compared to the model solution (most presumably due to salts in the

fermentation medium) must be taken into account. Additionally, in experiments with cell- and protein-free fermentation broth glucose rejection of 95 % was observed. The final pH of the recycled feed solution in each experiment was higher than 3, which ensured sufficient amounts of pyruvic acid ions ($\text{pK}_{\text{a,pyruvate}} \cong 2.5$) in the feed¹⁰⁷.

4.5.3 Ion and Water Transport Modeling in Electrodialysis

The rate of water transport could be evaluated from the slope in relationship between the water being transferred and the time. As was observed the amount of the water transported was directly proportional to the current density (Figure 4.19). By mean of linear regression parameters α and β (Equation 3.50) were estimated (Table 4.8) from experimental results.

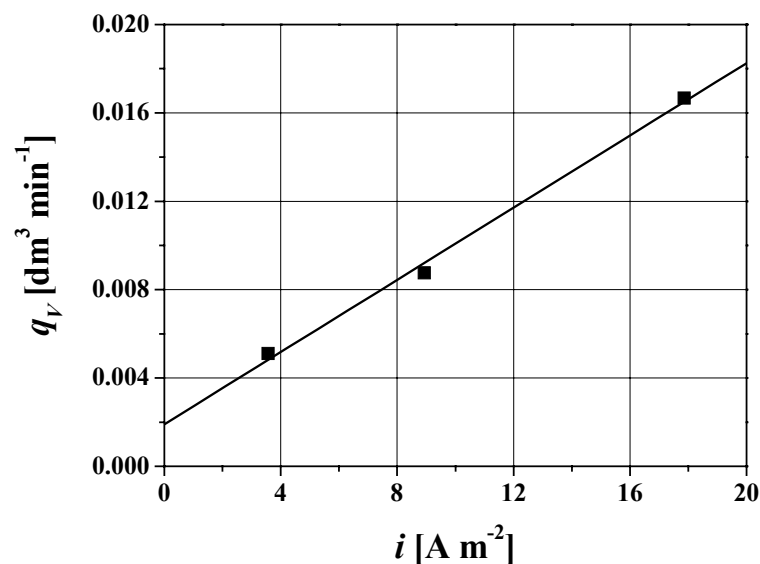


Figure 4.19 The relationship between the water transport rate and the current densities

Parameters A and B (Equation 3.53, Table 4.8) were estimated by the non-linear regression analysis from the data set obtained in the electrodialysis of the pyruvate model solution at 10 A. It should be mentioned that different ion exchange membranes as well as different solutions would affect the value of constants A and B ⁸⁸. Therefore, these constants should be determined experimentally for different ion exchange membranes and solutes used.

Table 4.8 Overall phenomenological coefficient of water transport and ion transport rate constant electro dialysis of the pyruvic acid

α [$\text{dm}^3 \text{min}^{-1}$]	β [$\text{dm}^3 \text{m}^2 \text{min}^{-1} \text{A}^{-1}$]	A [$\text{mmol A}^{-1} \text{min}^{-1}$]	B [$\text{A}^{-1} \text{min}^{-1}$]
$1.91 \cdot 10^{-3} \pm 0.63 \cdot 10^{-3}$	$8.17 \cdot 10^{-4} \pm 0.54 \cdot 10^{-4}$	$3.78 \cdot 10^5 \pm 1.20 \cdot 10^5$	152 ± 122

In order to verify the developed water and ion transport model for the electro dialysis of pyruvic acid, the calculated values obtained from the model simulation were compared to the collected data from experiments at different current. Both calculated as well as experimental results for the concentration of pyruvic acid in the acid compartment are plotted as shown in Figure 4.20.

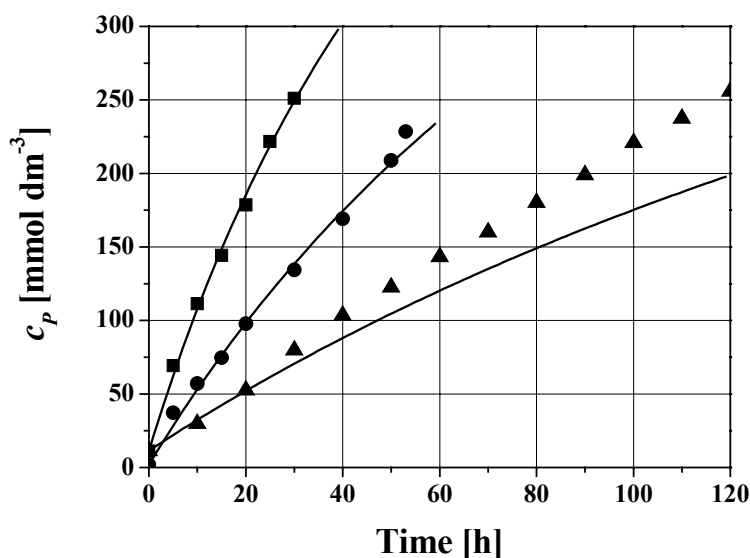


Figure 4.20 Variation results between both calculated (—) and measured data (10 A - ■, 5 A - ●, 2 A - ▲) for pyruvic acid concentration in the acid compartment for the different current applied

The graph indicates that the developed water and ion transport model is reliable to describe the transport behavior for this electro dialysis system even for a different current (current density's). This model could be used for the prediction of the other condition for water and ion transport phenomena under similar operating conditions (same type of ions, same membranes and membrane area).

4.6 *In situ* Product Recovery (ISPR) Approach with Fully Integrated Electrodialysis

It was planned that three streams should leave the electro dialysis unit (according to Figure 3.12): the pyruvic acid reduced fermentation permeate, the pyruvate enriched acid stream and NH_4OH enriched base stream. The pyruvic acid reduced fermentation permeate contained glucose with some nutrients and could be reused in a continuous recycling process. Consequently, a reduction of raw material costs was expected. NH_4OH produced in the three-compartment electro dialysis could also be reused to decrease the amount of the fresh base needed for pH titration. Based on the preliminary experiments, it was expected that pyruvate could be concentrated in the acid stream thus allowing a simplified purification later on. The experimental set-up of the in-situ product recovery (ISPR) is already presented (Figure 3.9).

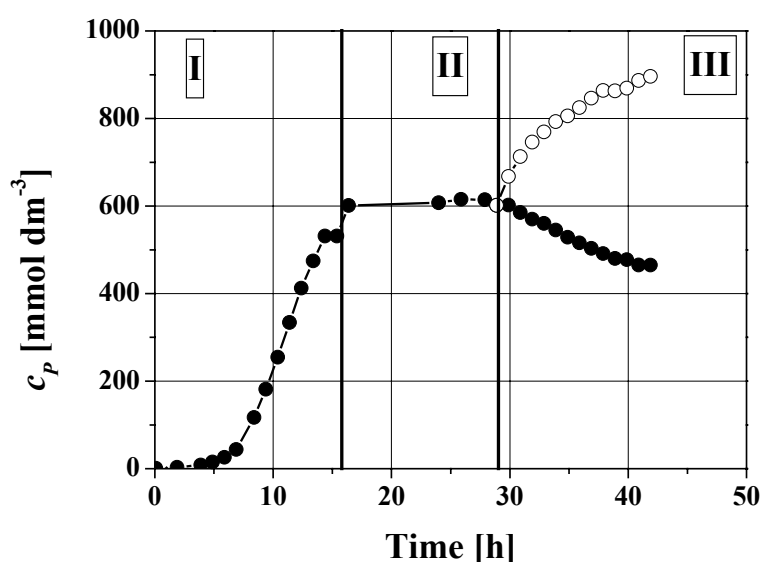


Figure 4.21 Pyruvate concentration (c_p) for bioreactor in the *in situ* product recovery (ISPR) approach with fully integrated three-compartment electro dialysis process. Pyruvate concentration in the bioreactor - ●, total amount of pyruvate produced referred to the real working volume of the bioreactor - ○

As indicated, fermentation suspension was first ultra-filtrated (cut-off: 500 kD) to produce a cell free permeate which was pumped through a second ultra-filtration unit (cut-off: 10 kD) to separate proteins and cell debris. Then cell and protein free fermentation solution entered the electro dialysis.

Fermentation permeate with reduced pyruvic acid was recycled into the bioreactor through a sterile micro-filtration unit to prevent a possible contamination by the non-sterile

pyruvate separation process. A constant flow of the NH_4OH containing base stream was pumped into the bioreactor to support pH regulation.

As shown by the pyruvate concentration (Figure 4.21) and formation courses (Figure 4.22), the process can be divided into three phases: a fed-batch period (I), a continuous period (II), and an ISPR period (III). Pyruvate concentration kept constant which indicates an equilibrium between pyruvate production (by retained cells) and wash-out. Then, pyruvate separation via electrodialysis was started after 29 h process time and lasted for approximately 14 h. During the period III the pyruvate concentration in the bioreactor decreased more than 20 % (Figure 4.21). At the same time, the microbial pyruvate production was still active – though on a reduced level. Whereas the volumetric pyruvate formation rate was about $60 \text{ mmol dm}^{-3} \text{ h}^{-1}$ during period II, it dropped down to approximately half of its original value during the ISPR phase (Figure 4.22).

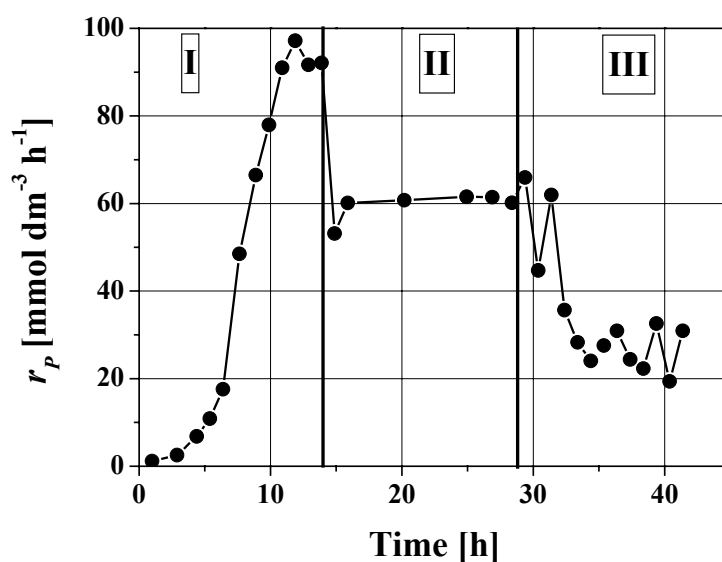


Figure 4.22 Pyruvate production rate (r_p) for bioreactor in the *in situ* product recovery (ISPR) approach with fully integrated three-compartment electrodialysis process. Pyruvate production rate was calculated differentially.

When both curves (Figures 4.21 and 4.22) are compared, a 2.5 fold pyruvate concentration is observed. However, the current efficiency (56 %) and the pyruvate recovery (72 %) were not as high as measured in the preliminary investigations (see Table 4.6).

This finding was in contrast to the assumption that a pyruvate separation might prevent a potential inhibition and would consequently lead to higher (or longer lasting) pyruvate formation rates. However, the (unwanted) coseparation of medium components via electrodialysis – which for instance was not prevented by additional nutrient supplement¹⁰⁸ – caused this unexpected result. As a consequence, low $STY = 68 \text{ g dm}^{-3} \text{ d}^{-1}$, and low $Y_{P/G} = 1.19 \text{ mol mol}^{-1}$ (Table 4.9) were observed which do not represent a process improvement in comparison to the repetitive fed-batch process.

Table 4.9 Integral yield pyruvate/glucose ($Y_{P/G}$) and integral space-time yield (STY) obtained in the experiment and calculated separately for fed-batch, continuous and *in situ* product recovery (ISPR) phase of the experiment

Phase	$Y_{P/G} [\text{mol mol}^{-1}]$	$STY [\text{g dm}^{-3} \text{ d}^{-1}]$
Fed-batch	1.38	52
Continuous	1.62	132
ISPR	1.19	68

It can be stated that the fully integrated separation of pyruvic acid via electrodialysis was successfully realized. Indications are given in Figure 4.23 by showing the decrease of pyruvate concentration in the feed (representing the pyruvate concentration in the bioreactor) and the increase in the acid compartment of the electrodialysis unit.

This was most presumably a consequence of membrane fouling caused by the precipitation of medium components like hardness material⁸⁴, which was more intensive during the 14 h of the ISPR approach than during the 2.5 h of the preliminary batch experiments.

Finally, pyruvate was concentrated in ED up to 550 mmol dm^{-3} with purity higher than 95 %. Only 7% of glucose were also co-separated, which is comparable to the results of the preliminary experiments. If the total amount of pyruvate produced is referred to the real working volume of the bioreactor, a final concentration of about 900 mmol dm^{-3} (79 g dm^{-3}) would have been achieved.

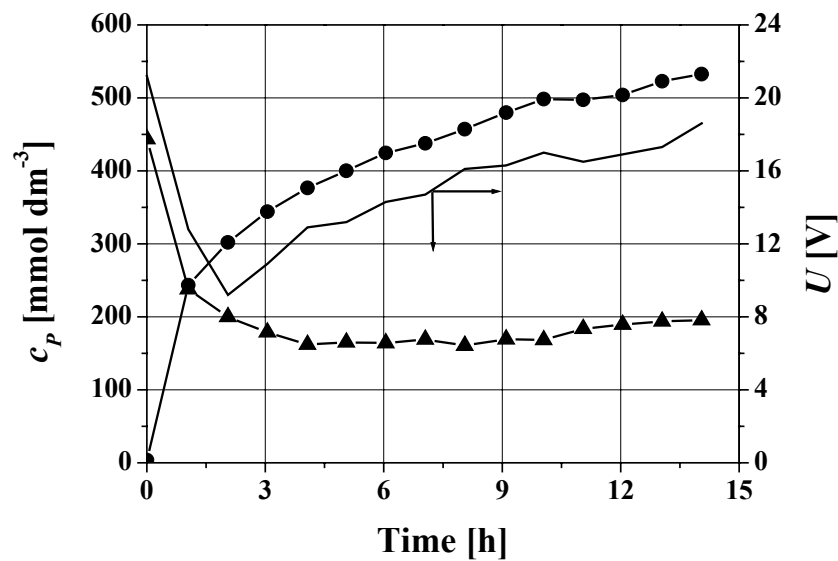


Figure 4.23 Pyruvate concentration in the feed - ▲, and in the acid compartment - ●, of the electro dialysis unit in the *in situ* product recovery (ISPR) approach with fully integrated three-compartment electro dialysis process. The voltage (U) drop in the processes is indicated with straight line

4.7 Unstructured Model for the Bioconversion of Glucose to Pyruvate

4.7.1 Data Generation

Fermentations were realized as a two-stage fed-batch process. During the first phase (cell growth and pyruvate production stage) acetate was fed according to the process control developed (see section 3.7.2). After biomass concentration remained constant for 3 hours, the second phase (pyruvate production stage) was started by stopping the acetate feed. Acetate controlled fed-batch fermentations were used to study influence of different glucose feeding strategies on molar pyruvate/glucose ($Y_{P/G}$) yield, integral space-time yield (STY) and final pyruvate titer c_P . Glucose feed was started after initial amount of glucose was depleted (approximately 10 hours fermentation time) and it was kept constant at 10, 20 and 30 g h⁻¹, respectively, in both phases. Influence of glucose was studied at acetate saturating conditions ($f=1$) to avoid possible process limitations and inhibitions concerning acetate.

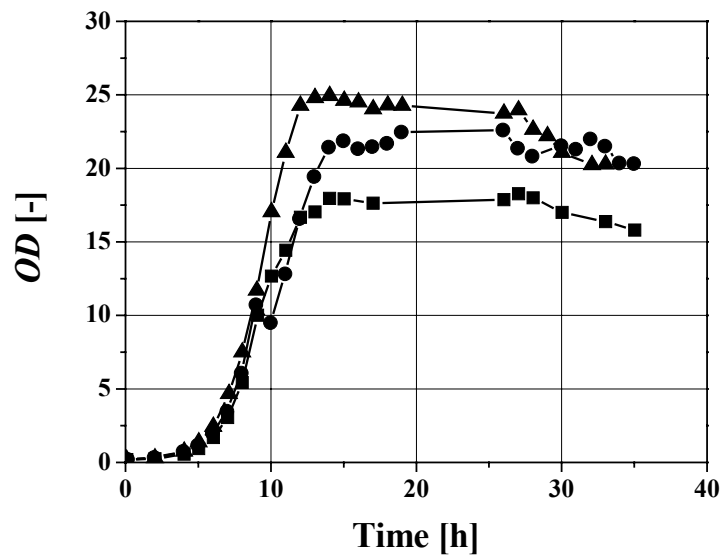


Figure 4.24 Influence of glucose feeding strategies on biomass concentration (OD) in acetate controlled fed-batch process using *Escherichia coli* YYC202 *ldhA::Kan* strain; $q_{V,G} = 10 \text{ g h}^{-1}$ - ■; $q_{V,G} = 20 \text{ g h}^{-1}$ - ●; $q_{V,G} = 30 \text{ g h}^{-1}$ - ▲

Influence of glucose feeding strategies on biomass growth and pyruvate concentration is shown in the Figures 4.24 and 4.25. There was no difference in the first 9 hours of fermentations and process is highly reproducible. Negative effect on biomass growth and pyruvate production was caused only by different glucose feeding strategies applied after 9 hours fermentation time. The lowest glucose feed rate applied ($q_{V,G} = 10 \text{ g h}^{-1}$) lead to the lowest maximal biomass concentration, final c_P and STY (Table 4.10). Contrary, increase of glucose feed rate, by keeping the same acetate feeding strategy, lead to an increase of the investigated process parameters.

Interestingly, there was no significant difference in the achieved $Y_{P/G}$ for different glucose feeding strategies. Except at the end of fermentations (Figure 4.26) there was no glucose accumulation in the experiments with $q_{V,G} = 10$ and $q_{V,G} = 20 \text{ g h}^{-1}$, respectively, indicating glucose limited conditions, for both, biomass growth and pyruvate production. The best results were achieved in the experiment with glucose accumulation ($q_{V,G} = 30 \text{ g h}^{-1}$), indicating necessity of glucose control at concentration level higher than zero, to ensure saturating conditions for glucose uptake.

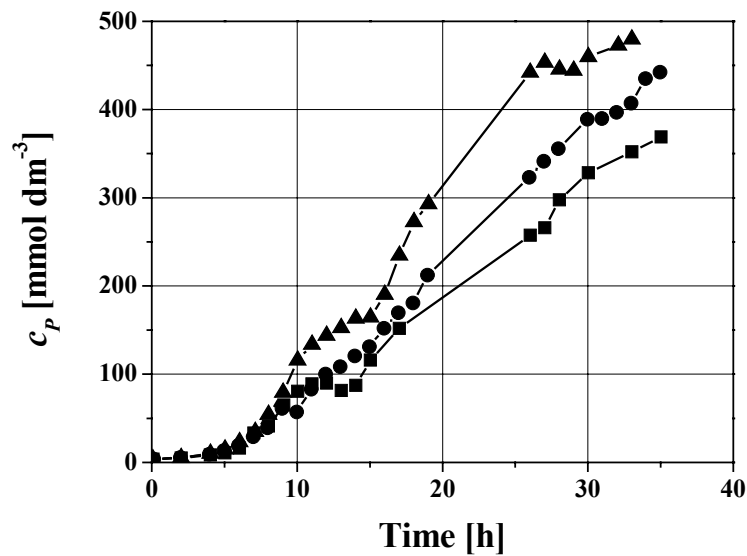


Figure 4.25 Influence of glucose feeding strategies on pyruvate concentration (c_P) in acetate controlled fed-batch process using *Escherichia coli* YYC202 *ldhA::Kan* strain; $q_{V,G} = 10 \text{ g h}^{-1}$ - ■; $q_{V,G} = 20 \text{ g h}^{-1}$ - ●; $q_{V,G} = 30 \text{ g h}^{-1}$ - ▲

Table 4.10 Influence of glucose feeding strategies on $Y_{P/G}$, STY and final c_P for acetate controlled fed-batch fermentations using *Escherichia coli* YYC202 *ldhA::Kan* strain.

*Calculated for 33 h of process time (normal fermentation time 35 h)

	$q_{V,G} = 10 \text{ g h}^{-1}$	$q_{V,G} = 20 \text{ g h}^{-1}$	* $q_{V,G} = 30 \text{ g h}^{-1}$
$OD [-]$	18.0	22.4	24.9
$Y_{P/G} [\text{mol mol}^{-1}]$	0.99	0.95	0.94
$STY [\text{g dm}^{-3} \text{ d}^{-1}]$	22.2	26.7	30.7
$c_P [\text{mmol dm}^{-3}] ([\text{g dm}^{-3}])$	368 (32.4)	442 (38.9)	480 (42.2)

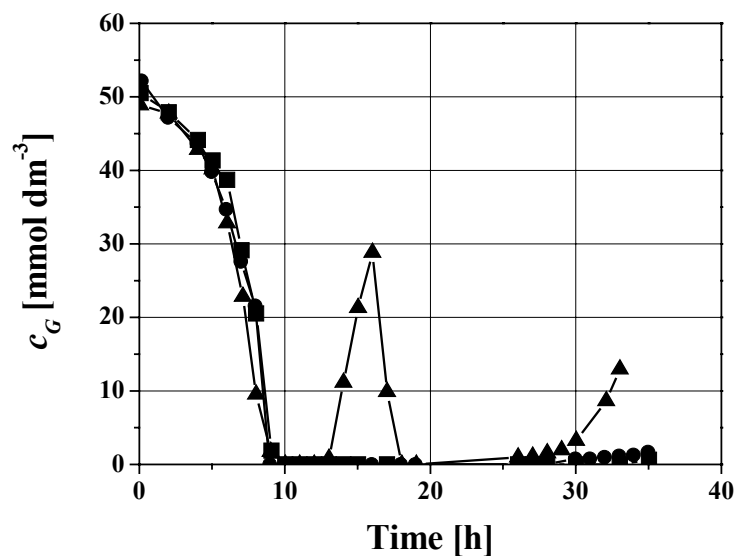


Figure 4.26 Influence of glucose feeding strategies on glucose concentration (c_G) in acetate controlled fed-batch process using *Escherichia coli* YYC202 *ldhA::Kan* strain; 10 g h⁻¹ glucose - ■; 20 g h⁻¹ glucose - ●; 30 g h⁻¹ glucose - ▲

4.7.2 Estimation of Parameters

Regarding parameter estimation, a non-linear regression (Nelder-Mead¹¹¹) was applied. Models are composed of five differential equations, five state variables and up to 10 parameters (see section 3.8). State variables, biomass (c_X), glucose (c_G), acetate (c_A), pyruvate concentrations (c_P), and reaction volume (V) were measured. Parameters estimation was carried out using data from fed-batch fermentation performed at $q_{V,G} = 10$ g h⁻¹. Validation of model parameters was performed for two different glucose feed rate $q_{V,G} = 20$ g h⁻¹ and $q_{V,G} = 30$ g h⁻¹. The resulting differential equations were solved by the "Scientist" software package.

Initial values of parameters $\mu_{MAX,G}$, $\mu_{MAX,A}$, $Y_{X/G,MAX}$, $Y_{X/A,MAX}$, Ks^G , and Ks^A , for Model 1 were those used for growth of *Escherichia coli* K12 on single substrate¹¹⁷. The initial value for parameter $Y_{P/G}$ was calculated from experimental results. Parameters V_{MAX} , Km^G , m_G and m_A , were set at a small value to avoid negative concentrations of calculated state variables. For discrimination of models (1a, 1b, 1c and 1d) minimal value of sum of square errors (difference between experimental and calculated data, Table 4.11) was set as a trial function. Interestingly, the Model 1b ($Y_{X,G} = \text{const.}$) has the smallest deviation of calculated data from experimental results. Additionally, parameter estimation for Model 1d ($Y_{X,G} = \text{const.}$, $Y_{X,A} = \text{const.}$) was resulted in the negative values of some estimated parameters.

Table 4.11 Sum of square errors for different models(Model 1)**negative values of estimated parameters*

Model	Sum of square errors
1a	$3.90 \cdot 10^2$
1b	$2.21 \cdot 10^2$
1c	$2.52 \cdot 10^2$
1d*	$3.45 \cdot 10^2$

Estimated values and confidence intervals of parameters, for the Model 1b, are shown in Table 4.12. Calculated values obtained by simulating the process together with experimental points, for biomass and pyruvate concentrations, are shown in Figure 4.27 and 4.28.

Table 4.12 Estimated values of parameters for the Model 1b

Parameter	
$Y_{X/G,MAX}$	$0.502 \pm 0.253 \text{ g g}^{-1}$
$Y_{X/A,MAX}$	$0.351 \pm 0.237 \text{ g g}^{-1}$
$Y_{P/G}$	$0.653 \pm 0.049 \text{ g g}^{-1}$
$\mu_{MAX,G}$	$0.202 \pm 0.102 \text{ h}^{-1}$
$\mu_{MAX,A}$	$0.323 \pm 0.331 \text{ h}^{-1}$
K_S^G	$0.055 \pm 0.079 \text{ g dm}^{-3}$
K_S^A	$0.124 \pm 0.050 \text{ g dm}^{-3}$
V_{MAX}	$0.809 \pm 0.506 \text{ g dm}^{-3} \text{ h}^{-1}$
Km^G	$0.299 \pm 0.782 \text{ g dm}^{-3}$
m_A	$0.011 \pm 0.035 \text{ g g}^{-1} \text{ h}^{-1}$

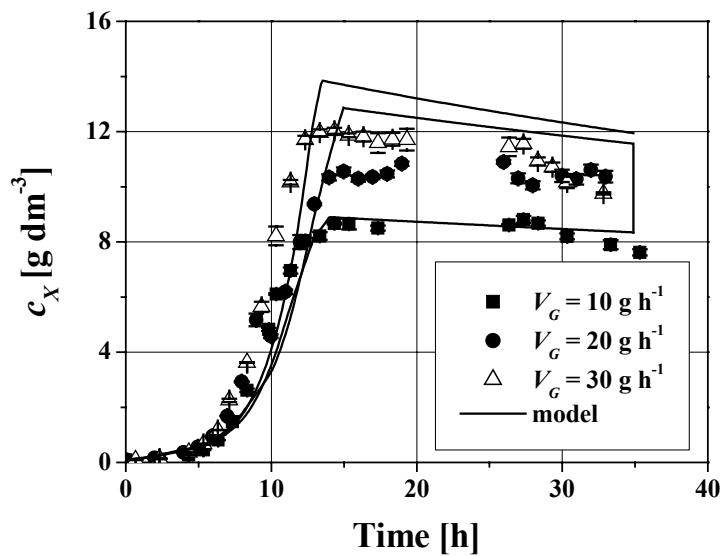


Figure 4.27 Simulation results of Model 1b and experimental data of biomass concentrations at three different glucose feed rates

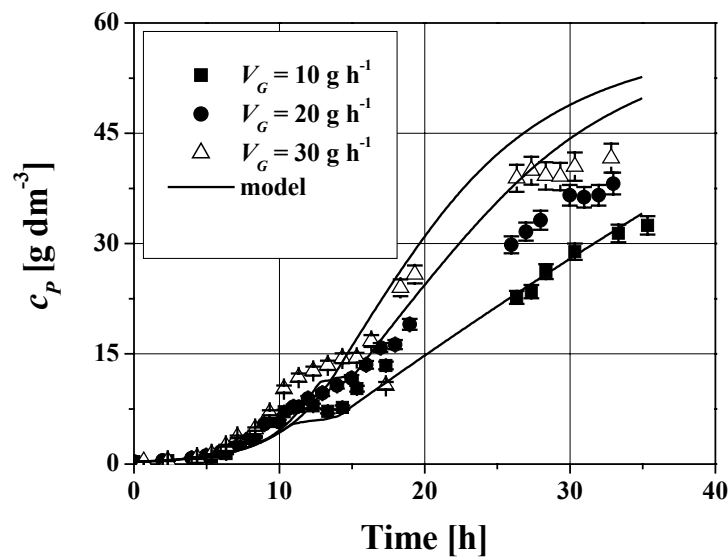


Figure 4.28 Simulation results of Model 1b and experimental data of pyruvate concentrations at three different glucose feed rates

As can be observed the model was able to describe dynamic behavior of the process. Unfortunately, except for the data set used for estimation of parameters, model was not able to fit well data sets ($q_{V,G} = 20 \text{ g h}^{-1}$ and $q_{V,G} = 30 \text{ g h}^{-1}$) used for its validation. Both, predicted

biomass and pyruvate concentrations (maximal and final) were too high comparing them to the experimental data.

In the next step of model development, multiple-substrate Monod kinetic was used for description of biomass growth. Same concept for pyruvate production used in the Model 1 was applied in the development of Model 2. Initial value of parameter μ_{MAX} was assumed to be sum of $\mu_{MAX,G}$ and $\mu_{MAX,A}$, estimated for the model 1b. Initial values of parameters $Y_{X/G,MAX}$, $Y_{X/A,MAX}$, Ks^G , and Ks^A , V_{MAX} , Km^G for Model 2 were estimated parameters of model 1b. The initial value for parameter $Y_{P/G}$ was calculated from experimental results. Parameters m_G and m_A , were set at a small value to avoid negative concentrations of calculated state variables. As in the evaluation of different concepts of Model 1, for discrimination of models (2a, 2b, 2c and 2d) minimal value of sum of square errors (difference between experimental and calculated data, Table 4.13) was set as a trial function. As in the case of Model 1 (Table 4.11), the Model 2b ($Y_{X,G} = \text{const.}$) has the smallest deviation of calculated data from experimental results. Furthermore, sum of square errors calculated for model 2b is lowest than one calculated for the model 1b. Additionally, parameter estimation for Model 2d ($Y_{X,G} = \text{const.}$, $Y_{X,A} = \text{const.}$), as in the case of Model 1, was resulted in the negative values of some estimated parameters.

Table 4.13 Sum of square errors for different models (Model 2)

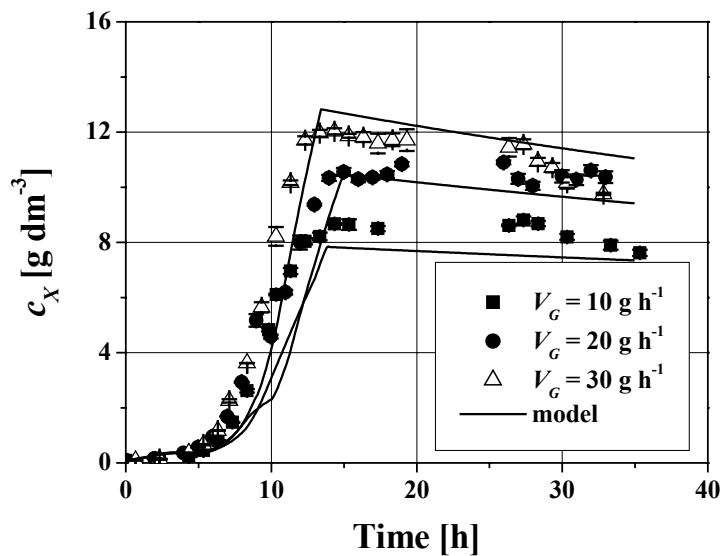
**negative values of estimated parameters*

Model	Sum of square errors
2a	$2.50 \cdot 10^2$
2b	$1.99 \cdot 10^2$
2c	$2.12 \cdot 10^2$
2d*	$3.37 \cdot 10^2$

Estimated values and confidence intervals of parameters, for the Model 2b, are shown in Table 4.14. Calculated values obtained by simulating the process together with experimental points, for biomass and pyruvate concentrations, are shown in Figure 4.29 and 4.30.

Table 4.14 Estimated values of parameters for the Model 2b

Parameter	
$Y_{X/G,MAX}$	$0.953 \pm 0.198 \text{ g g}^{-1}$
$Y_{X/A,MAX}$	$0.653 \pm 0.436 \text{ g g}^{-1}$
$Y_{P/G}$	$0.648 \pm 0.032 \text{ g g}^{-1}$
μ_{MAX}	$0.771 \pm 0.417 \text{ h}^{-1}$
K_S^G	$0.069 \pm 0.216 \text{ g dm}^{-3}$
K_S^A	$0.143 \pm 0.103 \text{ g dm}^{-3}$
V_{MAX}	$1.377 \pm 0.788 \text{ g dm}^{-3} \text{ h}^{-1}$
Km^G	$0.377 \pm 0.949 \text{ g dm}^{-3}$
m_A	$0.055 \pm 0.293 \text{ g g}^{-1} \text{ h}^{-1}$

**Figure 4.29** Simulation results of Model 2b and experimental data of biomass concentrations at three different glucose feed rates

As can be observed the model 2 b as well as model 1b was able to describe dynamic behavior of the process. Both predicted maximal and final biomass concentration fits very well data from the experiments of three different conditions. As in the case of model 1b

predicted pyruvate concentrations (maximal and final) were too high comparing them to the experimental data. It should be stressed that in fed-batch process the acetate concentration was kept very low (saturating conditions) and process behavior was controlled by the acetate feed rate rather than by kinetics itself. This fact accounts for the very large confidence region of parameters K_S^G , K_S^A , and m_A in both models (1b and 2b). Additionally, very large confidence region for parameters of bioconversion of glucose to pyruvate (observed in both models) are probably consequence of inadequate kinetic mechanism selected for its description.

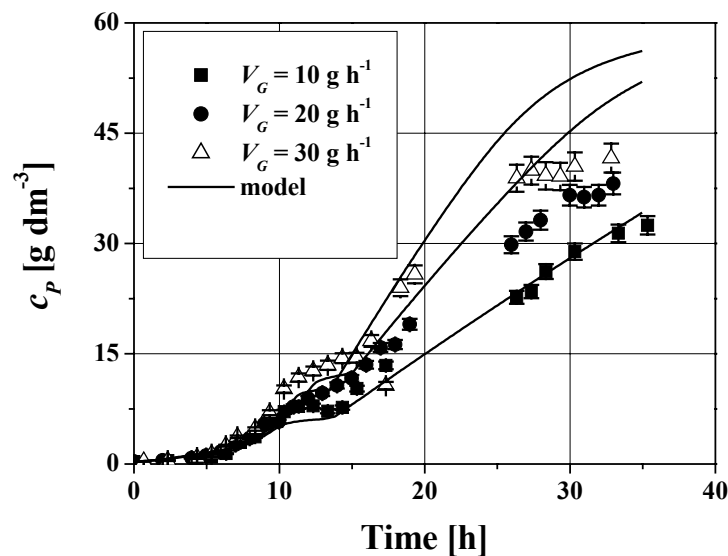


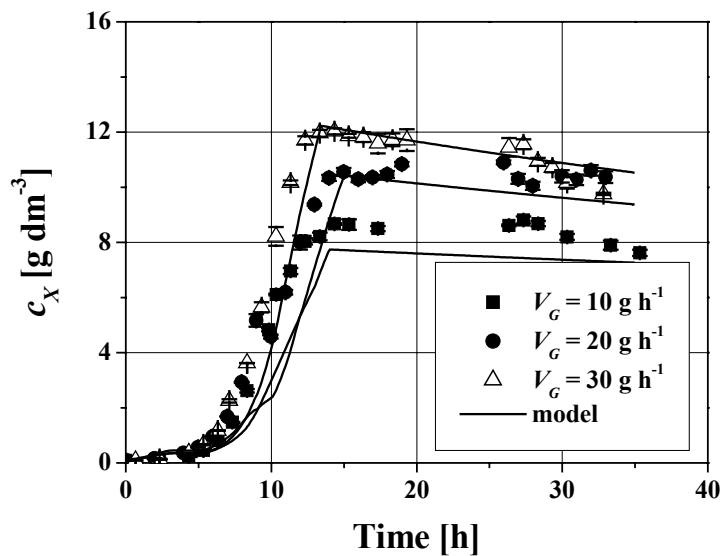
Figure 4.30 Simulation results of Model 2b and experimental data of pyruvate concentrations at three different glucose feed rates

In order to improve a model concerning pyruvate production the Model 3 was set up. Same concept for biomass growth description used in the Model 2b was applied in the development of Model 3. Simple Michaelis-Menten kinetics was used in modeling of pyruvate production. It was assumed that $Y_{P/G}$ is the function of pyruvate concentration. Estimation of parameters was performed and calculated sum of square errors for Model 3 was equal to $1.86 \cdot 10^2$ and the smallest comparing it to the sum of square errors calculated for Models 1 and 2.

Estimated values and confidence intervals of parameters, for the Model 3, are shown in Table 4.15. Calculated values obtained by simulating the process together with experimental points, for biomass and pyruvate, are shown in Figure 4.31 and 4.32.

Table 4.15 Estimated values of parameters for the Model 2b

Parameter	
$Y_{X/G,MAX}$	$0.953 \pm 0.198 \text{ g g}^{-1}$
$Y_{X/A,MAX}$	$0.653 \pm 0.436 \text{ g g}^{-1}$
$Y_{P/G,MAX}$	$0.846 \pm 0.025 \text{ g g}^{-1}$
μ_{MAX}	$0.771 \pm 0.417 \text{ h}^{-1}$
K_S^G	$0.069 \pm 0.216 \text{ g dm}^{-3}$
K_S^A	$0.143 \pm 0.103 \text{ g dm}^{-3}$
V_{MAX}	$1.506 \pm 0.264 \text{ g dm}^{-3} \text{ h}^{-1}$
Km^G	$0.345 \pm 0.114 \text{ g dm}^{-3}$
m_A	$0.055 \pm 0.293 \text{ g g}^{-1} \text{ h}^{-1}$

**Figure 4.31** Simulation results of Model 3 and experimental data of biomass concentrations at three different glucose feed rates

As can be observed the model 3 as well as models 1b and 2b was able to describe dynamic behavior of the process. Both predicted maximal and final biomass concentration fits data from the experiments at the three conditions very well. Contrary to the results obtained

with models 1b and 2b, Model 3 fits very well predicted maximal and final pyruvate concentration (maximal and final). Furthermore, narrow confidence region for parameters in charged in bioconversion of glucose to pyruvate for Model 3 (V_{MAX} , Km^G , and $Y_{P/G}$, Table 4.15) indicated adequate kinetic mechanism selected for its description.

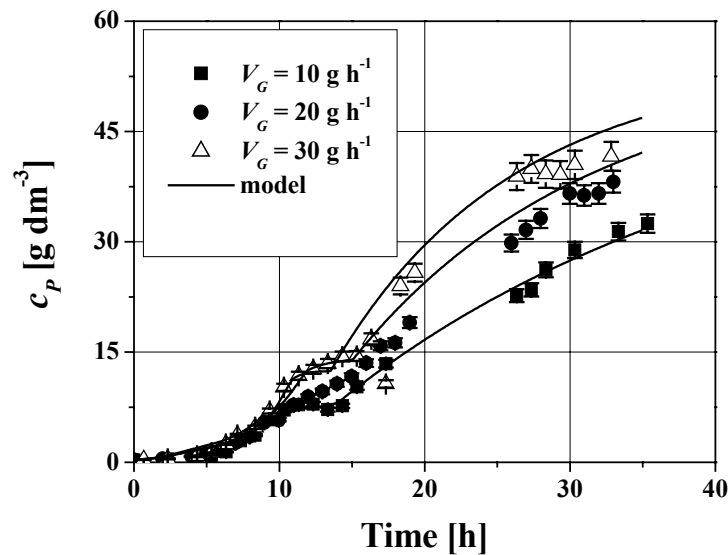


Figure 4.32 Simulation results of Model 2b and experimental data of pyruvate concentrations at three different glucose feed rates

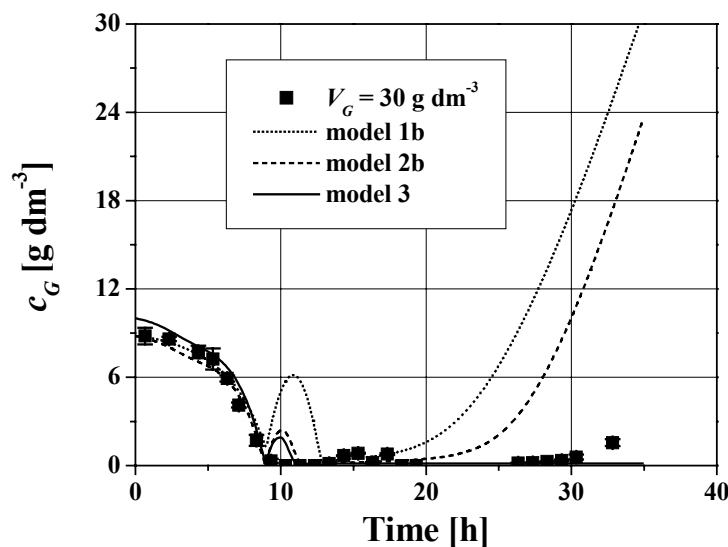


Figure 4.33 Comparison between calculated values obtained by simulation of models 1b, 2b and 3, and experimental data for glucose concentration in the fed-batch experiment with constant glucose flow of 30 g h^{-1}

Additionally, models 1b and 2b were not able to predict glucose concentration profile especially in the case of higher amount of glucose fed in the process ($q_{V,G} = 30 \text{ g h}^{-1}$). According to the calculated values obtained by simulation of the process, models 1b and 2b predicted accumulation of glucose in the pyruvate production stage, which was not the case in the experiment. Contrary, model 3 was able to simulate this behavior. All developed and investigated models were not able to simulate glucose accumulation at the end of the process. Furthermore, all models predict certain level of glucose accumulation (depending on the model from 2 to 6 g dm^{-3}) immediately after fed-batch phase was started (approximately 9 hours fermentation time) which was not confirmed with the experiment (Figure 4.33).

4.7.3 Validation of the Model

In order to validate the model 3 additionally, fed-batch experiment (see section 4.2.2) and repetitive fed-batch experiment (see section 4.4) were simulated, and the calculated values obtained by the model were compared with the experimental results. For the model validation in the fed-batch process experimental and calculated results for the biomass (Figure 4.34) and the pyruvate (Figure 4.35) concentrations were taken in account.

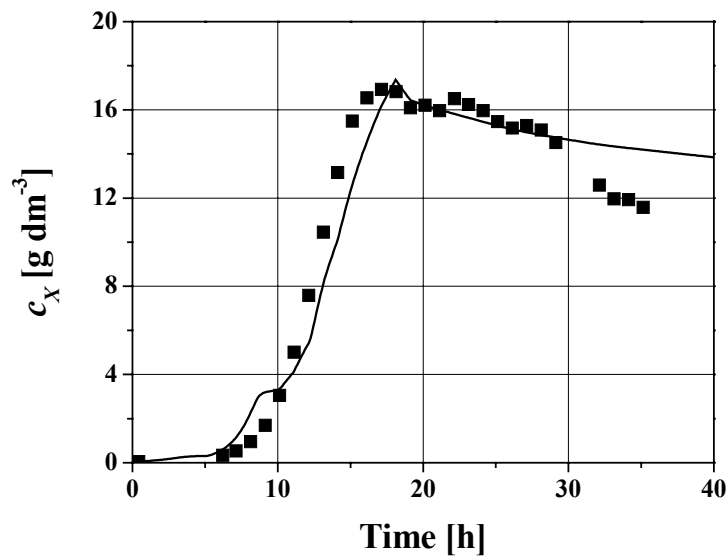


Figure 4.34 Comparison between calculated values obtained by simulation of model 3 (—), and experimental data (■) for biomass concentration in the fed-batch experiment with acetate accumulation ($f = 0.8$) using *Escherichia coli* YYC202 *ldhA::Kan* strain

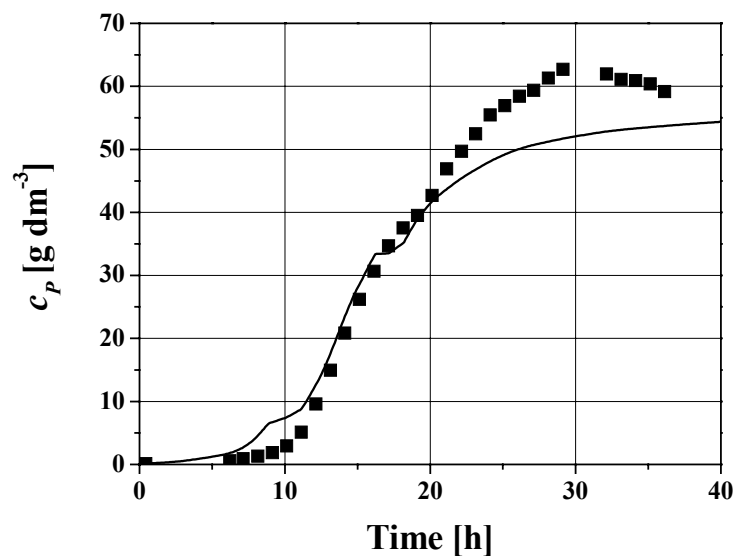


Figure 4.35 Comparison between calculated values obtained by simulation of model 3 (—), and experimental data (■) for pyruvate concentration in the fed-batch experiment with acetate accumulation ($f = 0.8$) using *Escherichia coli* YYC202 *ldhA::Kan* strain

A good agreement of the model with the both data sets: the biomass concentration and the pyruvate concentration was obtained. Higher differences in the case of biomass in the last phase of experiment (after 30 h, Figure 4.34) cannot be explained just by dilution of the system (included in the model). Most probably, model simplicity was the reason for this behavior. Precisely, biomass growth was assumed to be exponential in entire fermentation, and the death phase was not considered in the kinetic equation for description of the biomass growth (Equation 3.37), which was obviously the case in the experiment.

In the case of the pyruvate concentration good prediction was obtained in the first 20 hours of the fed-batch fermentation. Unfortunately, maximal pyruvate concentration calculated was approximately 10 % lower than maximal pyruvate concentration obtained in the experiment (Figure 4.35). As in the case of predicted biomass concentration model simplicity could be a reason for such a kind of the model response. Additionally, experiments used for estimation of parameters (see sections 4.7.1 and 4.7.2) were designed to ensure glucose limited conditions, which was not included in the part of the model in charged for conversion of glucose to pyruvate (Equation 3.40). Anyhow, Figures 4.34 and 4.35

demonstrate that the model simulations of the batch and fed-batch culture dynamics correlated reasonably well with the experimental batch and fed-batch culture kinetics obtained.

To illustrate model limits calculated glucose concentrations were compared with the experimental results (Figure 4.36). Obviously, model is able to predict process behavior in the batch phase of the experiment, which is not the case in the second, fed-batch phase. The glucose concentration in the experiment was regulated at 5 g dm^{-3} . The glucose concentration predicted by the model was 10 fold lower, (probably like in the case of the biomass and the pyruvate) because of model simplicity and some assumptions used in model development especially in the bioconversion part of the model. Precisely, bioconversion glucose-pyruvate was assumed to be one-step enzymatic reaction. In *Escherichia coli* metabolism production of pyruvate from glucose is much more complicate (nine enzymatic reactions plus transport of glucose via PTsystem). Interestingly, model was qualitatively able to predict glucose accumulation observed in the experiment (12 to 16 hour fermentation time).

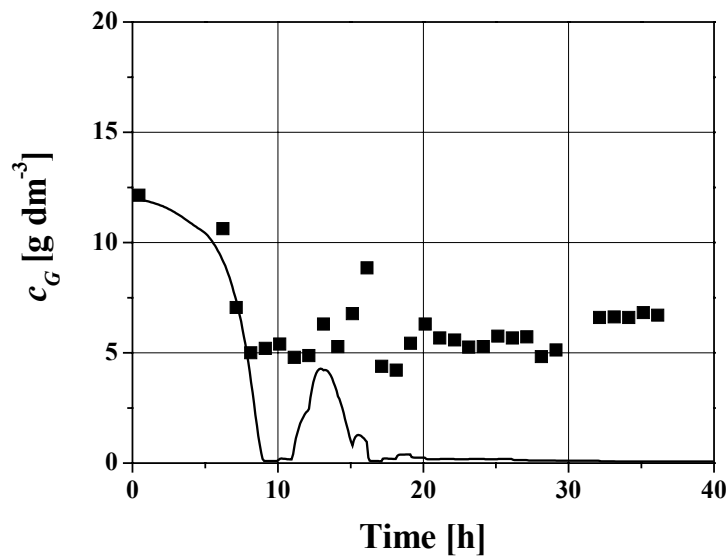


Figure 4.36 Comparison between calculated values obtained by simulation of model 3 (—), and experimental data (■) for glucose concentration in the fed-batch experiment with acetate accumulation ($f = 0.8$) using *Escherichia coli* YYC202 *ldhA::Kan* strain

Additionally, in Table 4.16 integral STY , integral $Y_{P/G}$ and final c_P calculated from experimental results and calculated by model simulation were compared.

Table 4.16 Comparison of integral STY , integral $Y_{P/G}$ and final c_P calculated from experimental results and calculated by model simulation

	Experiment	Model
$Y_{P/G}$ [mol mol ⁻¹]	1.11	0.97
STY [g dm ⁻³ d ⁻¹]	42.0	32.6
c_P [mmol dm ⁻³] ([g dm ⁻³])	62.0	54.2

Figures 4.37 and 4.38 demonstrate the model simulation and the experimental results for the biomass and the pyruvate concentration in the repetitive fed-batch experiment. As is indicated in the section 4.4 increase of the biomass at the end of the cycles was not growth dependent. Due to the apparently too slow cell recycling from the ultra-filtration unit into the bioreactor the biomass increases at the end of the cycles. Probably that was the main reason why experimental results for biomass concentration were just principally verified by the model. However, still exhibits a large deviation.

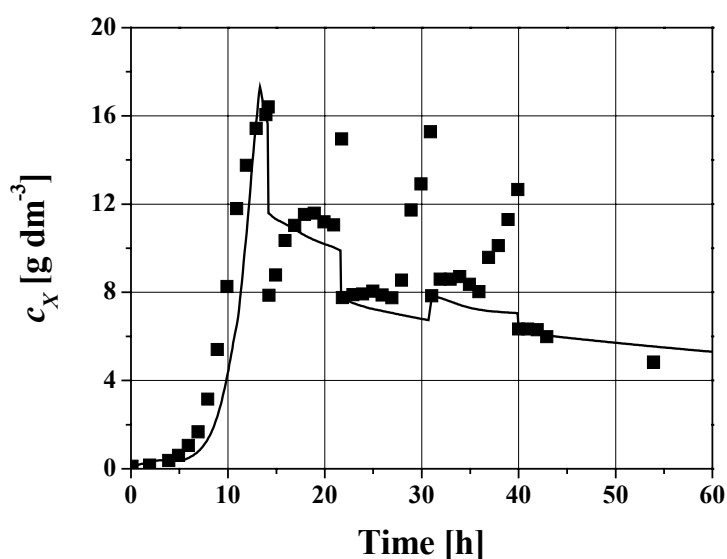


Figure 4.37 Comparison between calculated values obtained by simulation of model 3 (—), and experimental data (■) for biomass concentration in the repetitive fed-batch experiment using *Escherichia coli* YYC202 *ldhA::Kan* strain

As was in the case pyruvate concentration prediction in the fed-batch experiment, maximal pyruvate concentration calculated with the use of model was approximately 10 % or more

lower than one obtained in the experiment. Same explanations given in the description of model inadequacy for the fed-batch experiment can be used as well for the repetitive fed-batch experiment. It is obvious that maximal pyruvate production rate is not constant and it is dependent on the activity of the biomass from beginning to the end of the fermentation. For the first four cycles maximal pyruvate concentration achieved by the model is lowest than experimentally obtained values. Contrary, in the last cycle, maximal calculated pyruvate concentration is higher than one achieved in the experiment (Figure 4.38).

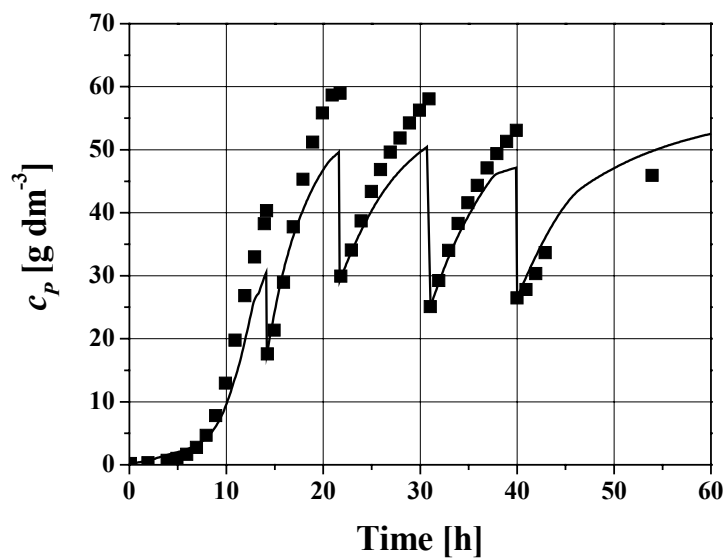


Figure 4.38 Comparison between calculated values obtained by simulation of model 3 (—), and experimental data (■) for pyruvate concentration in the repetitive fed-batch experiment using *Escherichia coli* YYC202 *ldhA::Kan* strain

5. CONCLUSIONS

Four process strategies for *E. coli* based pyruvate production were investigated.

A fed-batch process was completely developed. Glucose closed-loop control was established, and acetate open-loop control was developed on the basis of on-line measurement of exhaust gases. High co-production of lactate was detected by the use of *E. coli* YYC202 strain. That motivated the construction of a new non-lactate producing *E. coli* YYC202 *ldhA::Kan* strain. With the new strain, the final pyruvate titer in the fed-batch process is increased by 40 % and a yield ($Y_{P/G}$) to 1.11 mol mol⁻¹.

Evidence was obtained that high extracellular pyruvate concentrations are inhibiting for further pyruvate production.

Three alternative processes – a continuous process with cell retention, a repetitive fed-batch process and an *in situ* product recovery (ISPR) approach with fully integrated ED – were studied in order to test their applicability for microbial pyruvate production considering a potential product inhibition.

Continuous process experiments revealed long-term production strain instabilities leading to space-time yields (STY) of 104 – 117 g dm⁻³ d⁻¹ together with low pyruvate/glucose yields ($Y_{P/G}$) of 1.10 – 1.24 mol mol⁻¹.

Repetitive fed-batch experiments as a very promising process approach were carried out. STY was improved more than 5 fold compared to the published data with *Torulopsis glabrata*³⁶. The obtained integral $Y_{P/G} = 1.78$ mol mol⁻¹ (0.87 g g⁻¹), represents the highest value published so far for the production of pyruvate from glucose. The value coincides with high pyruvate concentrations (up to 700 mmol dm⁻³) and high pyruvate production rates (up to 19 g g_{CDW}⁻¹ d⁻¹).

The use of electrodialysis (ED) has shown that this separation process is well suited to separate pyruvate from fermentation broth – even in a fully integrated ISPR process. ED should also be favored with respect to a sustainable process development because it offers the opportunity to separate pyruvate without using solvents, to concentrate the product and to minimize process waste water in fully integrated ED. The model for the electrodialysis process was also developed.

The proposed model 3 for the bioconversion of glucose to pyruvate using *Escherichia coli* YYC202 *ldhA::Kan* strain fitted adequately the experimental data of the different

processes. The developed model is able to give further information allowing process optimization.

6. LITERATURE

- [1] Nakazawa, H., Enei, H., Okumura, S., Yoshida, H., Yamada, H.: Enzymatic preparation of L-tryptophan and 5-hydroxy-L-tryptophan. *FEBS Lett.* 25 (1972) 43-45
- [2] Yamada, H., Kumagai, H., Kashima, N., Torii, H., Enei, H., Okumura, S.: Synthesis of L-tyrosine from pyruvate, ammonia and phenol by crystalline tyrosine phenol lyase. *Biochem. Biophys. Res. Commun.* 46 (1972) 370-374
- [3] Nakazawa, H., Enei, H., Okumura, S., Yamada, H.: Synthesis of L-tryptophan from pyruvate, ammonia and indole. *Agr. Biol. Chem.* 36 (1972) 2523-2528
- [4] Yamada, H., Kumagai, H.: Microbial and enzymatic processes for amino acid production. *Pure. Appl. Chem.* 50 (1978) 1117-1127
- [5] Takao, S., Yokota, A., Tanida, M.: Enzymatic production of tryptophan coupled to pyruvic acid fermentation. *J. Ferment. Technol.* 62 (1984) 329-334
- [6] Kawasaki, K., Yokota, A., Tomita, F.: L-tryptophan production by a pyruvic acid-producing *Escherichia coli* strain carrying the *Enterobacter aerogenes* tryptophanase gene. *J. Ferment. Bioeng.* 82 (1996) 604-606
- [7] Yokota, A., Oita, S., Takao, S.: Tryptophan production by a lipoic acid auxotroph of *Enterobacter aerogenes* having both pyruvic acid productivity and high tryptophanase activity. *Agric. Biol. Chem.* 53 (1989) 2037-2044
- [8] Li, Y., Chen, J., Lun, S. -Y.: Biotechnological production of pyruvic acid. *Appl. Microbiol. Biotechnol.* 57 (2001) 451-459
- [9] Stanko, R. T.: Method for preventing body fat deposition in mammals. US Patent 4,351,835 (1982)
- [10] Stanko, R. T.: Method for preventing body fat deposition in mammals. US Patent 4,548,937 (1985)
- [11] Stanko, R. T., Robertson, R. J., Galbreath, R. W., Reilly, J. J., Greenawalt, K. D. Jr., Goss, F. L.: Enhanced leg exercise endurance with a high-carbohydrate diet and dihydroxyacetone and pyruvate. *J. Appl. Physiol.* 69 (1990) 1651-1656
- [12] DeBoer, L. W. V., Bekx, P. A., Han, L., Steinke, L.: Pyruvate enhances recovery of rat hearts after ischemia and reperfusion by preventing free radicals generation. *J. Appl. Physiol.* 265 (1993) 1571-1576
- [13] Borle, A., Stanko, R. T.: Pyruvate reduces anoxic injury and free radical formation in perfused rat hepatocytes. *J. Appl. Physiol.* 270 (1993) 535-540

- [14] Izumi, Y., Olney, J. W.: Use of pyruvate to prevent neuronal degeneration associated with ischemia. US Patent 5,395,822 (1995)
- [15] Howard, J. W., Fraser, W. A.: Pyruvic acid. *Org. Synth. Coll.* 1 (1932) 475-476
- [16] Sugiyama, S., Fukunaga, S., Ito, K., Ohigashi, S., Hayashi, H.: Catalysts for vapor-phase dehydration of ethylene glycol and their application to pyruvic acid synthesis. *J. Catal.* 129 (1991) 12-18
- [17] Feldman, C. F.: Process for the production of pyruvic acid. US Patent 4,136,111 (1979)
- [18] Sugiyama, S., Fukunaga, S., Kawashiro, K., Hayashi, H.: Catalytic conversion of diethyl tartrate into pyruvate over silica-supported potassium disulfate. *Bull. Chem. Soc. Jpn.* 65 (1992) 2083-2085
- [19] Ai, M., Ohdan, K.: Formation of pyruvic acid by oxidative dehydrogenation of lactic acid. *Chem. Lett.* 5 (1995) 405
- [20] Tsujino, T., Ohigashi, S., Sugiyama, S., Kawashiro, K., Hayashi, H.: Oxidation of propylene glycol and lactic acid to pyruvic acid in aqueous phase catalyzed by lead-modified palladium-on-carbon and related systems. *J. Mol. Catal.* 71 (1992) 25-35
- [21] Imanari, M., Kujira, K., Iwane, H.: Process for preparing pyruvate. US Patent 5,225,593 (1993)
- [22] Kiyoura, T.: Process for producing pyruvic acid. US Patent 4,247,716 (1981)
- [23] Anton, D. L., DiCosimo, R., Witterholt, V. G.: Process for the preparation of pyruvic acid using permeabilized transformants of *H. polymorpha* and *P. pastoris* which express glycolate oxidase and catalase. US Patent 5,538,875 (1996)
- [24] Eisenberg, A., Seip, J. E., Govagan, J. E., Payne, M. S., Anton, D. L., DiCosimo, R.: Pyruvic acid production using methylotropic yeast transformants as catalyst. *J. Mol. Catal. B: Enzymatic* 2 (1997) 223-232
- [25] Burdick, B. A., Schaeffer, J. R.: Co-immobilized coupled enzyme systems on nylon mesh capable of gluconic and pyruvic acid production. *Biotechnol. Lett.* 9 (1987) 253-258
- [26] Izumi, Y., Matsumura, Y., Tani, Y., Yamada, H.: Pyruvic acid production from 1,2-propanediol by thiamin-requiring *Acinetobacter* sp. 80-M. *Agric. Biol. Chem.* 46 (1982) 2673-2679
- [27] Ogawa, J., Soong, C.-L., Ito, M., Shimizu, S.: Enzymatic production of pyruvate from fumarate – an application of microbial cyclic-imide-transforming pathway. *J. Mol. Catal. B: Enzymatic* 11 (2001) 355-359

- [28] Schinsschel, C., Simon, H.: Preparation of pyruvate from (R)-lactate with *Proteus* species. *J. Biotechnol.* 31 (1993) 191-203
- [29] Moriguchi, M., Shuto, K., Hashimoto, T.: Production of pyruvic acid from saccharified citrus peel extract by dried cells of *Debaryomyces coudertii*. *J. Ferment. Technol.* 62 (1984) 243-248
- [30] Yokota, A., Takao, S.: Pyruvic acid production by lipoic acid auxotrophs of *Enterobacter aerogenes*. *Agric. Biol. Chem.* 53 (1989) 705-711
- [31] Besnainou, B., Giani, D., Sahut, C.: Method for producing pyruvic acid by fermentation. US Patent 4,918,013 (1990)
- [32] Miyata, R., Yonehara, T., Yotsumoto, K., Tsutsui, H.: Method for producing pyruvic acid by fermentation. US Patent 4,971,907 (1990)
- [33] Yonehara, T., Miyata, R.: Fermentative production of pyruvate from glucose by *Torulopsis glabrata*. *J. Ferment. Bioeng.* 78 (1994) 155-159
- [34] Miyata, R., Yonehara, T.: Improvement of fermentative production of pyruvate from glucose by *Torulopsis glabrata* IFO 0005. *J. Ferment. Bioeng.* 82 (1996) 475-479
- [35] Hua, Q., Yang, C., Shimizu, K.: Metabolic flux analysis for efficient pyruvate fermentation using vitamin-auxotrophic yeast of *Torulopsis glabrata*. *J. Biosci. Bioeng.* 87 (1999) 206-213
- [36] Miyata, R., Yonehara, T.: Breeding of high-pyruvate-producing *Torulopsis glabrata* with acquired reduced pyruvate decarboxylase. *J. Biosci. Bioeng.* 88 (1999) 173-177
- [37] Hua, Q., Shimizu, K.: Effect of dissolved oxygen concentration on the intracellular flux distribution for pyruvate fermentation. *J. Biotechnol.* 68 (1999) 135-147
- [38] Li, Y., Chen, J., Liang, D.-F., Lun, S.-Y.: Effect of nitrogen concentration on the production of pyruvate by *Torulopsis glabrata*. *J. Biotechnol.* 81 (2000) 27-34
- [39] Hua, Q., Araki, M., Koide, Y., Shimizu, K.: Effects of glucose, vitamins, and DO concentrations on pyruvate fermentation using *Torulopsis glabrata* IFO 0005 with metabolic flux analysis. *Biotechnol. Prog.* 17 (2001) 62-68
- [40] Li, Y., Chen, J., Lun, S.-Y., Rui, X.-S.: Efficient pyruvate production by a multi-vitamin auxotroph of *Torulopsis glabrata*: key role and optimization of vitamin levels. *Appl. Microbiol. Biotechnol.* 55 (2001) 680-685
- [41] Yokota, A., Shimizu, H., Terasawa, Y., Takaoka, N., Tomita, F.: Pyruvic acid production by a lipoic acid auxotroph of *Escherichia coli* W1485. *Appl. Microbiol. Biotechnol.* 41 (1994) 638-643

- [42] Yokota, A., Terasawa, Y., Takaoka, N., Shimizu, H., Tomita, F.: Pyruvic acid production by an F₁-ATPase-defective mutant of *Escherichia coli* W1485lip2. *Biosci. Biotech. Biochem.* 58 (1994) 2164-2167
- [43] Yokota, A., Henmi, M., Takaoka, N., Hayashi, C., Takezawa, Y., Fukumori, Y., Tomita, F.: Enhancement of glucose metabolism in a pyruvic acid-hyperproducing *Escherichia coli* mutant defective in F₁-ATPase activity. *J. Ferment. Bioeng.* 83 (1997) 132-138
- [44] Takao, S., Tanida, M.: Pyruvic acid production by *Schizophyllum commune*. *J. Ferment. Technol.* 60 (1982) 277-280
- [45] Andreeva, R. I., Vysotskii, E. S., Rodicheva, E. K., Shcherbakova, G. Y.: Production of pyruvic acid by the luminescent bacterium. *Mikrobiologiya* 50 (1981) 776-780
- [46] Vise, A. B., Lascelles, J.: Some properties of a mutant strain of *Escherichia coli* which requires lysine and methionine or lipoic acid for growth. *J. Gen. Microbiol.* 48 (1967) 87-93
- [47] Willetts, A.: Bacterial metabolism of propane-1,2-diol. *Biochim. Biophys. Acta.* 588 (1979) 302-309
- [48] Mueller, P. J., von Frommannshausen, B.: Bistability in the glucose and energy metabolism of ammonia-limited chemostat cultures of *Escherichia coli* ML 30. *Z. Allg. Mikrobiol.* 22 (1982) 185-190
- [49] Moriguchi, M.: Fermentative production of pyruvic acid from citrus peel extract by *Debaryomyces coudertii*. *Agric. Biol. Chem.* 46 (1982) 955-961
- [50] Cooper, B.: Preparation of pyruvic acid. US Patent 4,900,668 (1990)
- [51] Yanase, H., Mori, N., Masuda, M., Kita, K., Shima, M., Kato, N.: Pyruvate production by *Enterococcus casseliflavus* A-12 from gluconate in an alkaline medium. *J. Ferment. Bioeng.* 73 (1992) 287-291
- [52] Steinbuechel, A., Schlegel, H. G.: Excretion of pyruvate by mutants of *Alcaligenes eutrophus* which are impaired in the accumulation of poly(β -hydroxybutyric acid) (PHB), under conditions permitting synthesis of PHB. *Appl. Microbiol. Biotechnol.* 31 (1989) 168-175
- [53] Bott, M., Gerharz, T., Takors, R., Zelić, B.: Verfahren zur fermentativen Herstellung von Pyruvat. German Patent Application 10129714.4 (2001)

- [54] Gerharz, T., Zelić, B., Takors, R., Bott, M.: Verfahren sowie Mikroorganismen zur mikrobiellen Herstellung von Pyruvat aus Kohlenhydraten sowie Alkoholen. German Patent Application 10220234.6 (2002)
- [55] Zelić, B., Gerharz, T., Bott, M., Vasić-Rački, Đ., Wandrey, C., Takors, R.: Fed-batch process for pyruvate production by recombinant *Escherichia coli* YYC202 strain. *Chem. Eng. Technol.* (2003) In print
- [56] Strathmann, H.: Electrodialysis. In: Baker RW (Ed) Membrane separation systems, recent developments and future directions. Noyes Data Corp, New Jersey, 1991
- [57] Bailly, M., Bar, D.: Hybrid separation schemes for producing organic acids: the potential, promise and production. *Chem. Eng.* 109 (2002) 51-53
- [58] Tichy, S., Vasić-Rački, Đ., Wandrey, C.: Electrodialysis as an integrated downstream process in amino acid production. *Chem. Biochem. Eng. Q.* 4 (1990) 127-135
- [59] von Eysmond, J., Vasić-Rački, Đ., Wandrey, C.: The continuous production of acetic acid by electrodialysis integrated fermentation. Modeling and computer simulation. *Chem. Biochem. Eng. Q.* 7 (1993) 139-148
- [60] Weuster-Botz, D., Karutz, M., Joks, B., Schärtges, D., Wandrey, C.: Integrated development of fermentation and downstream processing for L-isoleucine production with *Corynebacterium glutamicum*. *Appl. Microbiol. Biotechnol.* 46 (1996) 209-219
- [61] Börgardt, P., Krischke, W., Trösch, W., Brunner, H.: Integrated bioprocess for the simultaneous production of lactic acid and dairy sewage treatment. *Bioprocess. Eng.* 19 (1998) 321-329
- [62] Kim, Y. H., Moon, S.-H.: Lactic acid recovery from fermentation broth using one-stage electrodialysis. *J. Chem. Technol. Biotechnol.* 76 (2001) 169-178
- [63] Madzingaidzo, L., Danner, H., Braun, R.: Process development and optimisation of lactic acid purification using electrodialysis. *J. Biotechnol.* 96 (2002) 223-239
- [64] Escherich, T.: Die darmbakterien des Neugeborenen und Säuglingen. *Fortschritte. Med.* 3 (1885) 515-522; 547-554
- [65] Neidhardt, F. C., ed.: *Escherichia coli* and *Salmonella*. ASM, Washington, 1996
- [66] Blattner, F. R., Plunkett, G. III., Bloch, C. A., Perna, N. T., Burland, V., Riley, M., Collado-Vides, J., Glasner, J. D., Rode, C. K., Mayhew, G. F., Gregor, J., Wayne Davis, N., Kirkpatrick, H. A., Goeden, M. A., Rose, D. J., Mau, B., Shao, Y.: The complete genome sequence of *Escherichia coli* K-12. *Science* 277 (1997) 1453-1474

- [67] Puehler, A.: Prokaryotes and man: chances, promises and risks. In: Lengeler, J. W., Drews, G., Schlegel, H. G.: *Biology of prokaryotes*. Thieme Verlag, Stuttgart, 1999, 916-917
- [68] Stephanopoulos, G.: Metabolic fluxes and metabolic engineering. *Metabolic Eng.* 1 (1999) 1-11
- [69] Schlegel, H. G.: *Allgemeine Mikrobiologie*, 7. Auflage, Thieme Verlag, Stuttgart, 1992
- [70] Lehninger, A. L., Nelson, D. L., Cox, M. M.: *Principles of Biochemistry*. Worth Publishers, New York, 1993
- [71] Prescott, L. M., Harley, J. P., Klein, D. A.: *Microbiology*. Wm. C. Brown Publishers, Boston, 1996
- [72] Axe, D. D., Bailey, J. E.: Transport of lactate and acetate through the energized cytoplasmic membrane of *Escherichia coli*. *Biotechnol. Bioeng.* 47 (1995) 8-19
- [73] Baronofsky, J.J., Schreurs, W. J. A., Kashket, E. R.: Uncoupling by acetic acid limits growth of and acetogenesis by *Clostridium thermoaceticum*. *Appl. Environ. Microbiol.* 48 (1984) 1134-1139
- [74] Bailey, J. E., Ollis, D. F.: *Biochemical engineering fundamentals*. McGraw-Hill Book Company, New York, 1977
- [75] Aiba, S., Humphrey, A. E., Millis, N. F.: *Biochemical engineering*. Academic Press, Inc., New York, 1973
- [76] Cabral, J. M. S., Tramper, J.: Bioreactor design. In: Straathof A. J.J., Adlercreutz, P. (ed): *Applied biocatalysis*. Harwood Academic Publishers, Amsterdam, 2000
- [77] Efors, S.-O.: Continuous and fed-batch operation of fermentation processes. In: Berovič, M. (ed): *Bioprocess engineering course*. National institute of chemistry, Ljubljana, 1998
- [78] Fontes, S., Bosander, P.: Modelling & simulation of separation processes. *Filtration Separation.* 37 (2000) 24-26
- [79] Boniardi, N., Rota, R., Nano, G., Mazza, B.: Lactic acid production by electro dialysis part II: Modelling. *J. Appl. Electrochem.* 27 (1997) 135-145
- [80] Audinos, R.: Ion-exchange membrane processes for clean industry chemistry. *Chem. Eng. Technol.* 20 (1997) 247-258
- [81] Madzingaidzo, L., Danner, H., Braun, R.: Process development and optimization of lactic acid purification using electro dialysis. *J. Biotechnol.* 96 (2002) 223-239
- [82] Korngold, E.: Electro dialysis – membranes and mass transfer. In Belfort, G. (ed): *Synthetic membrane processes*. Academic Press, New York, 1984

- [83] Boniardi, N., Rota, R., Nano, G., Mazza, B.: Lactic acid production by electro dialysis part I: Experimental tests. *J. Appl. Electrochem.* 27 (1997) 125-133
- [84] Lindstrand, V., Sundström, G., Jönsson, A.-S.: Fouling of electro dialysis membranes by organic substances. *Desalination* 128 (2000) 91-102
- [85] Lee, E. G., Moon, S.-H., Chang, Y. K., Yoo, I.-K., Chang, H. N.: Lactic acid recovery using two-stage electro dialysis and its modelling. *J. Membr. Sci.* 145 (1998) 53-66
- [86] Law, M., Wen, T., Solt, G. S.: Thickness and concentration profile on the boundary layer in the electro dialysis. *Desalination* 109 (1997) 95-103
- [87] Hsu, J.-P., Yang, K.-L., Ting, K.-C.: Effect of convective boundary layer on the current efficiency of a membrane bearing nonuniformly distributed fixed charges. *J. Phys. Chem. B* 101 (1997) 8984-8989
- [88] Ling, L.-P., Leow, H.-F., Sarmidi, M. R.: Citric acid concentration by electro dialysis: ion and water transport modelling. *J. Membr. Sci.* 199 (2002) 59-67
- [89] Kedem, O.: The role of volume flow in electro dialysis. *J. Membr. Sci.* 206 (2002) 333-340
- [90] Silhavy, J., Berman, M., Enquist, L.: Experiments with gene fusions. Cold Spring Harbor Laboratory. 1984
- [91] Bunch, P. K., Mat-Jan, F., Lee, N., Clark, D. P.: The *ldhA* gene encoding the fermentative lactate dehydrogenase of *Escherichia coli*. *Microbiology* 143 (1997) 187-195
- [92] Buchholz, A., Takors, R., Wandrey, C.: Quantification of intracellular metabolites in *Escherichia coli* K12 using liquid chromatographic-electrospray ionization tandem mass spectrometric techniques. *Anal. Biochem.* 295 (2001) 129-137
- [93] Schuhmann, W., Wohlschläger, H., Huber, J., Schmidt, H. L., Stadler, H.: Development of an extremely flexible automatic analyzer with integrated biosensors for on-line control of fermentation processes. *Anal. Chim. Acta.* 315 (1995) 113-122
- [94] Gerigk, M. R., Maass, D., Kreutzer, A., Sprenger, G., Bongaerts, J., Wubbolts, M., Takors, R.: Enhanced pilot-scale fed-batch L-phenylalanine production with recombinant *Escherichia coli* by fully integrated reactive extraction. *Bioprocess. Biosyst. Eng.* 25 (2002) 43-52
- [95] Svrcek, W. Y., Elliott, R. F., Zajic, J. E.: The extended kalman filter applied to a continuous culture model. *Biotechnol. Bioeng.* 16 (1974) 827-846

- [96] Kelle, R., Hermann, T., Weuster-Botz, D., Eggeling, L., Krämer, R., Wandrey, C.: Glucose-controlled L-isoleucine fed-batch production with recombinant strains of *Corynebacterium glutamicum*. *J. Biotechnol.* 50 (1996) 123-136
- [97] Mulchandani A., Bassi, A. S.: Principles and applications of biosensors for bioprocess monitoring and control. *Crit. Rev. Biotechnol.* 15 (1995) 105-124
- [98] Hitzmann, B., Broxtermann, O., Cha, Y. L., Sobiah, O., Stärk, E., Scheper, T.: The control of glucose concentration during yeast fed-batch cultivation using fast measurement complemented by an extended Kalman filter. *Bioprocess Eng.* 23 (2000) 337-341
- [99] Wiechert, W.: Interaktive Datenanalyse bei biotechnischen Prozessdaten. PhD Thesis. University Bonn, Germany. 1990
- [100] Stephanopoulos, G., San, K. Y.: Studies on on-line bioreactor identification, I: theory. *Biotechnol. Bioeng.* 26 (1984) 1176-1188
- [101] Bastin, G., Dochain, D.: On-line estimation and adaptive control of bioreactors. Elsevier Science, Amsterdam. 1990
- [102] Ferenci, T.: "Growth of bacterial cultures" 50 years on: towards and uncertainty principle instead of constants in bacterial growth kinetics. *Res. Microbiol.* 150 (1999) 431-438
- [103] Postma, P. W., Lengeler, J. W., Jacobson, G. R.: Phosphoenolpyruvate: Carbohydrate phosphotransferase systems of bacteria. *Microbiol. Rev.* 57 (1993) 543
- [104] Luli, G. W., Strohl, W. R.: Comparison of growth, acetate production, and acetate inhibition of *Escherichia coli* strains in batch and fed-batch fermentations. *Appl. Environ. Microbiol.* 56 (1990) 1004
- [105] Tita-Nwa, F.: Lab-scale process development for (*Escherichia coli* based) pyruvate production focusing on acetate feeding in fed-batch and diafiltration Mode. Master thesis. IBT-2, Forschungszentrum Juelich, 2002
- [106] Li, Y., Hugenholtz, J., Chen, J., Lun, S.-Y.: Enhancement of pyruvate production by *Torulopsis glabrata* using a two-stage oxygen supply control strategy. *Appl. Microbial Biotechnol.* 60 (2002) 101-107
- [107] Kim, Y. H., Moon, S.-H.: Lactic acid recovery from fermentation broth using one-stage electrodialysis. *J. Chem. Technol. Biotechnol.* 76 (2001) 169-178
- [108] Danner, H., Madzingaidzo, L., Thomasser, C., Neureiter, M., Braun, R.: Thermophilic production of lactic acid using integrated membrane bioreactor systems coupled with monopolar electrodialysis. *Appl. Microbial Biotechnol.* 59 (2002) 160-169

- [109] Pramanik, J., Keasling, J. D.: Stoichiometric model of *Escherichia coli* metabolism: Incorporation of growth-rate dependent biomass composition and mechanistic energy requirement. *Biotechnol. Bioeng.* 56 (1997) 398-421
- [110] Weuster-Botz, D., Paschold, H., Striegel, B., Gieren, H., Kula, M.-R., Wandrey, C.: Continuous computer controlled production of formate dehydrogenase (FDH) and isolation on a pilot scale. *Chem. Eng. Technol.* 17 (1994) 131-137
- [111] Nelder, J. A., Mead, R.: A simplex method for function minimisation. *Comput. J.* 7 (1965) 308-331
- [112] Weuster-Botz, D., Paschold, H., Striegel, B., Gieren, H., Kula, M.-R., Wandrey, C.: Continuous computer controlled production of formate dehydrogenase (FDH) and isolation on a pilot scale. *Chem. Eng. Technol.* 17 (1994) 131-137
- [113] Tomar, A., Eiteman, M. A., Altman, E.: The effect of acetate pathway mutations on the production of pyruvate in *Escherichia coli*. *Appl. Microbiol. Biotechnol.* (2003) in press
- [114] Patnaik, P. R.: Are microbes intelligent beings?: An assessment of cybernetic modeling. *Biotechnol. Adv.* 18 (2000) 267-288
- [115] Patnaik, P. R.: Enhancement of protein activity in a recombinant fermentation by optimizing fluid dispersion and initial plasmid copy number distribution. *Biochem. Eng. J.* 9 (2001) 111-118
- [116] Patnaik, P. R.: Effect of fluid dispersion on cybernetic control of microbial growth on substitutable substrates. *Bioprocess Biosyst. Eng.* 25 (2003) 315-321
- [117] Venkatesh, K. V., Doshi, P., Rengaswamy, R.: An optimal strategy to model microbial growth in a multiple substrate environment. *Biotechnol. Bioeng.* 56 (1997) 635-644
- [118] Dunn, I. J., Heinzle, E., Ingham, J., Prenosil, J. E.: Biological reaction engineering: Principles, applications and modelling with PC simulation. VCH Verlagsgesellschaft, Weinheim, 1992
- [119] Bae, W., Rittman, B. E.: A structured model of dual-limitation kinetics. *Biotechnol. Bioeng.* 49 (1996) 683-689
- [120] Han, K., Levenspiel, O.: Extended Monod kinetics for substrate, product and cell inhibition. *Biotechnol. Bioeng.* 32 (1988) 430-437
- [121] von Eysmond, J., Vasic-Racki, Dj., Wandrey, C.: Acetic acid production by *Acetogenium kivui* in continuous culture – kinetic studies and computer simulations. *Appl. Microbiol. Biotechnol.* 34 (1990) 344-349

- [122] Bonomi, A., Augusto, E. F. P., Barbosa, N. S., Mattos, M. N., Magossi, L. R., Santos, A. L.: Unstructured model proposal for the microbial oxidation of D-sorbitol to L-sorbose. *J. Biotechnol.* 31 (1993) 39-59
- [123] Bader, F. G.: Analysis of double-substrate limited growth. *Biotechnol. Bioeng.* 20 (1978) 183-202
- [124] SCIENTIST handbook, MicroMath[®], Salt Lake City, 1986-1995
- [125] Dhurjati, P., Ramkrishna, D., Flickinger, M. C., Tsao, G. T.: A cybernetic view of microbial growth: modeling of cells as optimal strategists. *Biotechnol. Bioeng.* 27 (1985) 1-9
- [126] Ramakrishna, R., Ramkrishna, D.: Cybernetic modeling of growth in mixed, substitutable substrate environments: Preferential and simultaneous utilization. *Biotechnol. Bioeng.* 52 (1996) 141-151
- [127] Zelić, B., Gostović, S., Vasić-Rački, Đ., Vuorilehto, K., Takors, R.: Process strategies to enhance pyruvate production with recombinant *Escherichia coli*: From repetitive fed-batch to *ISPR* with fully integrated electrodialysis. *Biotechnol. Bioeng.* (2003) submitted

7. APPENDIX

7.1 List of Symbols

A	area; [m^2]
A	ion transport rate constant; [$\text{mmol A}^{-1} \text{min}^{-1}$]
B	ion transport rate constant; [$\text{A}^{-1} \text{min}^{-1}$]
ACR	acetate consumption rate; [$\text{mmol dm}^{-3} \text{h}^{-1}$]
b	change in volumetric consumption rate; [$\text{g dm}^{-3} \text{h}^{-2}$]
c	concentration; [g dm^{-3}] or [mmol dm^{-3}] or [mol m^{-3}]
\hat{c}	estimated concentration; [g dm^{-3}]
CE	current efficiency; [-]
CTR	volume-specific CO_2 transfer rate; [$\text{mmol dm}^{-3} \text{h}^{-1}$]
D	diffusion coefficient; [$\text{m}^2 \text{s}^{-1}$]
D	dilution rate; [h^{-1}]
E	extinction; [-]
f	parameter; [-]
F	Faraday's constant; [C mol^{-1}]
F	function
g_i	random disturbances; [$\text{g dm}^{-3} \text{h}^{-1}$]
i	current density; [A m^{-2}]
K_m	Michaelis-Menten constant; [mol dm^{-3}]
K_S	Monod constant; [mol dm^{-3}]
m	maintenance; [h^{-1}]
q_M	mass flow rate; [g h^{-1}]
M	molecular weight; [g mol^{-1}]
M	random error; [g dm^{-3}]
N	mole flux; [$\text{mol s}^{-1} \text{m}^{-2}$]
OD_{600}	optical density at $\lambda = 600 \text{ nm}$; [-]
\hat{Q}	estimated volumetric consumption rate; [$\text{g dm}^{-3} \text{h}^{-1}$]
q_V	volumetric flow rate; [$\text{dm}^3 \text{h}^{-1}$]
r	reaction (production, consumption) rate; [$\text{mmol dm}^{-3} \text{h}^{-1}$] [$\text{g dm}^{-3} \text{h}^{-1}$]
s	tracking output difference; [g dm^{-3}]

STY	space-time yield; [g dm ⁻³ d ⁻¹]
t	time; [h] [min] [s]
t	transport number; [-]
u	weighting factor; [-]
V	volume; [dm ³]
v_{MAX}	maximal reaction rate; [h ⁻¹]
V_R	fermentation broth volume; [dm ³]
Y	yield; [mol mol ⁻¹] [g g ⁻¹]

Greek letters

α	phenomenological coefficient; [dm ³ min ⁻¹]
β	phenomenological coefficient; [dm ³ m ² min ⁻¹ A ⁻¹]
δ	thickness of the boundary layer; [m]
λ	wavelength; [nm]
μ	specific growth rate; [h ⁻¹]
μ_{MAX}	maximal specific growth rate; [h ⁻¹]
π	specific production rate [mmol g _{CDW} ⁻¹ h ⁻¹]
ρ	density; [g dm ⁻³]
ω	recycle ratio; [-]

7.1.1 List of Abbreviations

A	acetate
<i>aceEF</i>	pyruvate dehydrogenase
<i>ackA</i>	acetate kinase
Ac-CoA	acetyl-coenzyme A
ADP	adenosine di-phosphate
AMP	adenosine mono-phosphate
ATP	adenosine tri-phosphate
CDW	cell dry weight
CFB	cell free fermentation broth
CPFB	cell and protein free fermentation broth
CoA	coenzyme A
CSTR	stirred-tank reactors

DW	dry weight
ED	electrodialysis
F	function
FAD	flavine adenine dinucleotide
G	glucose
G6P	glucose-6-phosphate
GDP	guanosine diphosphate
GTP	guanosine triphosphate
HPr	histidine protein
ISPR	<i>in situ</i> product recovery
L	lactate
<i>ldhA</i>	lactate dehydrogenase
L-DOPA	L-dihydroxyphenyl alanine
MV3	minimal variance controller
NAD	nicotinamide adenine dinucleotide
NADH	nicotinamide adenine dinucleotide reduced
NADP	nicotinamide adenine dinucleotide phosphate
NADPH	nicotinamide adenine dinucleotide phosphate reduced
P	pyruvate
PEP	phosphoenolpyruvate
<i>pflB</i>	pyruvate formate lyase
<i>poxB</i>	pyruvate oxidase
PPP	pentose phosphate pathway
<i>pps</i>	phosphoenolpyruvate synthetase
<i>pta</i>	phosphotransacetylase
PTS	phosphotransferase system
<i>pyk</i>	pyruvate kinase
TCA	tricarboxylic acid
WSED	water splitting electrodialysis

7.1.2 Subscripts

0	influent, initial
IN	intra cellular
EX	extra cellular

P	permeate
P	product
S	substrate
X	biomass

7.2 List of Chemicals and Enzymes

All chemicals used were in the pure form "pro analysi" or "reinst" except otherwise stated.

25 % ammonia	Merck
acetone	Merck
$\text{AlCl}_3 \cdot 6\text{H}_2\text{O}$	Merck
antifoam S 289	Sigma-Aldrich
ATP	Boehringer
Bacto Tryptone [®]	Difco
$\text{CaCl}_2 \cdot 2\text{H}_2\text{O}$	Merck
$\text{CuCl}_2 \cdot 2\text{H}_2\text{O}$	Merck
$\text{CoCl}_2 \cdot 6\text{H}_2\text{O}$	Merck
$\text{FeSO}_4 \cdot 7\text{H}_2\text{O}$	Merck
glucose	Merck
glucose monohydrate	Roquette Italia S. P. A.
glucose-6-phosphate-dehydrogenase	Boehringer
glycerin	Merck
H_3BO_3	Merck
HCl (32 %)	Merck
HEPES	Merck
hexokinase	Boehringer
isopropyl	Merck
kanamycin disulphate	Merck
KH_2PO_4	Merck
K_2CO_3	Merck
K_2HPO_4	Merck
maleic acid	Merck
methanol	Merck
$\text{MgCl}_2 \cdot 6\text{H}_2\text{O}$	Merck

MgSO ₄	Merck
MnSO ₄ · H ₂ O	Merck
NaCl	Merck
NAD	Boehringer
NaH ₂ PO ₄ · H ₂ O	Merck
Na ₂ HPO ₄	Merck
Na ₂ MoO ₄ · 2H ₂ O	Merck
NaOH (45 %)	Merck
Na ₂ SO ₄	Merck
NH ₄ Cl	Merck
(NH ₄) ₂ SO ₄	Merck
perchloric acid	Merck
potassium acetate	Merck
sodium pyruvate	Merck
tetracycline hydrochloride	Merck
tris-(hydroxymethyl)-aminomethane	Merck
Tween 20	Merck
yeast extract	Merck
ZnSO ₄ · 7H ₂ O	Merck

7.3 List of Equipments

A/D converter	SMP Interface	Siemens
autoclaves	different	Tutnauer GMBH,
balances	IP 65, 3807MP	Sartorius AG
bioreactor	7.5 L	Infors
biosensor strip	glucose	SensLab ²
centrifuges	different	Heraeus, Beckmann
centrifugal pumps		Iwaki
conductivity meter	LF537	WTW
dilutor	Micro LAB 1000	Hamilton
electro dialysis stack		Goema
feeding system	YFC 01Z	Sartorius AG
fluorescence detector	RF-535	Shimadzu
gas analyzer	Binos 100 2M	Fisher-Rosemount

homogenisator	Vortex	Bender and Holbein
HPLC		Sykam
laboratory robot	Biomek 2000	Beckman Instrument
laminar flow chamber		Heraeus
LC-MS: a) HPLC		Gynkotek
b) MS		Thermo Finnigan
micro-titer plate photometer	Thermomax	Molecular Devices
micro-titer plate shaker	Titrimax	Heidolph
off-line glucose measurement	Accutrend Sensor®	Roche Diagnostic
on-line glucose measurement	OLGA GL2b	IBA GmbH
oven		Heraeus
peristaltic pumps	U101, U501, U504 601F/625L	Watson-Marlow
pH electrode	F-615-B130-DH	Broadley James
pH meter	632	Methrom
photometer	UV-160 A	Shimadzu
pO ₂ electrode	12 mm OxyProbe	Broadley James
power unit	NGRE 100/10	Rohde & Schwarz
rotation shaker	3033	GFL GmbH
ultra low freezer	C 21085	New Brunswick Scientific

7.4 HPLC and LC-MS Parameters

7.4.1 HPLC for Organic Acids

HPLC	Sycam
Column	Aminex HPX-87H, 300 × 7.8 mm, BioRad
Detector	S3300, UV-Detector, Sycam
Eluent	5 mmol dm ⁻³ H ₂ SO ₄ (isocratic)
Flow	0.5 mL min ⁻¹
Injection volume	100 µL
Oven temperature	40 °C
Wavelength extinction	215 nm

7.4.2 HPLC for Amino Acids

HPLC	Sycam
Column	Licrospher 100, RP 18-5 EC, 125 × 4 mm, Merck
Detector	RF-535, Fluorescence detector, Shimadzu
Eluent A	phosphate buffer (10 mM, pH 7.2) 0.5 % tetrahydrofuran
Eluent B	50 % phosphate buffer (10 mM, pH 7.2) 35 % methanol 15 % acetonitrile
Gradient	0 min 80 % B 7 min 90 % B 8.5 min 100 % B 11 min 100 % B 12 min 80 % B
Flow	0.9 mL min ⁻¹
Injection volume	5 µL
Guard column exposition	90 s
Oven temperature	40 °C
Wavelength extinction	330 nm
Wavelength emission	450 nm

7.4.3 LC-MS

HPLC autosampler	Gina 50, Gynkotek
HPLC pump	M 480, Gynkotek
Column	β-Nucleodes-OH, Macherey-Nagel
Detector	LCQ ion trap mass spectrometer, Thermo Finnigan
Eluent A	12 mM aqueous ammonium acetate
Eluent B	80 %, v/v, methanol 20 % v/v, eluent A
Gradient	0 - 15 min 2 % Eluent B, 98 % Eluent A 15 - 30 min linear increase to 100 % Eluent B 30 - 45 min 100 % Eluent B 45 - 47 min linear decrease to 2 % Eluent B, 98 % Eluent A

	47 - 60 min 2 % Eluent B, 98 % Eluent A
Flow a) HPLC	0.5 mL min ⁻¹
b) MS	40 µL min ⁻¹
Injection volume	20 µL
ESI Parameters:	
temperature of heated capillary	250 °C
electro-spray capillary voltage	4.5 kV
sheath gas	80 units = 1.2 L min ⁻¹
auxiliary gas	no
detection of negative ions	full scan mode

7.4.4 HPLC Chromatograms

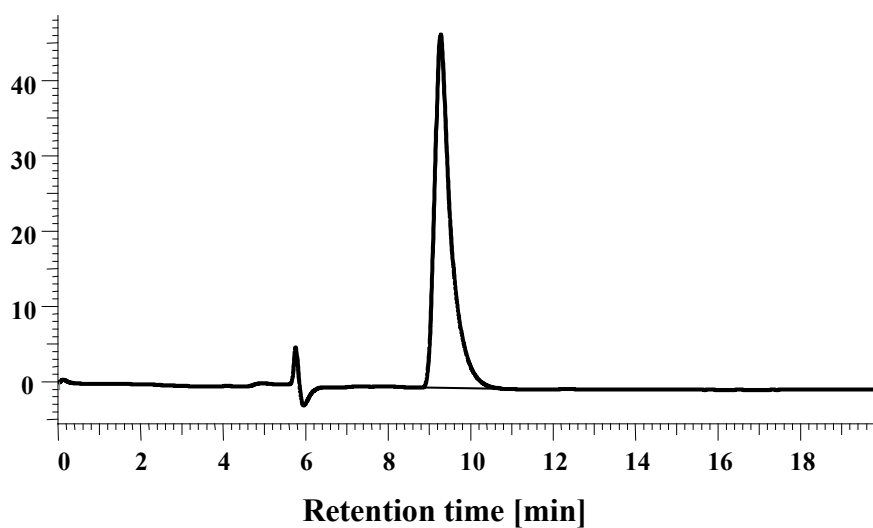


Figure 7.1 HPLC chromatogram of pyruvate standard solution

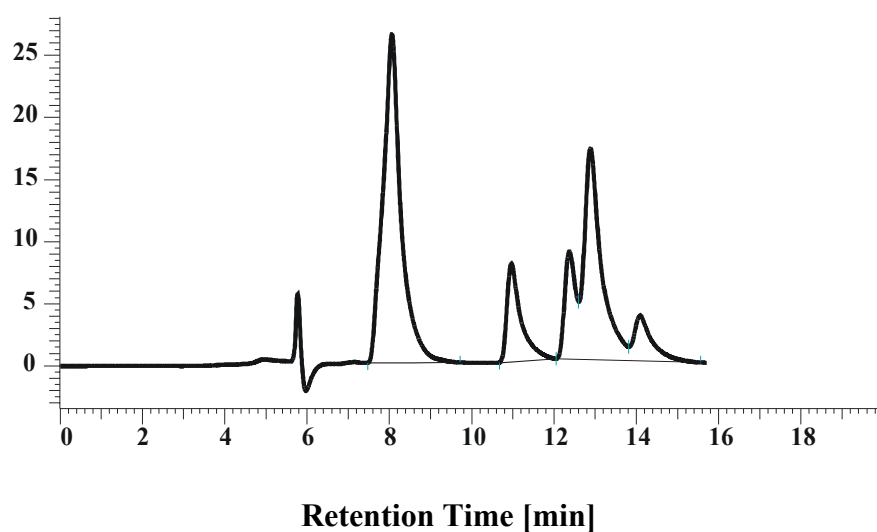


Figure 7.2 HPLC chromatogram of standard mix (citrate, succinate, lactate, fumarate, acetate) solution

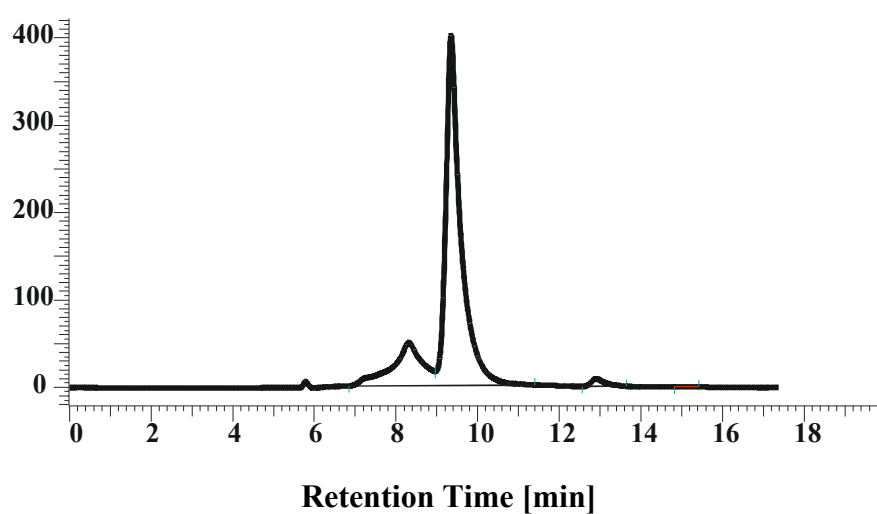


Figure 7.3 HPLC chromatogram of reaction mixture

Table 7.1 Retention times for organic acids determined by HPLC

Compound	Time [min]	Compound	Time [min]
Citrate	8.06	Lactate	12.37
Pyruvate	9.28	Fumarate	12.90
Succinate	10.97	Acetate	14.10

7.5 Ecological Validation of the Process

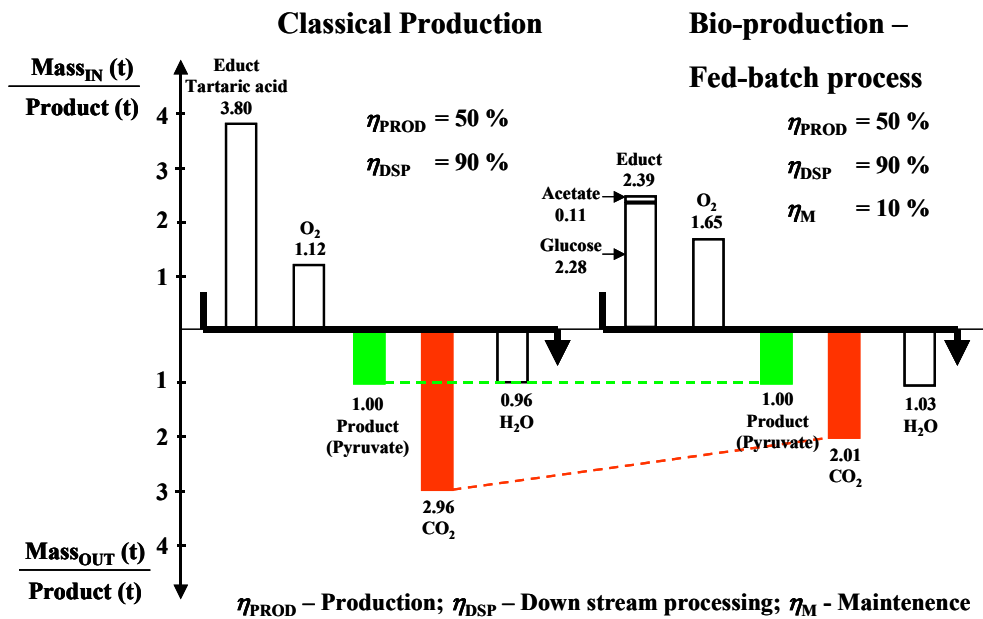


Figure 7.4 Ecological validation of the process. Comparison of CO₂ emissions in the classical pyruvate production process (pyrolysis of tartaric acid) and in the fed-batch pyruvate production process using *Escherichia coli* YYC202 *ldhA::Kan* strain for the production of 1 t pyruvate

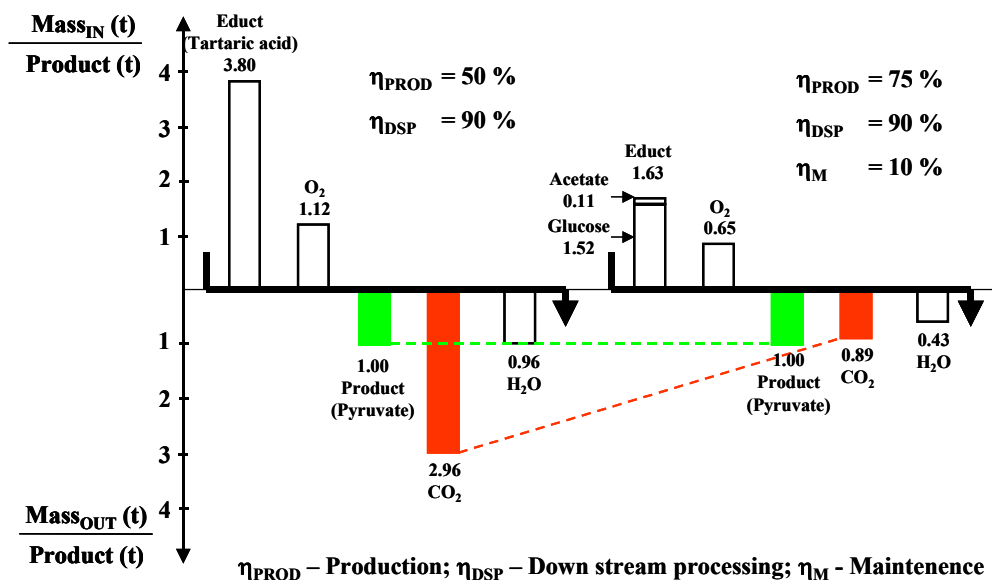


Figure 7.5 Ecological validation of the process. Comparison of CO₂ emissions in the classical pyruvate production process (pyrolysis of tartaric acid) and in the repetitive fed-batch pyruvate production process using *Escherichia coli* YYC202 *ldhA::Kan* strain for the production 1 t pyruvate

7.6 Economical Validation of the Process

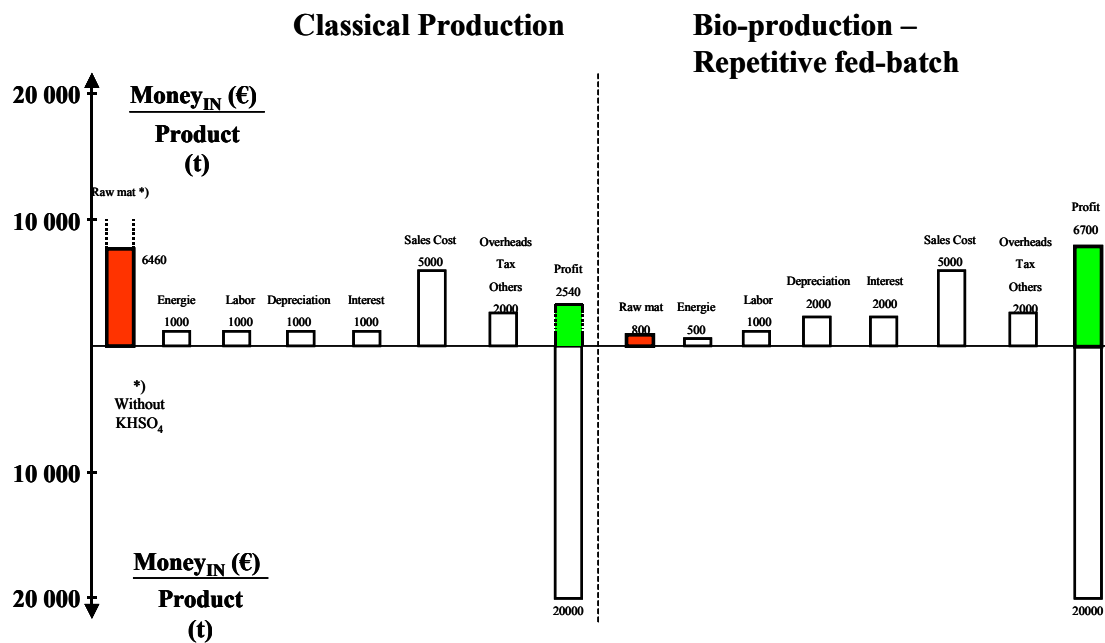


Figure 7.6 Ecological validation of the process. Comparison of CO_2 emissions in the classical pyruvate production process (pyrolysis of tartaric acid) and in the fed-batch pyruvate production process using *Escherichia coli* YYC202 *ldhA::Kan* strain for the production of 1 t pyruvate

Curriculum vitae

Personal details:

- Bruno Zelić
- born in Osijek, July 15th 1973., Croatia
- married with Aisa, daughter Anaïs

Education:

- 1979 - 1987: primary school "Tin Ujević", Osijek;
- 1987 - 1991: high school "Ruđer Bošković", Osijek;
- 1991 - 1996: undergraduate study, Faculty of chemical engineering and technology, University of Zagreb;
- 1996 - 1999: graduate study, Faculty of chemical engineering and technology, University of Zagreb;
- 1999 - 2003: doctoral study, Faculty of chemical engineering and technology, University of Zagreb

Professional experience

- June 1996 – November 1999: young researcher, Faculty of chemical engineering and technology, University of Zagreb
- December 1998 – February 1999: study stay, Forschungszentrum Jülich, Institute of Biotechnology 2, Germany
- November 1999 - : assistant, Faculty of chemical engineering and technology, University of Zagreb
- September 2000 – August 2002: PhD thesis, Forschungszentrum Jülich, Institute of Biotechnology 2, Germany

Rewards:

- 1994: Rector's price for the best student work;
- 1995: Rector's price for the best student work;
- 1998: Award for the best work of the young researcher presented at the conference, Biotechnical Foundation, Faculty of Food Technology and Biotechnology, University of Zagreb;
- 1999: Award for the young researchers and artists, Society of university professors and other scientist, University of Zagreb
- 2003: Award of Croatian society of chemical engineers and technologist

Bibliography

Scientific papers in CC journals:

1. Zelić, Bruno; Pavlović, Nediljko; Delić, Vladimir; Vasić-Rački, Đurđa: Kinetic model for the bioconversion of glucose to 2,5-diketo-D-gluconic acid. *Bioprocess Engineering*. 21 (1999) 45-50

Article in a journal stated in NN 2/97

1. Zelić, Bruno; Pavlović, Nediljko; Delić, Vladimir; Vasić-Rački, Đurđa: Optimization of pH and temperature in the process of bioconversion of glucose to 2, 5-diketo-D-gluconic acid. *Chemical and Biochemical Engineering Quarterly*. 16 (2002) 7-11
2. Zelić, Bruno; Pavlović, Nediljko; Vasić-Rački, Đurđa: Traženje optimalnih radnih uvjeta u procesu dekolorizacije otopine 2,5-diketo-D-glukonske kiseline EVOP metodom. *Kemija u industriji*. 46 (1997) 233-243

Papers sent to magazines

1. Zelić, Bruno; Gerharz, Tanja; Bott, Michael; Vasić-Rački, Đurđa; Wandrey, Christian; Takors, Ralf: Fed-batch Process for Pyruvate Production by Recombinant *Escherichia coli* YYC202 strain. *Chemical Engineering and Technology*. (2003) In print
2. Zelić, Bruno; Gostović, Srđan; Vuorilehto, Kai; Vasić-Rački, Đurđa; Takors, Ralf: Process strategies to enhance pyruvate production with recombinant *Escherichia coli*: From repetitive fed-batch to ISPR with fully integrated electro dialysis. *Biotechnology and Bioengineering*. (2003)

Invited lectures

1. Liese, Andreas; Hummel, Werner; Dausmann, Thomas; Haberland, Juergen; Kriegesmann, Angus; Zelić, Bruno; Wandrey, Christian. Verfahrensoptimierung und Scale-up der diastereoselektiven Reduktion von Dienen. 19. DECHEMA Jahrestagungen der Biotechnologen, Leipzig, Germany (2001)
2. Zelić, Bruno; Pavlović, Nediljko; Vasić-Rački, Đurđa. Analysis of Microbial Growth of *Erwinia citreus* in Continuous Culture. In: Flamant Gilles (Ed.): Specific Processes and Technologies, Nancy, Societe Francaise de Genie des Procedes, 13 (1999) 303-310

Conference papers with international peer-review

1. Vrsalović, Ana; Zelić, Bruno; Vasić-Rački, Đurđa: Optimization of biocatalyst production in bakers yeast cultivation. In: Glavic, Peter ; Brodnjak-Voncina, Darinka (Ed.): Zbornik referatov s posvetovanja 2.del. Maribor, FKKT Maribor (2000) 523-528
2. Zelić, Bruno; Pavlović, Nediljko; Delić, Vladimir; Vasić-Rački, Đurđa: Kinetic model for the bioconversion of glucose to 2, 5-diketo-D-gluconic acid. Poli, G. (Ed.): Proceedings, Milano, The Italian Association of Chemical Engineering (1997) 3105-3108

Other conference papers

1. Zelić, Bruno; Pavlović, Nediljko; Vasić-Rački, Đurđa: Modelling of the bioconversion of glucose to 2,5-diketo-D-gluconic acid in continuous process. Biotechnology 2000, Biochemical Engineering Science and Processes, Frankfurt am Main, DECHEMA (2000) 287-289

Abstracts in Book of abstracts and unpublished papers

1. Zelić, Bruno, Vasić-Rački, Đurđa; Wandrey, Christian; Takors, Ralf: Improvement of classical pyruvate production by novel *Escherichia coli* process. In: Zrnčević, Stanka (Ed.): Knjiga sažetaka, Zagreb, HDKI i HKD (2003) 237, oral presentation
2. Zelić, Bruno; Gerharz, Tanja; Bott, Michael; Wandrey, Christian; Takors, Ralf: Process development for *Escherichia coli* based pyruvate production. In: Grote, Ralf; Antranikian, Garabed (Ed.): Book of Abstracts, Hamburg, TUHH-Technologie GmbH (2002) 194, poster
3. Zelić, Bruno; Gerharz, Tanja; Bott, Michael; Wandrey, Christian; Takors, Ralf: Alternative Approach for High Energy Extensive Pyruvate Production: *E. coli* Based Process Development. In: Marquardt, Wolfgang; Wagner, Wolfram (Ed.): Book of Abstracts, Weinheim: Wiley-VCH Verlag GmbH (2002) 718, oral presentation
4. Zelić, Bruno; Vasić-Rački, Đurđa; Wandrey, Christian; Takors, Ralf: Development of environmental friendly and sustainable bio-production pyruvate process. In: Koprivanac, Natalija (Ed.): Knjiga sažetaka, Kutina, HDKI (2002) 36, oral presentation
5. Zelić, Bruno; Takors, Ralf; Vasić-Rački, Đurđa; Wandrey, Christian: Process development for *Escherichia coli* based pyruvate production. In: Vicković, Ivan (Ed.): Sažetci, Koprivnica, HKD i HKDI (2001) 220, poster

6. Vrsalović, Ana; Zelić, Bruno; Vasić-Rački, Đurđa. Modeliranje kontinuirane biokatalitičke oksidacije etanola uz ADH u membranskom reaktoru. In: Butula, Ivan (Ed.): Knjiga sažetaka, Zagreb, HDKI (2000) 83, poster
7. Vrsalović, Ana; Brkić, Žana; Zelić, Bruno. Statistička analiza ponovljivosti podataka u bioprocesu uzgoja pekarskog kvasca. In: Štern, Ivica (Ed.): Knjiga sažetaka, Zagreb, FKIT (2000) 42, poster
8. Zelić, Bruno: Usporedba polinomnog i Monodovog modela rasta biomase. Štern, Ivica (Ed.): Knjiga sažetaka, Zagreb FKIT (2000) 43, poster
9. Zelić, Bruno; Pavlović, Nediljko; Vasić-Rački, Đurđa: Modeliranje biokonverzije glukoze u 2,5-diketo-D-glukonsku kiselinu. In: Bošnjak, Marijan; Janović, Zvonimir; Vasić-Rački, Đurđa (Ed.): Zbornik radova, 9. Ružičkini dani, Zagreb, Hrvatsko društvo kemijskih inženjera i tehnologa (1998) 63, poster
10. Zelić, Bruno; Pavlović, Nediljko; Delić, Vladimir; Vasić-Rački, Đurđa: Optimiranje pH i temperature u procesu biokonverzije. In: Gojo, Miroslav; Trajkov, Nada; Smolec, Sonja (Ed.): Sažeci, XV. hrvatski skup kemičara i kemijskih inženjera, Zagreb, Hrvatsko društvo kemijskih inženjera i tehnologa, 2 (1997) 267, poster
11. Zelić, Bruno; Pavlović, Nediljko: Razvoj matematičkog modela biokonverzije glukoze u 2,5-DKG. Susret mladih kemijskih inženjera, Zagreb, Hrvatsko društvo kemijskih inženjera i tehnologa (1996) 34, oral presentation
12. Zelić, Bruno; Pavlović, Nediljko; Delić, Vladimir; Vasić-Rački, Đurđa: Kinetički model biokonverzije glukoze u 2,5-DKG. Knjiga sažetaka, 8. Ružičkini dani, Zagreb, Hrvatsko društvo kemijskih inženjera i tehnologa (1996) 123, poster
13. Zelić, Bruno; Wandrey, Christian; Takors, Ralf: Process development for Escherichia coli based pyruvate production. Der Internen Arbeitssitzungen der Fachausschuesse "Bioverfahrenstechnik" (GVC) und "Technik biologischer Prozesse" (Dechema), Bad Honnef, Germany (2002), oral presentation

Dissertations, master thesis:

1. Zelić, Bruno: Razvoj kinetičkog modela biokonverzije glukoze u 2,5-diketo-D-glukonsku kiselinu. Master thesis, Zagreb, Fakultet kemijskog inženjerstva i tehnologije, (1999) Supervisor: Vasić-Rački, Đurđa

Graduation thesis

1. Zelić, Bruno: Razvoj matematičkog modela biokonverzije glukoze u 2,5-diketo-D-glukonsku kiselinu. Graduation thesis, Zagreb : Fakultet kemijskog inženjerstva i tehnologije, (1996) Supervisor: Vasić-Rački, Đurđa

Other papers

1. Gerharz, Tanja; Zelić, Bruno; Takors, Ralf; Bott, Michael.: Produktion von Pyruvat aus Glucose mit Escherichia coli, , In: Heiden, Stefanie; Erb, Rainer (Ed.): Biokatalyse, Spektrum akademischer Verlag GmbH, Heidelberg (2001) 29-33

Patents

1. Bott, Michael; Gerharz, Tanja; Takors, Ralf; Zelić, Bruno: Vefahren zur fermentative Herstellung von Pyruvat. German Patent Application 10129714.4 (2001)
2. Gerharz, Tanja; Zelić, Bruno; Takors, Ralf; Bott, Michael: Verfahren sowie Mikroorganismen zur mikrobiellen Herstellung von Pyruvat aus Kohlenhydraten sowie Alkoholen. German Patent Application 10220234.6 (2002)